Magma storage at Ocean Islands: insights from Cape Verde

Barker AK[1,2], Rydeblad E[1,3], Silva SMDM[4]

1 Mineralogy, Petrology, Tectonics, Department of Earth Sciences, Uppsala University, Villavägen 16, Uppsala SE-752 36, Sweden

2 Centre of Natural Hazards and Disaster Sciences (CNDS), Villavägen 16, Uppsala SE-752 36, Sweden

3 Department of Earth Science and Engineering, South Kensington Campus, Imperial College London, SW7 2AZ, UK

4 Faculty of Science and Technology, University of Cabo Verde, CP 279, Praia, Santiago, Cabo Verde

Abstract

The Cape Verde archipelago is a group of Ocean Islands in the Central Atlantic that forms two chains of islands trending Northwest and Southwest. Several of the islands are considered to be volcanically active, with frequent eruptions on Fogo. We examine the mineral chemistry and thermobarometry of the southern islands; Santiago, Fogo and Brava together with the Cadamosto Seamount. Our objective is to explore the magmatic storage system and implications for volcanic eruptions and associated hazards at Cape Verde. The volcanic rocks at Cape Verde are alkaline and dominantly mafic, whereas the island of Brava and the Cadamosto Seamount are unusually felsic. Clinopyroxene compositions range from 60 to 90 Mg# at Santiago and Fogo. In contrast, at Brava and the Cadamosto Seamount the clinopyroxene compositions are 5 to 75 Mg#. Mineral chemistry and zonation records fractional crystallization, recharge, aggregation of crystals, magma mixing and variations in thermal conditions of the magma at temperatures from 925 to 1250ºC. Magma storage depths at Santiago, Fogo, Brava and the Cadamosto Seamount are between 12 and 40 km, forming deep sub-Moho magma storage zones. Transient magma storage in the crust is suggested by fluid inclusion re-equilibration and pre-eruption seismicity. A global compilation of magma storage at Ocean Islands suggests deep magma storage is a common feature and volcanic eruptions are often associated with rapid magma ascent through the crust. Shallow magma storage is more variable and likely reflects local variations in crustal structure, sediment supply and tectonics. Petrological constraints on the magma plumbing system at Cape Verde and elsewhere are vital to integrate with deformation models and seismicity in order to improve understanding and mitigation of the volcanic hazards.

Introduction

Ocean Islands occur in all of the world's oceans and are formed by intraplate volcanism. Several Ocean Islands are volcanically active with eruptions at Reunion, Canary Islands, Cape Verde and Hawaii between 2007 and 2018 (e.g. Di Muro et al., 2014; Longpré et al., 2014; Worsley, 2015; Liu et al., 2018). Many of the Ocean Islands are inhabited and have lucrative tourist industries, which put people directly at risk from the volcanic hazards associated with eruptions. Additionally, submarine and subaerial eruptions can also be hazardous for the shipping and aviation industries respectively (O'Mangain et al., 2007; Di Muro et al., 2014). Consequently, understanding the magma plumbing systems from the magma storage zones to the volcanic centers is imperative for assessing and monitoring the volcanic hazards. We present insights into the magma storage at Cape Verde, to explore the nature of the volcanically active parts of the archipelago which is motivated by the recent eruptions at Fogo (Ribeiro, 1960; Worsley et al., 2015).

The Cape Verde archipelago is an Ocean Island group built upon the Cape Verde Rise (Ramalho et al., 2010a,b). The older and now heavily eroded islands of Maio, Sal and Boa Vista are found in the East, from where two volcanic chains emerge. The northern chain consists of São Nicolau, Santa Luzia, São Vicente and Santa Antão. The islands of Santiago, Fogo, and Brava as well as the Cadamosto Seamount form the southern island chain (Figure 1). The island of Fogo displays the iconic Pico do Fogo, peaking at 2829 m above sea level, located inside the Bordiera, on the Chã das Caldeiras, where the historic eruption sites are found; the latest eruption was November 2014 to February 2015 (Silva et al., 2015; Fernandes & Faria, 2015; González et al., 2015; Worsley 2015; Richter et al., 2016; Jenkins et al., 2017). Prior to that nine eruptions occurred at Fogo between 1760 and 1995, with a total of 28 eruptions since settlement in the 15th century (Ribeiro, 1960; Nascimento, 2015). Brava and the Cadamosto Seamount have no historical record of volcanic activity. However, Holocene volcanic activity is documented at Brava and the Cadamosto Seamount records eruption ages of 21 ka (Madeira et al., 2010; Faria & Fonseca, 2014; Samrock et al., 2019). Additionally, seismicity extends from Fogo to the Cadamosto Seamount suggesting that Brava and the Cadamosto Seamount are also underlain by active magmatic systems (Heleno et al., 2006; Grevemeyer et al., 2010).

The volcanic hazards on Fogo are in the form of ash and lapilli associated with strombolian activity and lava flows as well as occasional sub-plinian to plinian eruptions (Torres et al., 1997; Eilese et al., 2015). The residents of Fogo are vulnerable to the direct volcanic hazards associated with an eruption, especially the approximately one thousand who live and work inside the Bordeira close to Pico do Fogo, followed by the 11,000 residents of the East coast of Fogo (Faria & Fonseca, 2014). The eruptions in 1995 and 2014/2015 led to large-scale evacuation as well as significant damage to property, agricultural land and buildings (Silva et al., 2015; Worsley 2015; Jenkins et al., 2017). Potential volcanic hazards at

Brava are connected to pyroclastic and phreatomagmatic eruptions and endanger the 6,000 inhabitants (Faria & Fonseca, 2014).

In addition, the onshore and offshore geological record of the Cape Verde archipelago shows evidence for flank collapses and landslide deposits (Masson et al., 2002, 2008; Paris et al., 2018; Barrett et al., 2020). The Bordeira cliffs of Fogo were potentially exposed by a huge landslide (Day et al., 1999; Foeken et al., 2009; Ramalho et al., 2015; Martínez-Moreno et al., 2018). Tsunami deposits have been used to constrain the associated flank collapse and landslide to approximately 73 ka (Ramalho et al., 2015). Furthermore tsunami deposits associated with local flank collapses are found, among other locations, on Santiago and Maio (Paris et al., 2011, 2018; Ramalho et al., 2015; Madeira et al., 2019). Therefore the Cape Verde Islands are associated with multiple natural hazards that may pose a threat to the population both locally and farther afield.

Monitoring of the volcanism is the responsibility of the National Institute for Metrology and Geophysics. In addition the University of Cape Verde has been conducting geochemical monitoring in partnership with national and international institutions (Fonseca et al., 2003; Barrancos et al., 2015; Pérez et al., 2015; Dionis et al., 2015a, b). Seismicity and deformation is monitored throughout Cape Verde with 15 seismometers and a geodetic network (Faria & Fonseca, 2014). The Fogo-Brava seismic network consists of seven seismometers on Fogo and two on Brava and Fogo hosts three geodetic stations. Additional monitoring targets volcanic gas emissions with semi-frequent measurements of CO_2 and SO_2 emissions and fumerole temperatures (Faria & Fonseca, 2014; Worsley 2015). The National Institute for Metrology and Geophysics work with the National Civil Protection service to provide risk communication (Faria & Fonseca, 2014).

The magmatic system can be investigated through minerals in the erupted products. The minerals capture the compositional signature of the host magma during growth, therefore they respond to variations in magma composition. Consequently minerals provide a chronological record of magma evolution (Davidson et al., 2007). On this basis mineral thermobarometry offers a petrological method to estimate the crystallization conditions of magma chambers, including the temperature and pressure of crystal growth (e.g. Putirka, 2008). Igneous thermobarometers have been widely applied in many settings such as volcanic arcs (e.g. Till, 2017; Lai et al., 2018) and to investigate continental magmatism (Putirka et al., 2003; Putirka & Condit, 2003). Clinopyroxene-melt thermobarometers have also been applied in Ocean Islands settings to explore tholeiitic to alkaline systems e.g. Hawaii, Cape Verde, Canary Islands (e.g. Putirka, 1997; Klügel et al., 2000, 2005, Nikogosian et al., 2002; Aulinas et al., 2010; Hildner et al., 2011, 2012; Longpré et al., 2014; Mata et al., 2017). Despite large uncertainties associated with

crystallization pressure estimates, thermobarometry offers several advantages that complement geophysical methods for determining magma chamber depth location (Magee et al., 2018). Firstly a magma pocket requires significant dimensions to be detected by seismic arrays, even at dense seismic station distribution (e.g. Gudmundsson, 2012). Secondly seismicity picks up differences in seismic velocities, and thereby requires magma pockets to be melt rich, if they are mush zones with a significant proportion of crystals then the melt:solid ratio may not be high enough to observe variations in seismic wave velocities (e.g. Gudmundsson, 2012). Additionally, studies of deformation often employ petrological data as inputs to estimate the shape, size and depth of the point source, to model the inflation of a magma chamber (e.g. Amelung & Day, 2002; González et al., 2015). Petrological techniques can thus provide crucial information on magma storage for integration with geophysical models (Magee et al. 2018). Whereas geophysical methods are not only useful for investigating the magma storage system but also have distinct advantages in real-time monitoring of magma movement prior to eruptions (Magee et al., 2018).

Furthermore, thermobarometry determines pressure and temperature of mineral growth and is often sensitive to crystals growing in small magma pockets (e.g. Geiger et al., 2016; Stock et al., 2018). In many cases these magma pockets are not detected until earthquakes trace magma ascent prior to an eruption. Several cases have shown that other methods confirm the models for magma plumbing systems developed from thermobarometry (e.g. Longpré et al., 2014; Barker et al., 2019). However thermobarometry is not without limitations, restricted by the minerals present as well as magma compositions and experimental conditions of calibrations (e.g. Putirka, 2008). For instance, although clinopyroxene crystallizes over wide temperature, pressure and compositional ranges the felsic magmas in many settings evolve beyond clinopyroxene crystallization (e.g. Weidendorfer et al., 2016). Therefore other minerals or features such as fluid inclusions and volatile solubility in glass are required to trace the more evolved parts of the magmatic system (e.g. Schwarz & Klügel 2004; Jeffery et al., 2016).

All volcanic activity is fed from the magma plumbing system, therefore it is important to understand the magma storage, magmatic processes and where they occur as well as the processes that lead to magma ascent (Cooper, 2017; Putirka, 2017; Sparks & Cashman, 2017). To address the connection between the magmatic system and volcanic hazards at Cape Verde we will discuss magmatic processes recorded by mineral chemistry and the magma plumbing system derived from thermobarometric modelling for the southern Cape Verde archipelago. Mineral chemistry from the islands of Santiago, Fogo, Brava and the Cadamosto seamount will be examined to provide insights into the magmatic processes. These examples have been selected based on availability of mineral chemistry and geophysical data as well as relevance from a volcanic hazard perspective. Mineral-melt equilibrium

thermobarometry for Santiago, Fogo, Brava and the Cadamosto Seamount will be integrated into a model for the magmatic plumbing systems in southern Cape Verde. Evidence for the shallower parts of the magma plumbing systems and the volcanic hazards at Fogo will be reviewed. Finally, the magma plumbing system for Cape Verde will be compared with other Ocean Islands globally.

The Cape Verde Archipelago

The Cape Verde Rise is situated 2000 km East of the Mid-Atlantic Ridge in the Central Atlantic, between 15 and 17°N and approximately 500 km West of Dakar, Senegal (Figure 1). The Cape Verde Rise forms a gigantic bathymetric swell reaching circa 2 km above the surrounding ocean crust and covers an area of more than 0.3 million km^2 (Crough, 1982; McNutt, 1988; Jørgensen & Holm, 2002; Lodge and Helffrich, 2006; Holm et al., 2008; Masson et al., 2008; Brown et al., 2009). The Cape Verde islands and seamounts are located in the Southwest of the Cape Verde Rise (Figure 1; Rona, 1971; Egloff, 1972; Dash et al., 1976). The islands are arranged in a semi-circle opening to the West, with older heavily eroded islands occurring in the East and two subparallel chains of islands in the North and South, which extend westwards (Figure 1; Gerlach et al., 1988).

The northern and southern island chains are subparallel to the fracture zones found to the West of the Cape Verde archipelago (Figure 3; Jacobi and Hayes, 1982). Therefore fracture zones may influence the orientation of the island chains (Klerkx et al., 1974; Le Pichon and Fox, 1971; Doucelance et al., 2003). Evidence for fracture zone offsets is documented by magnetic lineations and gravity anomalies (Figure 3; Hayes and Rabinowitz, 1975; Dash et al., 1976; Williams et al. 1990; Verhoef et al. 1991; Roest et al. 1992; Ali et al., 2003). Additionally brittle deformation through normal, reverse and transverse faults has formed horst and graben structures on the Cape Verde Rise (Figure 3b; Efimov & Skolotnev, 2006; Skolotnev et al., 2007; 2009).

The Cretaceous ocean crust, formed at the Mid Atlantic Ridge, is overlain by a several kilometer thick sequence of hemipelagic sediments (Figure 2; Dash et al. 1976; Courtney & White, 1986; Williams et al., 1990; Ali et al., 2003; Müller et al., 2008; Pim et al., 2008). The oceanic lithosphere is approximately 85 km thick, confirmed by elevated seismic velocities extending to ca. 80 km and a Lower Velocity Zone that appears at 90±6 km depth (Cazenave et al., 1988; Lodge and Helffrich, 2006). Although the ocean crust beneath Cape Verde has normal thicknesses of 7 to 8 km, the islands are underlain by thickened crust (Pim et al., 2008; Wilson et al., 2010, 2013). The Moho beneath individual islands decreases westwards from >20 km beneath Maio, to 17 to 18 km beneath Santiago and to 12 to 14

km beneath Fogo (Lodge and Helffrich, 2006; Pim et al., 2008; Wilson et al., 2010, 2013). The sedimentary stratigraphy observed at Deep Sea Drilling Project (DSDP) Site 368 is composed of marl and nannofossil ooze, underlain by clay, claystone and minor chert associated with turbidites, plus black shale interbedded with dikes below (Lancelot et al., 1978; Faugères et al., 1989).

The Cape Verde islands display core complexes composed of intrusive carbonatite to alkaline assemblages as well as submarine pillow basalts (Serralheiro, 1970; De Paepe et al., 1974; Serralheiro, 1976; Stillman et al., 1982; Gerlach et al., 1988; Davies et al., 1989; Madeira et al., 2010; Ramalho et al., 2010b). The extrusives are dominantly mafic as exemplified by nephelinites and basanites at Santiago and Fogo (Gerlach et al., 1988; Davies et al., 1989; Barker et al., 2009; Hildner et al., 2011, 2012). However several volcanic centers such as the island of Brava and the Cadamosto Seamount exhibit largely felsic assemblages (Assunção et al. 1965; Machado et al. 1968; Madeira et al., 2008, 2010; Barker et al., 2012; Weidendorfer et al., 2016; Samrock et al., 2019). Cape Verde is one of the few Ocean Island groups hosting carbonatites, which are widespread on Brava with minor exposures on Fogo, Santiago and São Vicente (e.g., Assunção et al., 1965; Silva et al., 1981; Turbeville et al., 1987; Hoernle et al., 2002; Jørgensen and Holm, 2002; Mata et al., 2010; Mourão et al., 2010).

Geochronology of the Cape Verde archipelago

The Cape Verde islands exhibit a general age progression from the early Miocene, for the oldest exposures, which decrease westwards to the presently volcanically active parts of the archipelago (Figure 4; Bernard-Griffiths et al. 1975; Stillman et al., 1982; Mitchell et al. 1983; Torres et al. 2002; Plesner et al. 2003; Jørgensen and Holm 2002; Duprat et al., 2007; Holm et al. 2008; Foeken et al. 2009; Dyhr and Holm 2010; Madeira et al. 2010; Samrock et al., 2019). The older islands in the East are highly eroded displaying relatively flat and low topography in contrast to the shield volcanoes that occur further West. The earliest age of the eastern islands is recorded by submarine pillow basalts from the island of Sal at 26 Ma (Torres et al., 2002). The volcano-magmatic activity continues until approximately 1 Ma at Sal (Figure 4; Mitchell et al., 1983; Torres et al., 1997; Holm et al., 2008; Dyhr & Holm, 2010). The northern islands show volcanic activity from approximately 8 to 10 Ma to between 100,000 and 300,000 years ago at São Nicolau to Santa Antão (Figure 4; Plesner et al. 2003; Duprat et al., 2007; Holm et al. 2008). Seismic activity beneath Santa Antão suggests this region continues to be volcanically active (Faria & Fonseca, 2014).

There is evidence that volcanism in the southern islands commenced at Santiago approximately 11 Ma ago (Figure 4; Stillman et al., 1982; Mitchell et al., 1983; Torres et al., 2002; Ali et al, 2003). The majority of the volcano-magmatic activity on the southern islands emerges from 5.5 Ma at Santiago, 4.5 Ma at Fogo and 2.3 Ma at Brava (Holm et al., 2008; Foeken et al. 2009; Madeira et al., 2010; Ramalho et

al., 2010). The most recent volcanic eruptions from Santiago are dated to 740,000 years ago and 300,000 years ago at Brava (Holm et al., 2008; Madeira et al., 2010). The islands typically show multiple stages of volcanism interrupted by periods of quiescence (Figure 4; Holm et al., 2008; Foeken et al., 2009; Madeira et al., 2010; Ramalho et al., 2010a, 2010b, 2010c). Volcanic activity at the Cadamosto Seamount appears to occur in the last 20,000 to 100,000 years (Samrock et al., 2019). The island of Fogo displays historical volcanism with around 30 eruptions since discovery and settlement in 1460 including recent eruptions in 1995 and 2014 to 2015 (Ribeiro, 1960; Da Silva et al., 1999; Hildner et al., 2011, 2012; Silva et al., 2015; Fernandes & Faria, 2015; Worsley 2015). Additionally Fogo, Brava and the Cadamosto Seamount display ongoing seismic activity (Heleno et al., 2006; Grevemeyer et al., 2010; Faria & Fonseca, 2014).

The geology of Santiago

The island of Santiago is composed of an intrusive complex, followed by submarine and subaerial volcanics (Figures 5 & 6; Bebiano, 1932; Serralheiro et al., 1976; Ramalho, 2011). The Complexo Antigo consists of alkaline silicate intrusives and carbonatites. The submarine stage is represented by the Flamengos Formation and exhibits pillow lavas embedded in hyaloclastite with eruption ages of 4.0 to 5.5 Ma (Figures 4, 5 & 6; Serralheiro, 1976; Holm et al., 2008; Barker et al., 2009; Ramalho et al., 2020c; Ramalho, 2011). The shield stage is formed by subaerial lavas of the Pico da Antonía Formation between 1.5 and 3.2 Ma (Figures 4, 5 & 6; Serralheiro, 1976; Holm et al., 2008; Barker et al., 2010; Ramalho et al., 2020c). Occasional carbonatite lava flows belong to the Pico da Antonía Formation (Jørgensen and Holm, 2002). The Assomada and Monte das Vacas formations erupted post-erosional lavas and scoria cones between 0.7 and 1.1 Ma (Figures 4 & 6; Serralheiro, 1976; Holm et al., 2008; Barker et al., 2010; Ramalho et al., 2020c). Additionally, a sliver of the Jurassic ocean crust has been uplifted and emplaced at Baía de Angra, plus uplifted sediments are found at Tarrafal (Serralheiro, 1976; Gerlach et al., 1988; Ogg et al., 1995; Ramalho, 2011).

The geology of Fogo

The geology of Fogo can be divided into four units. The stratigraphy begins with the submarine stage composed of carbonatites and alkaline basalts from approximately 4.5 Ma (Figure 4; Day et al., 1999; Madeira et al., 2010). The emergence of Fogo as an island is recorded by the subaerial lavas of the Monte Barro Group (Day et al., 1999). Subsequently a large stratovolcano known as Monte Amarelo developed during the Quaternary, reaching up to 3 km above sea level (Figure 7; Day et al., 1999). A giant landslide

occurred at approximately 73 ka, leaving the Bordiera cliffs as a remnant of the caldera wall or flank collapse scarp (Figure 1; Elsworth & Day, 1999; Masson et al., 2008; Foeken et al., 2009; Paris et al., 2011, 2018; Ramalho et al., 2015; Madeira et al., 2019). The associated structure is filled with volcanic materials to form a plateau known as the Chã das Caldeiras, which hosts the majority of the volcanic activity from 62 ka to present (Figures 4 & 7; Ribeiro, 1960; Torres et al., 1997; Day et al., 1999; Foeken et al., 2009). The spectacular Pico do Fogo, rising 2829 m above sea level formed by Hawaiian and Strombolian activity that produced basanite to tephrite lapilli and lava (Figures 5 & 7; Torres et al., 1997). Historic eruptions emanated from the base of Pico do Fogo, the eastern flank of Pico do Fogo or from vents on the Chã das Caldeiras plain. The eruptions have typical durations of 2 months, and the last eruption was 23rd November 2014 to 7th February 2015 (Figure 5; Silva et al., 2015; Fernandes & Faria, 2015; Worsley 2015). The eight previous eruptions occurred in 1785, 1799, 1816, 1847, 1852, 1857, 1951 and 1995 (Figure 4; Ribeiro, 1960; Torres et al., 1997; Day et al., 1999).

The geology of Brava

Brava is smaller than Fogo and Santiago with an area of 64 km^2, located 18 km from Fogo on the Brava-Fogo platform, which is only 1400 mbsl (Figure 1; Da Silva et al., 1999; Madeira et al., 2010). The geology was first investigated by Bebiano (1932) and later by Machado et al. (1968). Recent work by Madeira et al. (2010) has divided the stratigraphy into three units. The submarine volcanism consists of hyaloclastite and pillow basalt breccias and flows that radiate from the centre of the island (Figure 8; Madeira et al., 2010). They are intruded by N-S and E-W oriented dikes. Subsequently the intrusive complex was emplaced in the submarine volcanics. The alkaline-carbonatite intrusives are represented by pyroxenites, ijolite-melteigites-urites and nepheline syenites plus carbonatites (Figure 8; Madeira et al., 2010; Mourão et al., 2010). Post-erosional volcanism is dominantly phonolitic and ranges from ignimbrites and tephra deposits due to phreatomagmatic eruptions, to phonolite lava flows and domes (Figures 5 & 8). Mafic volcanism is rare in the post-erosional sections, however carbonatites in the form of ignimbrites and lava flows are not uncommon (Figure 8; Madeira et al., 2010). Seismicity, particularly NE and SE of Brava associated with volcanic cones on the Brava-Fogo platform, indicate that Brava is magmatically active. Seismic swarms at depths of 2 to 10 km, along with seismic tremor suggest volcano-tectonic events related to submarine intrusions (Faria & Fonseca, 2014).

The Cadamosto Seamount

The Cadamosto Seamount is a large circular submarine volcano, with a diameter of approximately 15 km, and a height of 3 km, reaching water depths of up to 1380 mbsl (Figure 1; Hansteen et al., 2014). The seamount has three main craters in the summit area, where pillow and sheet flows have been observed (Figure 5). The samples are mainly phononephelinites to phonolites, with occasional basaltic samples (Barker et al., 2012; Hansteen et al., 2014; Samrock et al., 2019). New ^{40}Ar-^{39}Ar geochronology gives eruption ages of 20 to 97 ka confirming the young nature of the seamount (Samrock et al., 2019). Additionally the Cadamosto Seamount is seismically active with notable earthquakes of magnitudes 4.9 and 4.3 recorded in 1998 and 2004 respectively (Grevemeyer et al., 2010). The seismicity is interpreted to be formed by brittle rock failure resulting from submarine intrusion (Grevemeyer et al., 2010).

Volcanic eruptions and hazards at Fogo

The natural hazards faced by the population of Fogo are weather related, such as droughts that lead to famine, as well as flash floods and related landslides that destroy roads and buildings. Less common and therefore considered less of a risk are volcanic eruptions and associated earthquakes. The volcanic eruptions pose hazard to the communities living in the Chã das Caldeiras area (964 people) plus potentially the towns on the East Coast of Fogo (11,000 people). Lava flows are the greatest hazard, however volcanic gases and tephra also contribute to the volcanic hazards (Texier-Teixeira et al., 2014; Nascimento, 2015; Silva et al., 2015, 2017; Richter et al., 2016).

There have been 28 eruptions on Fogo since discovery of the island by Portugese sailors in 1460 (Ribeiro, 1960). The most recent eruption commenced on 22nd November 2014 and continued for 77 days, finally ceasing on 7th February 2015. The eruption consisted of a 6 km high eruption cloud causing tephra deposits in eight villages and towns, as well as other islands such as Brava to the West and São Vicente to the North (Nascimento, 2015). The lava flows rapidly cut off the road access to Chã das Caldeiras and went on to destroy the villages of Portela and Bandaeira including 75% of the buildings in the Chã das Caldeiras area and 25% of the agricultural land and water storage facilities (Jenkins et al., 2017).

The volcano monitoring activities carried out by the Institute of National Meteorology and Geophysics and the University of Cape Verde are essential to volcanic crisis management. Regular automated monitoring covers seismicity and deformation of the volcano (Fonseca et al., 2003; Faria & Fonesca, 2014; Dionis et al., 2015a, b; Fernandes & Faria, 2015). During the eruption in 1995, volcanic tremor and seismic swarms occurred between 1 and 5 km depths (Da Silva et al., 1999). Approximately seven weeks prior to the eruption in 2014-2015, earthquakes were detected originating at depths of >15 km (Fernandes & Faria, 2015). Additional geochemical monitoring of the volcanic gases is manual and therefore

sampling is conducted during specific campaigns and does not provide a continuous record of volcano degassing (Dionis et al., 2015a,b; Pérez et al., 2015). For instance, air quality was monitored during the 2014-2015 eruption by the deployment of an instrument at one station in São Filipe on the West coast of Fogo (Nascimento, 2015).

Magmatic processes

We use mineral chemistry from Cape Verde to explore the magmatic processes recorded by clinopyroxene (Davidson et al., 2007). Advantages of focusing on clinopyroxene include crystallization over a wide temperature range and during a large extent of magmatic differentiation. The volcanic rocks from Santiago and Fogo classify as basanite, tephrite, alkali basalt, nephelinite and melanepehlinite, with minor tephriphonolite occurring at Fogo. Whereas those from Brava and the Cadamosto Seamount are dominantly phonolite and phonotephrite combined with the presence of intrusive syenite at Brava (Figure 9; Barker et al., 2009, 2012; Hildner et al., 2011, 2012; Weidendorfer et al., 2016; Mata et al., 2017; Samrock et al., 2019).

Clinopyroxene from Santiago and Fogo classifies as diopside-augite, whereas Brava and the Cadamosto Seamount host both diopside-augite and green aegirine-augite (Barker et al., 2009, 2012; Hildner et al., 2011, 2012; Weidendorfer et al., 2016; Rydeblad, 2018). Clinopyroxene from Santiago and Fogo display compositions of dominantly 60 to 90 Mg# and 60 to 85 Mg# respectively (Figure 10; Mg# mol% = $(Mg/Mg + Fe^{total})$. The samples from Fogo also show minor abundances of clinopyroxene at 10 to 20 Mg# and 45 to 60 Mg#. Analysed clinopyroxene from Brava are dominantly aegirine-augite that display a much wider range of compositions from 5 to 65 Mg# (Figure 10). The nephelinites and ijolites host clinopyroxene with the highest frequency between 35 and 55 Mg#, whereas the syenites host clinopyroxene with 10 to 35 Mg# (Figure 10). The seven diopside-augite analyses have 45 to 65 Mg#. Clinopyroxene from the Cadamosto Seamount shows a skewed distribution with a range of 40 to 75 Mg# and mode at 40 to 55 Mg# (Figure 10). When the diopside-augite and aegirine-augite are distinguished, they range from 41 to 74 Mg# and 42 to 72 Mg# respectively (Figure 10). High Fe^{3+}/Fe^{total} observed for volcanic rocks from Cape Verde indicates crystallization under oxidizing conditions with high oxygen fugacity (Holm et al., 2006; Duprat et al., 2007; Mata et al., 2017). This may increase the Mg# of the clinopyroxene and would likely have a more significant effect as the iron content increases, thereby having the greatest influence on the clinopyroxene compositions from Brava and the Cadamosto Seamount (Freise et al., 2003). Additionally, the presence of häuyne and high sulphur contents in the Brava and Cadamosto Seamount samples would further contribute to higher Mg# contents in

clinopyroxene (Andújar et al., 2008; Barker et al., 2012; Weidendorfer et al., 2016). The clinopyroxene compositions reflect the overall composition of the volcanic centers with a restricted range of mafic volcanic rocks found at Santiago and Fogo with high clinopyroxene Mg#, therefore differentiation has played a limited role in these locations. At Brava and the Cadamosto Seamount the volcanic centers become more felsic with wider compositional ranges and lower clinopyroxene Mg#. Consequently, the clinopyroxene compositions exhibit wider ranges or skewed distributions recording the influence of extensive fractional crystallization.

More detailed examination of the mineral chemistry shows that clinopyroxene from Santiago and Fogo display increasing Al_2O_3, TiO_2 and low but increasing Na_2O and MnO with decreasing Mg# (Figure 11). In contrast, the clinopyroxene crystals from Brava and the Cadamosto Seamount form a different trend at low and decreasing Al_2O_3, TiO_2 with decreasing Mg#. The clinopyroxene crystals from Brava exhibit high Na_2O of 2.1 to 6.2 wt% compared to 0.3 to 1.3 wt% Na_2O in the clinopyroxene from Santiago and Fogo. At the Cadamosto Seamount Na_2O contents increase from diopside-augite with 0.8 to 2.7 wt% to the aegirine-augite population with Na_2O of 2.7 to 4.5 wt% (Figure 11). The MnO contents increase from 0.2 to 1.3 wt% in clinopyroxene with Mg# between 35 and 75 including all crystals from the Cadamosto Seamount (Figure 11). Clinopyroxene crystals with Mg# ≤35 from Brava show a decrease in MnO contents from 1.0 to 0.1 wt% as Mg# decreases (Figure 11).

The majority of the clinopyroxene crystals from Santiago and Fogo display strong correlations, with only a relatively small proportion of clinopyroxene from Fogo plotting at lower Mg# for given Al_2O_3 and TiO_2 contents (Figure 11). This suggests dominantly equilibrium growth during fractional crystallization of the magma and phenocryst formation (Mollo et al., 2013, 2018; Welsch et al., 2016). The extensive differentiation trends in the clinopyroxene chemistry and the liquid lines of descent observed in the whole rock geochemistry (Barker et al., 2009; Mata et al., 2017), suggest that equilibrium crystallization occurred during melt evolution (e.g. Mollo et al., 2018). Thus, much of the crystal population is in disequilibrium with the final host melt, and this disequilibrium is not homogenized by diffusion or mixing of magmas. Consequently, the erupted products host antecrysts crystallized under different conditions compared to the final melt compositions (e.g. Davidson et al., 2007; Barker et al., 2009; Mollo et al., 2013, 2018; Welsch et al., 2016). At Brava and the Cadamosto Seamount the clinopyroxene populations are more scattered illustrating greater compositional diversity. The equilibrium mineral-melt pairs indicate that the diopside-augite population grew in equilibrium with low Na_2O melts (<8 wt% Na_2O), whereas the host rocks have much higher Na_2O contents (8 to 14 wt% Na_2O; Barker et al., 2012; Weidendorfer et al., 2016). Therefore despite their similar compositions, the diopside-augite and aegirine-augite populations were likely aggregated from different melts (Figure 11).

Whole rock geochemistry for Santiago, Fogo and Brava confirms significant fractional crystallization. At Santiago the full range of compositions indicate a total of 24% fractional crystallization of predominantly clinopyroxene (Barker et al., 2009). The Fogo lavas record significant fractional crystallization to produce the basanites and tephrites, which requires crystallization of up to 21% clinopyroxene and minor olivine, Fe-Ti-oxides and apatite (Magnusson, 2016; Mata et al., 2017). Likewise, the magmatic system at Brava shows 15% olivine and 35% clinopyroxene crystallization, with subordinate Fe-Ti-oxides and apatite, which explains the ijolite and nephelinite compositions (Weidendorfer et al., 2016). Furthermore, a total of 90% fractional crystallization is required to produce the entire range of whole rock compositions (Weidendorfer et al., 2016). The lavas at Santiago and a few of those from Fogo display high MgO contents implying a role for aggregation of crystals (Barker et al., 2009; Magnusson, 2016; Mata et al., 2017). These accumulated crystals must have grown in very similar magmas following the liquid line of descent for clinopyroxene crystallization shown by their Mg# and Al_2O_3 content (Figure 11).

Now we consider zoning patterns in clinopyroxene crystals and the processes they reveal. Petrographically at Santiago we frequently observe patchy cores that are rounded by resorption. Apparent in this example the resorbed, patchy core passes into an area of concentric zonation, where oscillatory zoning emphasizes the different growth rates for different sectors of the crystal (Figure 12). The associated chemistry for the zoned clinopyroxene crystal from Santiago exhibits a plateau over the patchy core with only small variations. The outer oscillatory zonation displays trends of fractional crystallization with decreasing Mg# and MnO content simultaneous with increasing TiO_2 content (Figure 12; Streck, 2008). Additionally, at Santiago the oscillatory zonation records recharge events with increasing Mg# and MnO associated with a decrease in TiO_2 content. The behaviour of Mg# and MnO are also observed to be decoupled, which indicates the occurrence of magma mixing. The selected clinopyroxene crystal from Fogo also reveals a patchy core followed by two outer zones. The fractures highlight differences in resorption of the core. The zone surrounding the core shows oscillatory zoning and then passes into a relatively homogeneous rim (Figure 12). The patchy core shows small variations in Mg#, whereas the oscillatory zone exhibits large variations in Mg# and the rim shows homogeneously high Mg# (Figure 12). The variations in TiO_2 and MnO contents are not consistent with the variations in Mg#, therefore much of the variation cannot be attributed to fractional crystallization or recharge events. Instead the zonation records magma chamber dynamics associated with temperature and compositional differences causing convection and mixing (Figure 12; Streck, 2008; Rydeblad, 2018). The clinopyroxene crystal from the Cadmosto Seamount shows a resorbed core surrounded two concentric outer zones (Figure 12). The concentric zones are homogeneous and incongruent with curved boundaries. In the associated

chemical variations, we observe a decrease in both Mg# and TiO_2 in the outer zones of the crystal, reflecting differentiation in this felsic system (Figure 11, 12). The variation in MnO content in the outer zones, despite the decrease in Mg# suggests that MnO behaves differently in felsic alkali magmas than their mafic counter parts (Streck, 2008). However the offset in composition of Mg# and TiO_2 in the two outer zones and the change in MnO also points towards magma mixing or variations in thermal conditions of the magma (>32 μm; Figure 12). The small variations in the inner part of the crystal (<27 μm), reflect variations in magma chamber compositional and thermal conditions. The zonation and textures of clinopyroxene crystals from southern Cape Verde indicate that the host magmas were not homogeneous in composition or temperature. This is traced by significant differences in behaviour between the major cation species in the mineral structure such as MgO, FeO and CaO and the trace elements TiO_2, MnO and Al_2O_3. The latter record the chemical and thermal disequilibrium of the magma chamber (Mollo et al., 2013, 2018; Welsch et al., 2016).

Magma storage in southern Cape Verde

The volcanics at Cape Verde are highly alkaline, in contrast most thermobarometers for igneous minerals are calibrated for subalkaline tholeiitic and calc-alkaline systems (e.g. Nimis, 1995; Putirka, 2008, Neave & Putirka, 2017). The clinopyroxene thermobarometers that are appropriate for alkaline systems often target mafic and ultramafic compositions (Ashchepkov et al., 2011), and are thereby not suited to the range of differentiated compositions observed at Cape Verde. The only available clinopyroxene-melt thermobarometer that has been developed for evolved alkaline systems is calibrated for relatively high K/Na (Masotta et al., 2013). Unfortunately, the lavas from Cape Verde are highly enriched in Na, giving a low K/Na ratio and thus this formulation is not ideal for clinopyroxene from Cape Verde (Barker et al., 2012, 2019). The only thermobarometer that has been calibrated for a range of alkaline compositions, providing a method for intercomparison between all samples, is the clinopyroxene-melt equilibrium thermobarometer of Putirka (Putirka et al., 1996, 2003; Putirka 2008). The Putirka clinopyroxene-melt thermobarometer has been widely applied in many alkaline settings (e.g. Klügel et al., 2000, 2005, Nikogosian et al., 2002). It has also been shown to be consistent with independent depth estimates such as seismic tomography, seismic reflection profiles or earthquakes patterns (e.g. Longpré et al., 2014; Barker et al., 2019). Unfortunately the data used by Putirka (2008) for calibration of evolved alkali compositions is sparse and therefore also not ideal (Putirka et al., 1996, 2003; Putirka 2008). Hence, we compare the results from the models of Masotta with those of Putirka (Putirka et al., 1996, 2003; Putirka 2008; Masotta et al., 2013). Therefore, we employ models A and B for pressure and

418 temperature respectively from Putirka et al. (2003) for consistency with Hildner et al. (2011, 2012) and
419 additionally for the evolved compositions equations P-alk and T-alk from Masotta et al. (2013).

420 The clinopyroxene-melt thermobarometer is based upon jadeite (NaAl) and diopside-
421 hedenbergite (CaMgFe) exchange between clinopyroxene and melt for determination of temperature. The
422 corresponding pressure is estimated from the distribution of the jadeite component (NaAl) between
423 clinopyroxene and the equilibrium melt (Putirka, 2008). Employment of the clinopyroxene-melt
424 equilibrium thermobarometer thus requires demonstration of equilibrium between the clinopyroxene and
425 melt. There are two commonly used approaches to test for equilibrium. Firstly, testing for equilibrium
426 from Fe-Mg partitioning utilizing a Rhodes diagram, with Kd(Fe-Mg) of 0.275±0.067 (Putirka, 2008;
427 Barker et al., 2009, 2012). A second approach is to employ the variations between clinopyroxene
428 components as observed from the mineral chemistry and calculated from the melt composition (Putirka,
429 2008; Mollo et al., 2013). Typically, equilibrium is considered to be within ±0.06 DiHd, ±0.07 EnFs and
430 ±0.02 Jd of unity (Putirka, 1999). Mollo et al. (2013) proposed an additional multicomponent equilibrium
431 test, expressed as the difference between the DiHd component and tested on the alkaline compositions
432 characteristic of Mt. Etna. The multicomponent equilibrium test derives from a comparison between the
433 clinopyroxene components calculated from the equilibrium with the melt and directly from the
434 clinopyroxene composition.

435 Ideal mineral-melt pairs are considered to be analysis of groundmass glass and proximal crystal
436 rims. However it is rare to have much glass in lavas from Cape Verde, which tend to display a
437 microcrystalline groundmass (Barker et al., 2009, 2012; Hildner et al., 2011, 2012). Glassy melt
438 inclusions are typically modified during cooling of volcanic rocks and are therefore not suitable (Baker,
439 2008). Glass or groundmass separates would provide equilibrium melt compositions for crystal rims,
440 representing the final growth from the melt. Consequently, whole rock compositions that include minerals
441 and groundmass are more likely to represent core compositions (Barker et al., 2009). Employing the
442 whole rock composition of a sample as nominal melts for testing clinopyroxene-melt equilibrium is
443 therefore not only suitable but also necessary to understand the crystallization conditions of the entire
444 crystal population. Equilibrium between clinopyroxene and melt can be further optimized, by subtracting
445 the compositions of the modal mineral content from the whole rock composition (Barker et al., 2009).
446 Another approach to find an optimal equilibrium match between clinopyroxene and melt is to select
447 equilibrium melt compositions from a related suite of volcanic rocks (Barker et al., 2015; Neave &
448 Putirka, 2017). The minimum ΔDiHd for data from Santiago, Fogo, Brava and the Cadamosto Seamount
449 occurs at a temperature difference of 20ºC (Figure 13). The ΔDiHd ranges from +0.02 to +0.15,
450 meanwhile the temperature decreases to +0.4ºC at ΔDiHd of +0.03 and increases up to 75ºC as the ΔDiHd

increases to a maximum of +0.15. The multicomponent equilibrium appears to be equally good for evolved compositions such as at the Cadamosto Seamount as for the more mafic systems, for example Fogo.

Evaluation of the oxygen fugacity for the most recent eruptions at Fogo suggests fO_2 of +0.9 to +2.3 log ΔNNO with Fe^{3+}/Fe^{total} of 0.21 (Mata et al., 2017). These relatively oxidized conditions are confirmed by ultramafic xenoliths with fO_2 of up to +2.2 log ΔQFM (Ryabchikov et al., 1995). Other approaches have determined the Fe^{3+}/Fe^{total} to 0.19 to 0.26 at Santo Antão and São Nicolau (Holm et al., 2006; Duprat et al., 2007). Cape Verde like many Ocean Island Basalts is apparently relatively oxidized compare to Mid Ocean Ridge Basalts. Herzberg and Asimow (2008) calculate primary magma compositions for Ocean Island Basalts globally and find a range in Fe^{3+}/Fe^{total} of 0.15 to 0.25. Their findings are consistent with estimates of oxygen fugacity and Fe^{3+}/Fe^{total} at Cape Verde that represent relatively oxidized conditions. The influence of oxidation on the clinopyroxene compositions may impact the equilibrium especially that based on Mg# and clinopyroxene components that contain iron (Freise et al., 2003; Andújar et al., 2008). It is possible to vary Fe^{3+}/Fe^{total} in the thermobarometric modeling, and therefore we have adopted a Fe^{3+}/Fe^{total} of 0.21. However, the potential implications on the resulting crystallization conditions are unclear and the applicability of the calibration data to such oxidized conditions is also uncertain.

Conversion of pressure to depth has been performed with a crustal density of 2800 kg/m^3 for the mafic ocean crust (Barker et al., 2009, 2012; Hildner et al., 2011, 2012). Uncertainties associated with the experimental calibration data are ±33ºC and ±0.17 GPa (SEE; Putirka, 2008), which equates to depths of ±6 km. Hence, much of the range in pressure estimates described below are within error of the method (Figure 14).

Now turning to southern Cape Verde, the equilibrium clinopyroxene crystals from Santiago display compositions of 75 to 90 Mg#. These clinopyroxene crystals belong to alkaline basalts, basanites, tephrites and melanephelinites and are in equilibrium, ΔDiHd of 0.01 to 0.08, with compositions in the range of 52 to 65 Mg# (Figure 9, 13; Barker et al., 2009). The corresponding crystallization conditions are temperatures of 1165 to 1255ºC and pressures of 0.40 to 1.15 GPa (Figure 14; Barker et al., 2009).

From Fogo the clinopyroxene mineral chemistry shows the highest frequency compositions between 60 and 85 Mg# (Figure 10). The host rocks are tephrite, basanite, foidite and tephriphonolite and equilibrium, ΔDiHd of <0.12 and corresponding melt compositions for the main clinopyroxene population range between 30 and 54 Mg# (Figures 9 & 13; Hildner et al., 2011, 2012; Rydeblad, 2018). The resulting crystallization conditions are 1010 to 1255ºC and 0.45 to 1.35 GPa, which compare well

with existing data of 1010 to 1150ºC and 0.42 to 0.90 GPa for pre-eruptive magma storage conditions (Hildner et al., 2011, 2012; Mata et al., 2017). Mata et al. (2017) further divide the crystallization conditions for the 2014-2015 eruption at Fogo by host magma into 1045 to 1065ºC and 0.56 to 0.78 GPa for phonotephrites and 1100 to 1145ºC at 0.70 to 0.90 GPa for tephrites. This study extends the range of crystallization conditions to higher temperatures and pressures, thereby also characterizing the deeper part of the magma storage system (Figure 14; Hildner et al., 2011, 2012; Mata et al., 2017).

There are only a few analyses of diopside-augite from Brava that are hosted by nephelinite with Mg# 47 to 62 (Weidendorfer et al., 2016). They show equilibrium, ΔDiHd of 0.02 to 0.13, with low Na melt compositions of Mg# 20 to 32 (Figures 10 & 13). The Putirka et al. (2003) models estimate crystallization at 1170 to 1300ºC and 0.2 to 1.0 GPa (Figure 14). In comparison the Masotta et al. (2013) model indicates crystallization at lower temperatures of 930 to 980ºC and 0.29 to 0.67 GPa and shows less scatter than the estimate from Putirka et al. (2003).

Diopside-augite from the Cadamosto Seamount have 40 to 75 Mg# (Figure 10; Barker et al., 2012). The corresponding whole rocks are phonolite to phononephelinite and equilibrium melt compositions are 29 to 37 Mg# with ΔDiHd of 0.01 to 0.16 (Figures 9 & 13; Barker et al., 2012). The Putirka et al. (2003) model gives crystallization conditions of 970 to 1025ºC and 0.45 to 1.35 GPa, whereas the Masotta et al. (2013) model indicates 925 to 980ºC and 0.26 to 0.70 GPa (Figure 14). Hence the results from the Masotta et al (2013) model overlap with those estimated by the model of Putirka et al. (2003) and extend to lower temperature and pressure. These evolved magmas from Brava and the Cadamosto Seamount crystallized at lower temperatures compared to the clinopyroxene from Santiago and Fogo (Figure 14; Barker et al., 2012).

The clinopyroxene crystals feature significant zonation through which we track the magma chamber dynamics for samples from Fogo. Rapid decreases in clinopyroxene Mg# occur under several scenarios, sometimes with no discernable temperature or pressure changes, suggesting mixing processes (Figure 15a). A second scenario observed in the zonation is a rapid decrease in clinopyroxene Mg# with a decrease in temperature on the order of 30ºC and simultaneous decrease in pressure suggesting convection and ascent within the magma reservoir (Figure 15b). In contrast, rapid increase in clinopyroxene Mg# occurs with large variations in temperature (Figure 15b). This implies that the thermal and compositional gradients are not perfectly contemporaneous and that thermal and chemical mixing occur at different rates. Whereas there are also examples of gradual increase in clinopyroxene Mg# corresponding with slight increases in temperature and pressure (Figure 15c). In some places the outer

514 rims record a decrease in clinopyroxene Mg#, with simultaneous decreases in temperature and pressure
515 (Figure 15d), indicating magma evolution during ascent within the magma reservoir.

516 Integrating the thermobarometry from the different locations, we find that crystallization was in
517 the range of 12 to 40 km (Figure 14 & 16). Therefore, the magma storage beneath southern Cape Verde
518 occurs below the Moho in the oceanic lithospheric mantle. At Santiago and Fogo the highest frequency of
519 crystallization is at 30 to 40 km (Figure 16; Barker et al., 2009; Hildner et al., 2011, 2012; Rydeblad,
520 2018). We also observe in the samples from Fogo that the rims crystallize with highest frequency between
521 20 and 30 km and extend to lower pressures approaching the Moho (Figure 14). This suggests that the
522 more mafic magmas begin to crystallize clinopyroxene deep in the system and move upwards towards the
523 Moho as crystallization continues and zonation and final rim compositions progressively form (Figure
524 15d). Evolution of magma storage depths with differentiation is consistent with the increase in Al_2O_3
525 contents up to 13 wt% as MgO content decreases signaling magmatic differentiation and associated with
526 lower pressures of crystallization (Figure 11; Marianelli et al. 1999; Morgan et al., 2004). Hildner et al.
527 (2012) proposed that the pre-eruptive magma storage conditions become shallower with time in the
528 historic eruptions. However, no trends with time appear when we investigate the crystallization conditions
529 of the whole range of clinopyroxene compositions. The absence of systematic temporal variations is
530 confirmed by clinopyroxene from the 2014-2015 eruption recording pressures of 0.56 to 0.9 GPa, which
531 are deeper than for the 1995 and 1951 eruptions (Mata et al., 2017).

532 The dominance of the deep magma storage zone indicates that the magmatic processes of
533 differentiation, recharge, mixing and potentially convection recorded by the crystal populations take place
534 in this deep magma storage zone (Figures 12, 14 & 15). The accumulation of antecrysts and aggregation
535 of crystal populations is likely to also occur in this deep magma storage zone before magmas ascend and
536 erupt. Thus, the resorbed kaersutite crystals frequently found in lavas from Fogo probably crystallized in
537 the oceanic lithospheric mantle, consistent with amphibole thermobarometry yielding pressures of
538 approximately 0.6 GPa (Mata et al., 2017). Subsequently they would have been incorporated into magmas
539 with starkly different compositions leading to their break down (Hildner et al., 2011, 2012).

540

541 ***Controls on the depth of magma storage***

542 The location of the magma storage is controlled by the crustal structure beneath the South of the
543 Cape Verde archipelago. The islands and seamounts stand several kilometers above the seafloor at
544 approximately 4000 mbsl and beneath them is 1 to 2 km of sediments (Figure 2; Lancelot et al., 1978;

Pim et al., 2008). The sediments overlie relatively old 130-135 Ma Central Atlantic ocean crust which extends down to the Moho at depths of 12 to 18 km, that decrease from East to West (Ali et al., 2003; Lodge & Helffrich, 2006; Pim et al., 2008). Hence the deep mantle plume source generates magmas which ascend in to the oceanic lithospheric mantle where they stagnant below the mantle-crust boundary (Figure 16; Barker et al., 2009).

The density of the ocean islands and seamounts, as well as the ocean crust extending down to the crust mantle boundary at 12 to 18 km beneath Cape Verde is estimated to be 2.75 to 2.80 g/cm^3 (Ali et al., 2003; Lodge & Helffrich, 2006; Pim et al., 2008). The sediments would be expected to provide a low density layer between the mafic ocean crust and the Cape Verde islands and seamounts (Pim et al., 2008). The expected upper mantle density is 3.1 g/cm^3 (Tenzer et al., 2013). The density contrast between the upper mantle and the oceanic crust evidently controls the depth and pressures of magma storage (Figure 14 & 16). The basanite, tephrite and melanephelinite at Fogo and Santiago have calculated densities of 2.65 to 2.80 g/cm^3 (Bottinga & Weill, 1970; Bottinga et al., 1982). This range is similar to the mafic ocean crust and extends to slightly lower densities, therefore the mafic magmas would be expected to pool at the Moho or slowly ascend. However the actual density of magma is a function of both the melt density and the crystal cargo. Many of the erupted basanitic lavas have crystal contents of 5 to 20% and even more in ankaramite samples (Barker et al., 2009). Such crystal cargoes of dominantly clinopyroxene and olivine would increase the density of the magma, leading to a decrease in buoyancy and stagnation of the magma below the crust-mantle boundary.

Common magma storage depths, irrespective of magma composition and age are likely associated with significant magma intrusion, solidification and formation of crystal mush zones. This would serve to underplate the oceanic crust with mafic materials, building a magma storage zone of lower density than the surrounding upper mantle lithologies (Klügel et al., 2015). Evidence for this comes from Fogo lavas that host several cumulate nodules, containing olivine, clinopyroxene, kaersutite, spinel and phlogopite (Hildner et al., 2012). The spinel, kaersutite and phlogopite are consistent with crystallization in the oceanic lithospheric mantle. Therefore, these nodules are likely sampling cumulates formed in the deep magma storage zone. Furthermore, crustal thickening associated with underplating and potentially shallower intrusions contributes to localized uplift on individual islands, such as observed on Santiago and Brava (Madeira et al., 2010; Ramalho et al., 2010a, 2010b).

The phonolites and syenites at Brava and the Cadamosto Seamount have calculated densities of 2.35 to 2.48 g/cm^3 and even the clinopyroxene-equilibrium melts show densities of 2.45 to 2.48 g/cm^3, consistent with recent experimental constraints (Bottinga & Weill, 1970; Bottinga et al., 1982; Seifert et

al., 2013). Such densities for phonolitic magma carrying relatively low density minerals should promote magma buoyancy and ascent through the ocean crust. Although the viscosity of magma would also change during differentiation and influence the magma dynamics. The resulting increase in viscosity of the magma plus the entrained crystal population potentially inhibit magma ascent. Crystal contents of 40 to 50% cause the magma to behave as a rigid crystal network, trapping it in the magma storage zone (Cooper, 2017). The crystal content ranges from 10 to 50% for the Cadamosto Seamount, thus the crystal assemblages along with the magma evolution controls the viscosity and thereby promote continued magma storage in the upper oceanic lithospheric mantle (Barker et al., 2012).

The equilibrium clinopyroxene compositions at Brava and the Cadamosto Seamount are 45 to 75 Mg# with equilibrium melt densities of 2.45 to 2.48 g/cm^3 (Figure 10). However, it is likely that the host magma carrying the existing crystal cargo, would have continued to evolve with a corresponding density change to 2.35 g/cm^3. Such a change in density provides a larger density contrast between the mafic ocean crust and the most evolved phonolitic compositions that may have promoted magma ascent.

Insights into the shallower magmatic system

Evidence of magmatic processes occurring shallower in the crust at Cape Verde is limited. At the Cadamosto Seamount, the majority of the diopside-augite crystallization occurs below the Moho in the deep magma storage zone (Figure 16). However the magma differentiation and aegirine-augite crystallization is unaccounted for by this crystallization model. Furthermore, at the Cadamosto Seamount the $\delta^{18}O$ for clinopyroxene (diopside-augite) have mantle derived values of +5.3‰, whereas the feldspathoids show $\delta^{18}O$ of +6.3 to +7.1‰, elevated over the mantle equilibrium value of +6.25‰ ($\delta^{18}O$ SMOW; Zhao and Zheng 2003; Barker et al., 2012). Additionally the sulfur isotopes for whole rock powders gave $\delta^{34}S$ of +4.7 to +5.9‰, highly enriched compared to mantle values with $\delta^{34}S$ of +0.8 ± 0.2% (Sakai et al. 1984; Barker et al., 2012). Barker et al. (2012) interpreted these feldsapathoid and whole rock isotope signatures to be caused by assimilation of a few percent of oceanic sediments and anhydrite. Hence the magmas associated with the Cadamosto Seamount interact with the sediment crustal layer, which is likely located at 4 to 6 km below sea level (Figures 2 & 16; Lancelot et al., 1978; Pim et al., 2008). This evidence suggests that less differentiated magmas ascend from the deep magma storage zone and evolve to phonolitic compositions through assimilation during storage in the upper crust. Seismicity in the vicinity of the Cadamosto Seamount also records crustal magmatic activity at depths of 0.5 to 15 km, which is likely associated with shallow hydrothermal processes and slightly deeper volcano-tectonic events such as magma intrusion in the ocean crust (Figure 16; Grevemeyer et al., 2010). The

609 volcano-tectonics events provide evidence for crustal magma storage, consistent with assimilation of
610 sedimentary components by the magmas.

611 Brava hosts a carbonatite-silicate intrusive complex, where the silicate rock types are represented
612 by ijolite, nephelinite and nepheline syenite (Weidendorfer et al., 2016). Extreme fractional crystallization
613 takes place, up to 90%, which is reflected in the large range of clinopyroxene compositions of 5 to 65
614 Mg# (Figure 10). The presence of clinopyroxene from 3 to 90% fractional crystallization is consistent
615 with the wide range in clinopyroxene compositions (Figure 10). Significant crystallization may have
616 occurred in the deep magma storage zone (<30%; Weidendorfer et al., 2016), in the presence of olivine,
617 perovskite and magnetite as illustrated by the crystallization of clinopyroxene with Mg# 47 to 62 at and
618 below the Moho in the nephelinites from Brava (Figure 13). Given the challenges of mobilizing magmas
619 containing more than 40 to 50% crystals (Cooper, 2017), deep crystallization is likely followed by magma
620 ascent and intrusion into the upper crust beneath the volcanic edifice, where *in situ* differentiation and
621 crystallization continue. Thereby crystallizing the majority of the aegirine-augite and other phases of the
622 syenite in the ocean crust. Persistent and relatively shallow magma storage is required to provide the heat
623 source for the active geothermal system on Brava that contains a mixture of magmatic and biogenic gases
624 (Dionis et al., 2015a). Additionally, Brava is seismically active recording volcano-tectonic events at
625 depths of 2 to 10 km in the ocean crust and volcanic edifice (Figure 16; Faria & Fonseca, 2014). The
626 seismicity is consistent with continued magma differentiation in the volcanic edifice.

627 There is evidence for temporary magma storage at Fogo, associated with magma ascent and
628 eruption. Olivine and clinopyroxene hosted fluid inclusions from the eruptions in 1995 and 1951 re-
629 equilibrated at depths of 8 to 13 km (Figure 16; Hildner et al., 2011; 2012). Hildner et al. (2011, 2012)
630 report relatively rapid re-equilibration during stagnation at these lower crustal depths over timescales of
631 hours to days. Hence eruption related temporary magma pooling occurs in the lower ocean crust.
632 Seismicity associated with the 1995 eruption at Fogo locates depths of magma storage between 1 and 5
633 km in the volcanic edifice and oceanic crust (Figure 16; Da Silva et al., 1999). Additionally, the surface
634 deformation signals from the 1995 eruption have been explained by a 2 km deep magma source, fed from
635 a conduit that extends to depths of more than 16 km (Figure 16; Amelung and Day, 2002). Precursory
636 seismicity to the 2014 eruption commenced in early October before the eruption on 23rd November 2014
637 (Fernandes & Faria, 2015). The initial earthquakes were recorded at depths exceeding 15 km, associated
638 with the sub-Moho magma storage zone. On 22nd November the seismicity was dominated by high
639 frequency and magnitude long-period earthquakes at depths of 2 to 4 km (Fernandes & Faria, 2015;
640 Jenkins et al., 2017). The 2014/2015 surface deformation is consistent with a dike propagating vertically
641 from sub-Moho depths and arriving below Pico do Fogo where the magma flowed laterally towards the

642 Southwest before erupting (González et al., 2015). Therefore, the transient eruption related magma
643 pathways can be traced from the sub-Moho magma storage zone, through the lower ocean crust to the
644 magma pockets in the volcanic edifice feeding the magma to the eruption fissure.

645 Long-term magma storage in the crust is suggested by shallow seismicity and the sustained
646 geothermal system. Fogo hosts a geothermal system with typical temperatures of 90-100°C recorded at
647 degassing fumeroles and values up to 130 to 190°C reported in the months leading up to the 2014
648 eruption (Risby & Sandback 2014; Dionis et al., 2015b). The active degassing is composed of a mixture
649 between magmatic and biogenic-atmospheric gases (Dionis et al., 2015b). Shallow seismicity at depths of
650 300 to 400 m below the Chã das Caldeiras plateau are confirmed by drilling to correspond to the
651 geothermal system (Faria & Fonseca, 2014). This requires a relatively shallow long-term heat source to
652 sustain the geothermal activity, although it has not yet been detected by geophysical methods (Caranova
653 & Silva, 2012). The heat source may be associated with the volcano-tectonic earthquakes at depths of up
654 to 7 km, this would imply that these earthquakes are caused by magma intrusion (Faria & Fonseca, 2014).

655 This information of magma storage depths and magma ascent timescales provides vital
656 information to scientists at the Institute of National Meteorology and Geophysics and the University of
657 Cape Verde attempting to interpret seismicity, deformation and volcanic gas geochemistry. Thereby
658 contributing to the decision making and communication with the National Civil Protection of Cape Verde
659 in times of impending volcanic crisis (Faria & Fonsesa, 2014; Dionis et al., 2015a, b). Additional
660 information on the volcanic hazards offered by Earth science comes in the form of volcanic hazard maps.
661 Richter et al. (2016) have examined the probable pathways of lava flows following the 2014-2015
662 eruption. Their results suggest that the locations of Portela and Bandaeira continue to be a risk of future
663 lava flows.

664

665 ***Ocean Islands globally***

666 The southern chain of the Cape Verde hotspot therefore exhibits a predominantly deep magma
667 storage zone at depths of between 12 and 40 km traced by clinopyroxene thermobarometry, seismicity
668 and deformation (Figure 17). Magma ascent through the ocean crust is documented by fluid inclusions
669 and seismicity. Additionally, shallow crustal magma storage is found by seismicity and deformation in
670 the upper 5 km of the oceanic crust and volcanic edifice. Prior to the eruption in 2014/2015 seismicity
671 traced the magma ascent from below the Moho, through the crust to the upper crust in the months leading
672 up to the eruption (Fernandes & Faria, 2015; González et al., 2015; Jenkins et al., 2017).

673 A comparison with the Canary Islands, suggests that the clinopyroxene equilibrium
674 thermobarometry and seismicity also display similarly deep magma storage relative to a Moho depth of
675 13 to 15 km (Figure 17; Ranero et al., 1995). Gran Canaria records magma storage at 15 to 36 km below
676 the Moho with a subsidary zone at 3 to 4 km (Table 1; Aulinas et al., 2010). The island of Tenerife also
677 shows deep magma storage at 20 to 45 km (Longpré et al., 2008). Estimates for magma storage at La
678 Palma also range from 12 to 45 km placing the magma storage within the oceanic lithospheric mantle
679 (Klügel et al., 2000; 2005; Nikogosian et al., 2002; Galipp et al., 2006; Barker et al., 2015). Magma
680 storage for the 2011 eruption at El Hierro has been reported to occur at depths of 17 to 24 km consistent
681 with seismic activity (Longpré et al., 2014 and references therein). Fluid inclusions and deformation
682 suggest magma storage in the lower crust (Longpré et al., 2014). Additionally investigation of the
683 deformation places a magma storage zone in the upper crust (Figure 17). In the 2011 eruption offshore el
684 Hierro the seismicity migrated upwards and laterally tracking the movement of magma supplied from
685 sub-Moho magma storage through the crust to eruption at the seafloor (González et al., 2013).

686 At Madeira, magma storage from clinopyroxene equilibrium thermobarometry has been shown to
687 occur at depths of 15 to 35 km and therefore deep relative to Moho depths of 14 to 15 km (Figure 17;
688 Schwarz & Klügel 2004; Klügel and Klein, 2006). Furthermore, fluid inclusions record temporary
689 stagnation in the lower and upper crust (Schwarz & Klügel 2004; Klügel and Klein, 2006).

690 The Azores also record deep crystallization of clinopyroxene, olivine and plagioclase as well as
691 entrapment of primary fluid inclusions (Figure 17; Renzulli & Santi 2000; Beier et al., 2006; Dias et al.,
692 2007; Madureira et al., 2011; Zanon et al., 2013; Zanon & Pimentel 2015). In the lower crust magma
693 storage is recorded by continued crystallization of clinopyroxene, along with fluid inclusion equilibration
694 and the appearance of seismicity (Renzulli & Santi 2000; Beier et al., 2006; Dias et al., 2007; Silva et al
695 2012; Madureira et al., 2011; Zanon et al., 2013; Zanon & Pimentel 2015). A shallow crustal magma
696 pocket is picked out by seismicity, water solubility and plagioclase-olivine experimental phase petrology
697 (Renzulli & Santi 2000; Silva et al 2012; Jeffery et al., 2016).

698 Clinopyroxene crystallization in basanites traces magma storage at Tristan da Cunha to the
699 oceanic mantle lithosphere and for more evolved trachyandesite to the middle of the ocean crust (Figure
700 17; Weit et al., 2017). Earthquakes were felt on Tristan da Cunha commencing several months prior to the
701 eruption in 1961 and again associated with the nearby submarine eruption in 2004 (O'Mangain et al.,
702 2007). These earthquakes showed high signal to noise ratios on the nearest seismometers, thus the
703 earthquakes were deemed to have shallow epicenters and the seismicity was employed to locate the
704 eruption to 40 to 50 km South of Tristan da Cunha (O'Mangain et al., 2007).

Information for the magma storage system at Ascension is derived from melt inclusions, placing stagnation in the lower crust (Figure 17; Chamberlain et al., 2016). Additionally, seismic data suggests volcano-tectonic events some of which occur in the shallow crust of the Ascension rift zone (Hanson et al., 1996).

In the Pacific Ocean, the two hotspots with records of magma plumbing systematics are Hawaii and the Galapagos. Investigations at Hawaii record clinopyroxene crystallization in the oceanic lithosphere and through to the lower crust (Figure 17; Putirka et al. 1996; Putirka 1997; Chatterjee et al., 2005; Hammer et al., 2016). Whereas seismicity occurs in the upper crust beneath the central volcanoes and extends into the middle crust at rift zones (Poland et al., 2015). Wolf island in the Galapagos shows clinopyroxene crystallization in the lower crust (Stock et al., 2018). Lower crustal magma storage is confirmed by deformation, which places magma storage at 6 to 9 km depth as well as in the volcanic edifice at approximately 1 km (Stock et al., 2018).

Reunion hotspot in the Indian Ocean hosts Piton de la Fournaise volcano, which frequently displays volcanic activity, including an eruption in 2007. Magma storage at the Moho and below is traced by seismicity, as well as melt inclusions and volatile solubility which extend to much greater depths (Figure 17; Bureau et al., 1998; Peltier et al. 2009; Di Muro et al., 2014). Mid-crustal magma stagnation is indicated by melt inclusions and seismicity (Bureau et al., 1998; Peltier et al. 2009), whereas shallow magma storage below the volcanic edifice is shown by fluid inclusions, volatile solubility and seismicity above a deformation center (Figure 17; Famin et al., 2009; Peltier et al. 2009; Di Muro et al., 2014; Fontaine et al., 2014). Notably for the 2007 eruption at Piton de la Fournaise volcano, the seismicity started shallow and penetrated downwards with time, as the eruption was fed from progressively deeper (Massin et al., 2011).

Studies of the magma plumbing system associated with the volcanic islands of the Kerguelen archipelago are scarce. Partly due to their inaccessibility and relatively evolved character often hosting phonolites (e.g. Quilty & Wheller, 2000; Freise et al., 2003). However several islands seem to be volcanically active, as observed by passing vessels on long Ocean voyages (Quilty & Wheller, 2000). Volcanic eruptions have been reported from Heard Island in 1910, 1948 to 1954, 1985 to 1987 and 1996, whilst a submarine eruption likely occurred in 1992. An eruption was reported from McDonald Island in 1997 and satellite images show evidence for an eruption in 2001 (Quilty & Wheller, 2000; Wunderman, 2003; Stephenson et al., 2005). The only constraints on the magma storage suggest mid-crustal magma evolution of phonolitic magmas based on experimental petrology (Figure 17; Freise et al., 2003). Given the recent history of eruptions in the Kerguelen archipelago and potential hazard for shipping, we

737 recommend detailed investigation into the magma storage system. Sample material exists from several of
738 the islands that can be used for petrological investigation (Barling et al., 1994; Freise et al., 2003) and
739 InSAR would provide useful insights into the shallow magma storage system without the need for an
740 expedition or deployment of equipment.

741 This comparison shows that deep magma storage is common to Ocean Islands, however the
742 shallow crustal magma storage systems vary considerably and are therefore likely controlled by local
743 factors opposed to the tectonic setting (Figure 17). Magma storage in the crust may be controlled by
744 density differences such as the transition between the ocean crust and sediments, the presence of which
745 will vary depending on the supply of sedimentary materials to the Ocean Islands. Sedimentary layers
746 provide a low density zone between the mafic ocean crust and the base of the volcano, hence creating an
747 opportunity for magmas to stall. Evidence for magma-sediment interaction is observed in lavas from Cape
748 Verde and seismicity, plus intrusions at this level likely contribute to local uplift at Santiago and Brava
749 (Da Silva et al., 1999; Ramalho et al., 2010a, 2010b; Barker et al., 2012; Fernandes & Faria, 2015).
750 Magmas stalling deeper in ocean crust may be influenced by the gabbro-dike or lava-dike transitions,
751 where porosity and permeability change. Additionally at these contacts, the ocean crust changes from
752 massive gabbro to vertically aligned dikes and then to horizontal lava flows and random orientations of
753 pillow lavas in the volcanic pile. Such changes potentially modifying the relationship between the magma
754 and crust, leading to readjustment of magma flow. The characteristics of magmatic conduits will also
755 influence magma ascent, with high permeability associated with fractures or faults aiding direct magma
756 ascent, whereas sealing of previous pathways may enforce stalling of magma. Some Ocean Islands, such
757 as Tenerife, Canary Islands have well developed rift zones, which may promote magma ascent (Carracedo
758 et al., 2007). The regional fracture zones that potentially control the alignment of volcanic islands in Cape
759 Verde likely provide effective pathways for magma ascent (Klerkx et al., 1974; Le Pichon and Fox, 1971;
760 Jacobi and Hayes, 1982). Furthermore, magmatic properties may also influence magma dynamics on
761 ascent through the crust, with magma buoyancy affected by density contrasts with the wall rock as well as
762 viscosity associated with the crystal cargo and magma composition (Bottinga & Weill, 1970; Bottinga et
763 al., 1982; Seifert et al., 2013; Cooper, 2017). This may explain storage of mafic magmas in the lower
764 crust, as the magma density may have changed just enough for magma to ascend above the Moho and
765 then stall in the lower crust where a similar density is encountered.

766

767

768

Conclusions and recommendations

Globally at Ocean Islands, we observe that clinopyroxene crystallization tends to occur deep in the magmatic system; in the oceanic lithosphere and sometimes up into the lower crust. Therefore, clinopyroxene captures the magmatic processes and magma storage that occur deep in these relatively mafic volcanic islands. Recent, well monitored eruptions of Fogo, Cape Verde (2014-2015) and el Hierro, Canary Islands (2011) have been fed from deep magma storage zones and seismicity traced the ascent of magma through the crust to the eruption site (González et al., 2013, 2015). In contrast the eruption at Piton de la Fournaise, Reunion (2007) appears to have started with fracturing of the shallow magma storage zone followed by magma ascent from progressively deeper to feed the ongoing eruption (Massin et al., 2011).

Therefore, knowledge of the deep magma storage system from clinopyroxene crystallization is appropriate for volcanoes where eruptions are fed from deep magma chambers, allowing monitoring teams to interpret enhanced deep seismicity. However for others such as Piton de la Fournaise it is essential to understand the shallow magma storage system. The presence of such long-lived shallow magmatic systems may influence the eruption style, therefore the presence or absence of protracted shallow magma storage may be a useful indicator of likely eruptive behaviour. To investigate the temporary as well as long-term shallow magma storage zones a combination of methods is recommended. Petrological methods that lend themselves to investigating the shallower magmatic system are water solubility, experimental studies, glassy melt inclusions and to some extent fluid inclusions depending on the timescales available for re-equilibration (Renzulli & Santi 2000; Freise et al., 2003; Famin et al., 2009; Zanon et al., 2013; Di Muro et al., 2014; Jeffery et al., 2016). Ideally seismicity and deformation data are used both for developing models of the magma storage system as well as real-time monitoring (Magee et al., 2018).

Investigation of timescales of magmatic processes that provide indications of typical timescales for magma ascent from a magma storage zone to eruption are also important. Such indications may be assessed on a case by case basis from the extent of re-equilibration of fluid inclusions (Hildner et al., 2011, 2012). Further information about magmatic timescales that may give insights into the magma ascent processes involved in volcanic eruptions may be gleaned by exploring diffusion between compositional zones within crystals. An example of olivine diffusion chronometry from Fogo, Cape Verde suggests rapid ascent of magmas and corresponding eruption on the order of 3 to 12 hours (Hildner et al., 2011). We recommend integration of all types of petrological data to provide indications of magmatic processes and their location and timescales with geophysical methods such as seismicity to

track magma storage and transport as well as InSAR and geodetics to reveal deformation patterns and assess source location and geometry (Magee et al., 2018).

Acknowledgements

We are particularly grateful to the editors Matteo Massotta, Silvio Mollo and Christoph Beier, for the invitation to contribute to this volume and their professional editorial handling. We are grateful to Andreas Klügel, David Neave and Ricardo Ramalho for constructive reviews that helped improve this contribution.

References:

Ali, M.Y., Watts, A.B. and Hill, I., 2003. Structure of Mesozoic oceanic crust in the vicinity of the Cape Verde Islands from seismic reflection profiles. Marine Geophysical Researches, 24(3-4): 329-343.

Ali, M.Y., and Watts, A.B., (2003). A seismic reflection profile study of lithospheric flexure in the vicinity of the Cape Verde Islands. *Journal of Geophysical Research* **108(B5)**: 2239-2263.

Amelung, F., & Day, S. (2002). InSAR observations of the 1995 Fogo, Cape Verde, eruption: Implications for the effects of collapse events upon island volcanoes. *Geophysical Research Letters*, *29*(12), 47-1.

Andújar, J., Costa, F., Martí, J., Wolff, J.A. and Carroll, M.R., (2008). Experimental constraints on pre-eruptive conditions of phonolitic magma from the caldera-forming El Abrigo eruption, Tenerife (Canary Islands). *Chemical Geology*, *257*(3-4), pp.173-191.

Ashchepkov, I.V.; André, L.; Downes, H.; Belyatsky, B.A. (2011) Pyroxenites and megacrysts from Vitim picrite-basalts (Russia): Polybaric fractionation of rising melts in the mantle? *J. Asian Earth Sci. 42*, 14–37.

Assunção CFT, Machado F, Gomes RAD (1965) On the occurrence of carbonatites in the Cape Verde Islands. Boletim da Sociedade Geológica de Portugal 16:179–188

Aulinas M, Gimeno D, Fernandez-Turiel JL, Pérez-Torrado FJ, Rodriguez- González A, Gasperini D (2010) The Plio-Quaternary magmatic feeding system beneath Gran Canaria (Canary Islands, Spain): constraints from thermobarometric studies. Journal of the Geological Society 167:785-801.

Baker, D.R. (2008) The fidelity of melt inclusions as records of melt composition. *Contrib. Mineral. Petrol. 156*, 377–395.

831 Barker, A.K., Nilsson, D., Hansteen, T., (2019). Unravelling the crustal architecture of Cape Verde; the xenolith
832 record. Submitted to Special Issue: Mineral Textural and Compositional Variations as a Tool for Understanding
833 Magmatic Processes editor: Silvio Mollo Minerals, 9(2), 90.

834 Barker, A.K., Troll, V.R., Carracedo, J.C., Nicholls, P., (2015). The magma plumbing system for the 1971 Tenguía
835 eruption, La Palma, Canary Islands. Contrib Mineral Petrol 170(5) doi: 10.1007/s00410-015-1207-7

836 Barker, A.K., Troll, V.R., Ellam, R.M., Hansteen, T.H., Harris, C., Stillman, C.J., Andersson, A., (2012), Magmatic
837 evolution of the Cadamosto Seamount, Cape Verde: Beyond the spatial extent of EM1. Contributions to Mineralogy
838 and Petrology163, 949-965. doi: 10.1007/s00410-011-0708-2.

839 Barker, A.K., Holm, P.M., Peate, D.W., & Baker, J.A., (2010), A five million year record of compositional
840 variations in mantle sources to magmatism on Santiago, southern Cape Verde archipelago. Contributions to
841 Mineralogy and Petrology doi: 10.1007/s00410-009-0470-x

842 Barker, A., Holm, P., Peate, D. & Baker, J., (2009). A 5 million year record of compositional variations in mantle
843 sources to magmatism on Santiago, southern Cape Verde archipelago. Mineralogy & Petrology, 160: 33-154.

844 Barling, J., Goldstein, S. L., & Nucholls, I. A. (1994). Geochemistry of Heard Island (southern Indian Ocean):
845 characterization of an enriched mantle component and implications for enrichment of the sub-Indian Ocean mantle.
846 *Journal of Petrology*, *35*(4), 1017-1053.

847 Barrancos, J., Dionis, S., Quevedo, R., Fernandes, P., Rodríguez, F., Pérez, N., Silva, S., Cardoso, N., Hernández,
848 P., Melián, G., Padrón, E., Padilla, G., Asensio-Ramos, M., Calvo, D., Semedo, H. & Alfama, V., (2015). Sulphur
849 dioxide (SO2) emissions during the 2014-15 Fogo eruption, Cape Verde. Geophysical Research Abstracts Vol. 17,
850 2015. EGU General Assembly 2015.

851 Bebiano, J., (1932). A geologia do Arquipélago de Cabo Verde, Comunicações dos Serviços Geológicos de
852 Portugal, (18), 167–187.

853 Beier, C., Haase, K.M. and Hansteen, T.H., (2006). Magma evolution of the Sete Cidades volcano, São Miguel,
854 Azores. *Journal of Petrology*, *47*(7), pp.1375-1411.
855

856 Bernard-Griffiths, J., Cantagrel, J.-M., Alves, C., Mendes, F., Serralheiro, A., & Macedo, J., (1975).
857 Geochronologie: Donnés radiometriques potassium-argon sur quelques formations magmatiques des îlles de
858 l'archipel du Cap Vert, C. R. Seances Acad. Sci. Ser. D., 280, 2429–2432.

859 Bottinga, Y., & Weill, D. F. (1970). Densities of liquid silicate systems calculated from partial molar volumes of
860 oxide components. *American Journal of Science*, *269*(2), 169-182.
861
862 Bottinga, Y., Weill, D., & Richet, P. (1982). Density calculations for silicate liquids. I. Revised method for
863 aluminosilicate compositions. *Geochimica et Cosmochimica Acta*, *46*(6), 909-919.
864

Brown, M. C., Singer, B. S., Knudsen, M. F., Jicha, B. R., Finnes, E., & Feinberg, J. M. (2009). No evidence for brunhes age excursions, santo antão, cape verde. *Earth and Planetary Science Letters*, *287*(1-2), 100-115.

Bureau, H., Pineau, F., Me¤ trich, N., Semet, M. P. & Javoy, M. (1998). A melt and fluid inclusion study of the gas phase at Piton de la Fournaise volcano (Reunion Island). Chemical Geology 147, 115-130.

Caranova, R., & Silva, R. P. (2012) Geothermal resource assessment in volcanic islands-Fogo Island, Cape Verde.

Carracedo, J-C., Perez-Torrado, F., Rodriguez- Gonzalez, A., Paris, R., Troll, V.R., Barker, A.K. (2015) Volcanic and structural evolution of Pico do Fogo, Cape Verde. Geology Today 31 (4), 146-152. 10.1111/gto.12101

Carracedo, J.C., Rodríguez Badiola, E., Guillou, H., Paterne, M., Scaillet, S., Pérez Torrado, F.J., Paris, R., Fra-Paleo, U., Hansen, A., (2007). Eruptive and structural history of Teide volcano and rift zones of Tenerife, Canary Islands. Geological Society of America Bulletin 19, 1027–1051. http://dx.doi.org/10.1130/B26087.1.

Cazenave, A., Dominh, K., Rabinowicz, M., & Ceuleneer, G. (1988). Geoid and depth anomalies over ocean swells and troughs: evidence of an increasing trend of the geoid to depth ratio with age of plate. *Journal of Geophysical Research: Solid Earth*, *93*(B7), 8064-8077.

Chamberlain, K.J., Barclay, J., Preece, K., Brown, R.J. and Davidson, J.P., (2016). Origin and evolution of silicic magmas at ocean islands: Perspectives from a zoned fall deposit on Ascension Island, South Atlantic. Journal of Volcanology and Geothermal Research, 327, pp.349-360.

Chatterjee, N., Bhattacharji, S. and Fein, C., (2005). Depth of alkalic magma reservoirs below Kolekole cinder cone, Southwest rift zone, East Maui, Hawaii. Journal of Volcanology and Geothermal Research, 145(1-2), pp.1-22.

Cooper, K. M. (2017). What does a magma reservoir look like? The “crystal's-eye” view. *Elements*, *13*(1), 23-28.

Courtney, R. C. & White, R.S. (1986). Anomalous heatflow and geoid across the Cape Verde Rise: Evidence for dynamic support from a thermal plume in the mantle. *Geophysical Journal of the Royal Astronomical Society*. **87**: 815-867.

Crough, S. (1982). Geoid height anomalies over the Cape Verde Rise. Marine Geophysical Researches, 5, 263–271.

Da Silva, S.H., Day, S.J. and Fonseca, J.F.B.D., (1999). Fogo Volcano, Cape Verde Islands: seismicity-derived constraints on the mechanism of the 1995 eruption. Journal of volcanology and geothermal research, 94(1-4), pp.219-231.

Dash, P., Ball, M.M., King G.A., Butler, L.W. and Rona, P.A. (1976). Geophysical investigation of the Cape Verde Archipelago. *Journal of Geophysical Research* **81(29)**: 5249-5259.

Davidson, J. P., Morgan, D. J., & Charlier, B. L. (2007). Isotopic microsampling of magmatic rocks. *Elements*, *3*(4), 253-259.

Davies, G., Norry, M., Gerlach, D. & Cliff, R., (1989). A combined chemical and Pb.Sr.Nd isotope study of the Azores and Cape Verde hot spots, the geodynamic implications. In: Saunders, A.D. & Norry, M.J. (eds) Magmatism in the Ocean Basins. Geological Society, Special Publications, London 42, pp. 231-255.

Day, S., Heleno, S. & Fonseca, J., (1999). A past giant lateral collapse and present day flank instability of Fogo, Cape Verde Islands. Journal of Volcanology and Geothermal Research, 94: pp. 191-218.

De Paepe, P.D., Klerkx, J., Hertogen, J. & Plinke, P., (1974). Oceanic tholeiites on Cape Verde Islands - petrochemical and geochemical evidence. Earth and Planetary Science Letters, 22(4): 347-354.

Di Muro, A., Métrich, N., Vergani, D., Rosi, M., Armienti, P., Fougeroux, T., Deloule, E., Arienzo, I., & Civetta, L. (2014). The shallow plumbing system of Piton de la Fournaise Volcano (La Reunion Island, Indian Ocean) revealed by the major 2007 caldera-forming eruption. *Journal of Petrology*, *55*(7), 1287-1315.

Dias, N.A., Matias, L., Lourenço, N., Madeira, J., Carrilho, F. and Gaspar, J.L., (2007). Crustal seismic velocity structure near Faial and Pico Islands (AZORES), from local earthquake tomography. *Tectonophysics*, *445*(3-4), pp.301-317.

Dionis, D., Melián, G., Rodríguez, R., Hernández, P., Padrón,E., Pérez, N., Barrancos, B., Padilla, G., Sumino, H., Fernandes, P., Bandomo,Z., Victória, S., Pereira, J. & Semedo, H., (2015b). Diffuse volcanic gas emission and thermal energy release from the summit crater of Pico do Fogo, Cape Verde. Bulletin of Volcanology. Bull Volcanol. 77:10.

Dionis, S., Pérez, N., Hernández, P., Melián,G., Rodríguez, F., Padrón, E., Sumino, H., Barrrancos, J., Padilla, G., Fernandes, P., Bandomo, Z., Silva, S., Pereira J. & Semedo, H. (2015a) Diffuse CO_2 degassing and volcanic activity at Cape Verde islands, West Africa. Earth, Planets and Space 67:48.

Doucelance, R., Escrig, S., Moreira, M., Gariépy, C. and Kurz, M. D., (2003). Pb-Sr-He isotope and trace element geochemistry of the Cape Verde Archipelago.Geochimica et Cosmochimica Acta, 67(19), 3717-3733.

Duprat, H., Friis, J., Holm, P., Grandvuinet, T., & Sørensen, R., (2007). The volcanic and geochemical development of São Nicolau, Cape Verde Islands: Constraints from field and 40Ar/39Ar evidence, Journal of Volcanology and Geothermal Research, 162(1-2), 1 – 19.

Dyhr CT, Holm PM (2010) A volcanological and geochemical investigation of Boa Vista, Cape Verde Islands; 40Ar/39Ar geochronology and field constraints. J Volcanol Geotherm Res 189:19–32

Efimov, V. N., & Skolotnev, S. G. (2006). New data on the structure of sedimentary cover at the Cape Verde Seamount and the Cape Verde Basin (central Atlantic) based on continuous seismic profiling data. In *Doklady earth sciences* (Vol. 407, No. 2, pp. 376-380). MAIK Nauka/Interperiodica.

Egloff, J. (1972). Morphology of ocean basin seaward of northwest Africa: Canary Islands to Monrovia, Liberia. *AAPG Bulletin*, *56*(4), 694-706.

Eisele, S., Reißig, S., Freundt, A., Kutterolf, S., Nürnberg, D., Wang, K. L., & Kwasnitschka, T. (2015). Pleistocene to Holocene offshore tephrostratigraphy of highly explosive eruptions from the southwestern Cape Verde Archipelago. Marine Geology, 369, 233-250.

Elsworth, D., & Day, S. J. (1999). Flank collapse triggered by intrusion: the Canarian and Cape Verde Archipelagoes. Journal of Volcanology and Geothermal Research, 94(1-4), 323-340.

Famin, V., Welsch, B., Okumura, S., Bachèlery, P., & Nakashima, S. (2009). Three differentiation stages of a single magma at Piton de la Fournaise volcano (Reunion hot spot). *Geochemistry, Geophysics, Geosystems*, *10*(1).

Faria, B. & Fonseca, J.F.B.D. (2014). Investigating volcanic hazard in Cape Verde Islands through geophysical monitoring: network description and first results. Natural Hazards and Earth System Sciences, v.14, pp.485–494.

Faria, B. (2010) Monitorização Geofísica do Vulcão do Fogo e Níveis de Alerta, Ph.D thesis, Universidade Técnica de Lisboa, (in Portuguese).

Faugères, J., Legigan, P., Maillet, N., and Latouche, C., (1989), Pelagic, turbiditic, and contouritic sequential deposits on the Cape Verde Plateau (Leg 108, Site 659, Northwest Africa): Sediment record during Neogene time: Proceedings of the Ocean Drilling Program, Scientific Results, v. 108, p. 311–327.

Fernandes, R., & Faria, B. (2015). FOGO-2014: monitoring the Fogo 2014 eruption, Cape Verde. In EGU General Assembly Conference Abstracts Vol. 17 id.12709

Foeken, J., Day, S., & Stuart, F., (2009). Cosmogenic 3He exposure dating of the Quaternary basalts from Fogo, Cape Verdes: Implications for rift zone and magmatic reorganisation, Quaternary Geochronology, 4(1), 37–49.

Fonseca, J. F., Faria, B. V., Lima, N. P., Heleno, S. I., Lazaro, C., d'Oreye, N. F., Ferreira, A.M.G, Barros, I.J.M., Santos, P., Bandomo, Z., Day, S. J., Osorio, J.P., Baio, M., Matis, J.L.G (2003). Multiparameter monitoring of Fogo Island, Cape Verde, for volcanic risk mitigation. *Journal of volcanology and geothermal research*, *125*(1-2), 39-56.

Fontaine, F. R., Roult, G., Michon, L., Barruol, G., & Muro, A. D. (2014). The 2007 eruptions and caldera collapse of the Piton de la Fournaise volcano (La Réunion Island) from tilt analysis at a single very broadband seismic station. *Geophysical Research Letters*, *41*(8), 2803-2811.

Freise, M., Holtz, F., Koepke, J., Scoates, J. and Leyrit, H., (2003). Experimental constraints on the storage conditions of phonolites from the Kerguelen Archipelago. Contributions to Mineralogy and Petrology, 145(6), pp.659-672.

Galipp K, Klügel A, Hansteen TH (2006) Changing depths of magma fractionation and stagnation during the evolution of an oceanic island volcano: La Palma (Canary Islands). Journal Volcanol Geotherm Res 155:285–306

Geiger, H., Barker, A.K., Troll, V.R., (2016). Locating the depth of magma supply for volcanic eruptions, insights from Mt. Cameroon. *Sci. Rep.* **6,** 33629; doi: 10.1038/srep33629

Geissler, W.H., Jokat, W., Jegen, M., Baba, K., (2016). Thickness of the oceanic crust and the mantle transition zone in the vicinity of the Tristan da Cunha hot spot estimated from ocean-bottom and ocean-island seismometer receiver functions. Tectophysics this volume.

Gerlach, D.C., Cliff, R.A., Davies, G.R., Norry, M. and Hodgson, N., (1988). Magma sources of the Cape-Verdes Archipelago - isotopic and trace-element constraints. Geochimica Et Cosmochimica Acta, 52(12): 2979-2992.

González, P. J., Bagnardi, M., Hooper, A. J., Larsen, Y., Marinkovic, P., Samsonov, S. V., & Wright, T. J. (2015). The 2014–2015 eruption of Fogo volcano: Geodetic modeling of Sentinel- 1 TOPS interferometry. *Geophysical research letters*, *42*(21), 9239-9246.

González, P.J., Samsonov, S.V., Pepe, S., Tiampo, K.F., Tizzani, P., Casu, F., Fernández, J., Camacho, A.G. and Sansosti, E., (2013). Magma storage and migration associated with the 2011–2012 El Hierro eruption: implications for crustal magmatic systems at oceanic island volcanoes. Journal of Geophysical Research: Solid Earth, 118(8), pp.4361-4377.

Grevemeyer I, Helffrich G, Faria B, Booth-Rea G, Schnabel M, Weinrebe RW (2010) Seismic activity at Cadamosto seamount near Fogo Island, Cape Verdes—formation of a new ocean island? Geophys J Int 180:552–558. doi:10.1111/j.1365-246X. 2009.04440.x

Gudmundsson, A. (2012). Magma chambers: Formation, local stresses, excess pressures, and compartments. *Journal of Volcanology and Geothermal Research*, *237*, 19-41.

Hammer, J., Jacob, S., Welsch, B., Hellebrand, E. and Sinton, J., (2016). Clinopyroxene in postshield Haleakala ankaramite: 1. Efficacy of thermobarometry. Contributions to Mineralogy and Petrology, 171(1), p.7.

Hanson, J. A., Given, H. K., & Berger, J. (1996). Earthquake activity near Ascension Island, South Atlantic Ocean, as seen by a combined seismic/hydrophone array. *Geothermics*, *25*(4-5), 507-519.

Hansteen, T., Kwasnitschka, T., Klügel, A., (2014). Cape Verde Seamounts - Cruise No. M80/3: December 29, 2009 - February 1, 2010 - Dakar (Senegal) - Las Palmas de Gran Canaria (Spain). DFG-Senatskommission für Ozeanographie, Bremen, 1–42. doi:10.2312/cr_m80_3, 42 pp.

Hayes, D. E. and Rabinowitz, P. D., (1975), Mesozoic Magnetic Lineations and the Magnetic Quiet Zone off Northwest Africa, *Earth Planet. Sci. Lett.* **28**, 105–115.

Heleno, S.I.N., Faria, B.V.E., Bandomo, Z. & Fonseca, J.F.B.D., (2006). Observations of high-frequency harmonic tremor in Fogo, Cape Verde Islands, *J. Volc. Geotherm. Res.*, **158,** 361–379.

Herzberg, C.; Asimow, P. D. (2008) Petrology of some oceanic island basalts: PRIMELT2. XLS software for primary magma calculation. *Geochemistry, Geophysics, Geosystems*, *9*(9).

Hildner, E.; Klügel, A.; Hansteen, T. (2012) Barometry of lavas from the 1951 eruption of Fogo, Cape Verde Islands: Implications for historic and prehistoric magma plumbing systems. Journal of Volcanology and Geothermal Research 217-218 73–90.

Hildner, E.; Klügel, A.; Hauff F. (2011) Magma storage and ascent during the 1995 eruption of Fogo, Cape Verde archipelago. *Contributions to Mineralogy and Petrology*, *162*, 751-772, doi:10.1007/s00410-011-0623-6.

Hoernle K. Tilton G, Le Bas MJ, Duggen S, Garbe-Schönberg D (2002) Geochemistry of oceanic carbonatites compared with continental carbonatites: mantle recycling of oceanic crustal carbonate. Contributions to Mineralogy and Petrology, 142(5), 520-542.

Holm, P. M., Grandvuinet, T., Friis, J., Wilson, J. R., Barker, A. K. and Plesner, S., (2008). An 40Ar/39Ar study of the Cape Verde hot spot: Temporal evolution in a semistationary plate environment. Journal of Geophysical Research: Solid Earth (1978 – 2012), 113 (B8).

Holm, P.M.; Wilson, J.R.; Christensen, B.P.; Hansen, L.; Hansen, S.L.; Hein, K.H.; Mortensen, A.K.; Pedersen, R.; Plesner, S.; Runge, M.K. (2006) Sampling the Cape Verde mantle plume: Evolution of melt compositions on Santo Antão, Cape Verde Islands. *Journal of Petrology*, *47*, 145-189.

Jacobi, R. D., & Hayes, D. E. (1982). Bathymetry, microphysiography and reflectivity characteristics of the West African margin between Sierra Leone and Mauritania. In *Geology of the Northwest African continental margin* (pp. 182-212). Springer, Berlin, Heidelberg.

Jeffery, A. J., Gertisser, R., O'Driscoll, B., Pacheco, J. M., Whitley, S., Pimentel, A., & Self, S. (2016). Temporal evolution of a post-caldera, mildly peralkaline magmatic system: Furnas volcano, São Miguel, Azores. *Contributions to Mineralogy and Petrology*, *171*(5), 42.

Jenkins, S. F., Day, S. J., Faria, B. V. E., & Fonseca, J. F. B. D. (2017). Damage from lava flows: insights from the 2014–2015 eruption of Fogo, Cape Verde. *Journal of Applied Volcanology*, *6*(1), 6.

Jørgensen, J. & Holm, P. (2002). Temporal variation and carbonatite contamination in primitive ocean island volcanic from São Vicente. Cape Verde Islands. Chemical Geology (192), pp. 249–267.

Klerkx, J., Deutsch, S., and De Paepa, P., (1974). Rubidium, strontium content and strontium isotopic composition of strongly alkalic basaltic rocks from the Cape Verde Islands. *Contributions to Mineralogy and Petrology* **45**: 107-118.

Klingelhöfer, F., Minshull, T.A., Blackman, D.K., Harben, P. and Childers, V., (2001). Crustal structure of Ascension Island from wide-angle seismic data: implications for the formation of near-ridge volcanic islands. Earth and Planetary Science Letters, 190(1-2), pp.41-56.

Klitgord, K., & Schouten, H. (1987). Plate kinematics of the Central Atlantic: in Tucholke, BE, and Vogt, PR, eds. *The Geology of North America: the Western Atlantic Region: Geol. Soc, America, Decade of North American Geology*.

Klügel, A., Klein, F., (2006). Complex magma storage and ascent at embryonic subma- rine volcanoes from Madeira Archipelago. Geology 34, 337–340.

Klügel, A., Longpré, M. A., García-Cañada, L., & Stix, J. (2015). Deep intrusions, lateral magma transport and related uplift at ocean island volcanoes. Earth and Planetary Science Letters, 431, 140-149.

Klügel A, Galipp K, Hansteen TH (2005) Magma storage and underplating beneath Cumbre Vieja volcano, La Palma (Canary Islands). Earth Planet Sci Lett 236:211–226

Klügel A, Hoernle KA, Schmincke HU, White JDL (2000) The chemically zoned 1949 eruption on La Palma (Canary Islands): petrologic evolution and magma supply dynamics of a rift- zone eruption, J Geophys Res 105(B3):5997–6016

Kokfelt, T. F., Holm, P.M., Hawkesworth, C.J., Peate, D.W. (1998). A lithospheric mantle source for the Cape Verde Island magmatism: Trace element and isotopic evidence from the Island of Fogo. *Mineralogical Magazine* 62A, 801-802.

Lai, Z., Zhao, G., Han, Z., Huang, B., Li, M., Tian, L., Bu, X. (2018). The magma plumbing system in the Mariana Trough back-arc basin at 18° N. *Journal of Marine Systems*, *180*, 132-139.

Lancelot, Y., Seibold, E., Cepek, P., Dean, W., Eremeev, V., Gardner, J., Jansa, L., Johnson, D., Krasheninnikov, V., Pflaumann, U., Rankin, J. G., Trabant, P. and Bukry, D., (1978). Site 368: Cape Verde Rise, in Initial Rep. Deep Sea Drill. Proj., vol. 41, pp. 233–326, eds Lancelot, Y., Seibold, E., Cepek, P., Dean, W., Eremeev, V., Gardner, J., Jansa, L., Johnson, D., Krashenin- Nikov, V., Pflaumann, U., Rankin, J. G., Trabant, P. and Bukry, D., Washington (U.S. Government Printing Office).

Le Maitre RW, Streckeisen A, Zanettin B, Le Bas MJ, Bonin B, Bate- man P, Bellieni G, Dudek A, Efremova A, Keller J, Woolley AR (2002) Igneous rocks. A classification and glossary of terms, Recommendations of the IUGS subcomission on the systematics of igneous rocks

Le Pichon, X.L., and Fox, P.J., (1971). Marginal offsets, fracture zones and the early opening of the North Atlantic. *Journal of Geophysical Research* **75**: 6294-6307.

Leva, C., Rümpker, G., Link, F. and Wölbern, I., (2019). Seismological evidence for subcrustal magmatic injection beneath Fogo volcano, Cape Verde hotspot. EarthArXiv 10.31223/osf.io/f6zdp

Liu, C., Lay, T., & Xiong, X. (2018). Rupture in the 4 May 2018 MW 6.9 earthquake seaward of the Kilauea east rift zone fissure eruption in Hawaii. *Geophysical Research Letters*, *45*(18), 9508-9515.

Lodge, A. and Helffrich, G., (2006). Depleted swell root beneath the Cape Verde Islands. Geology, 34(6): 449-452.

Longpré, M. A., Klügel, A., Diehl, A., & Stix, J. (2014). Mixing in mantle magma reservoirs prior to and during the 2011–2012 eruption at El Hierro, Canary Islands. *Geology*, *42*(4), 315-318.

Longpré, M. A., Troll, V. R., & Hansteen, T. H. (2008). Upper mantle magma storage and transport under a Canarian shield- volcano, Teno, Tenerife (Spain). *Journal of Geophysical Research: Solid Earth*, *113*(B8).

Machado F, Azeredo Leme J, Monjardino J, Seita MF (1968) Carta geológica de Cabo Verde, notícia explicativa da Ilha Brava e dos Ilhéus Secos. Garcia de Orta 16:123–130

Madeira, J., Ramalho, R. S., Hoffmann, D. L., Mata, J., & Moreira, M. (2019) A geological record of multiple Pleistocene tsunami inundations in an oceanic island: The case of Maio, Cape Verde. *Sedimentology*. https://doi.org/10.1111/sed.12612

Madeira J, Mata J, Mourão C, da Silveira AB, Martins S, Ramalho R, Hoffmn DL (2010) Volcano-stratigraphy and structural evolution of Brava Island (Cape Verde) based on 40Ar/39Ar, U-Th and field constraints. J Volcanol Geotherm Res 196:219–235

Madeira, J., Brum da Silveira, A., Mata, J., Mourão, C., & Martins, S. (2008). The role of mass movements on the geomorphologic evolution of island volcanoes: examples from Fogo and Brava in the Cape Verde archipelago. *Comun. Geol*, *95*, 93-106.

Madureira, P., Mata, J., Mattielli, N., Queiroz, G., and Silva, P. (2011) Mantle source heterogeneity, magma generation and magmatic evolution at Terceira Island (Azores archipelago): Constraints from elemental and isotopic (Sr, Nd, Hf, and Pb) data. Lithos, 126, 402–418.

Madureira, P., Mata, J., & Moreira, M. (2008). The Ne isotopic signature of Terceira lavas (Azores): evidence for Ne recycling?. *e-Terra*, *5*(11).

Magee, C., Stevenson, C. T., Ebmeier, S. K., Keir, D., Hammond, J. O., Gottsmann, J. H., O'Driscoll, B. (2018). Magma plumbing systems: a geophysical perspective. *Journal of Petrology*, *59*(6), 1217-1251.

Magnusson, E., (2016). Temporal evolution of historic mafic lavas from Fogo, Cape Verde. Examensarbete vid Institutionen för geovetenskaper, ISSN 1650-6553 ; 365. urn:nbn:se:uu:diva-296417

Marianelli, P., Metrich, N., Sbrana, A. (1999) Shallow and deep reservoirs involved in magma supply of the 1944 eruption of Vesuvius. Bulletin of Volcanology, 61, 48-63

Martínez-Moreno, F. J., Santos, F. M., Madeira, J., Pous, J., Bernardo, I., Soares, A., Esteves, M., Adão, F., Ribeiro, J., Mata, J., & da Silveira, A. B. (2018). Investigating collapse structures in oceanic islands using magnetotelluric surveys: The case of Fogo Island in Cape Verde. *Journal of Volcanology and Geothermal Research*, *357*, 152-162.

Masotta, M.; Mollo, S.; Freda, C.; Gaeta, M.; Moore, G. (2013) Clinopyroxene–liquid thermometers and barometers specific to alkaline differentiated magmas. *Contributions to Mineralogy and Petrology*, *166*(6), 1545-1561.

Massin, F., Ferrazzini, V., Bachèlery, P., Nercessian, A., Duputel, Z., & Staudacher, T. (2011). Structures and evolution of the plumbing system of Piton de la Fournaise volcano inferred from clustering of 2007 eruptive cycle seismicity. *Journal of Volcanology and Geothermal Research*, *202*(1-2), 96-106.

Masson, D.G., Le Bas, T.P., Grevemeyer, I. & Weinrebe, W., (2008). Flank collapse and large-scale landsliding in the Cape Verde Islands, off West Africa, *Geochem. Geophys. Geosyst.*, **9,** Q07015, doi:10.1029/ 2008GC001983.

Mata, J., Martins, S., Mattielli, N., Madeira, J., Faria, B., Ramalho, R. S., Silva, P., Moreira, M., Caldeira, R., Moreira, M., Rodrigues, J., & Martins, L. (2017). The 2014–15 eruption and the short-term geochemical evolution of the Fogo volcano (Cape Verde): Evidence for small-scale mantle heterogeneity. *Lithos*, *288*, 91-107.

Mata, J., Moreira, M., Doucelance, R., Ader, M. and Silva, L. C., (2010). Noble gas and carbon isotopic signatures of Cape Verde oceanic carbonatites: implications for carbon provenance. Earth and Planetary Science Letters, 291(1), 70-83.

McBride, J. H., White, R. S., Henstock, T. J., & Hobbs, R. W. (1994). Complex structure along a Mesozoic sea-floor spreading ridge: BIRPS deep seismic reflection, Cape Verde abyssal plain. *Geophysical Journal International*, *119*(2), 453-478.

McNutt, M. K., (1988) Thermal and mechanical properties of the Cape Verde Rise, J. Geophys. Res., 93, 2784–2794.

Mitchell, J. G., M. J. LeBas, J. Zielonka, and H. Furnes (1983), On dating the magmatism of Maio, Cape Verde Islands, Earth Planet. Sci. Lett., 64, 61–76.

Mollo, S., Blundy, J., Scarlato, P., De Cristofaro, S. P., Tecchiato, V., Di Stefano, F., Vetere, F., Holtz, F., & Bachmann, O. (2018). An integrated PT-H2O-lattice strain model to quantify the role of clinopyroxene fractionation on REE+ Y and HFSE patterns of mafic alkaline magmas: Application to eruptions at Mt. Etna. *Earth-Science Reviews*, *185*, 32-56.

Mollo, S., Putirka, K., Misiti, V., Soligo, M., & Scarlato, P. (2013). A new test for equilibrium based on clinopyroxene–melt pairs: clues on the solidification temperatures of Etnean alkaline melts at post-eruptive conditions. *Chemical Geology*, *352*, 92-100.

Morgan, D. J., Blake, S., Rogers, N. W., DeVivo, B., Rolandi, G., Macdonald, R., & Hawkesworth, C. J. (2004). Timescales of crystal residence and magma chamber volume from modelling of diffusin profiles in phenocrysts: Vesuvius 1944. *Earth and Planetary Science Letters* **222**, 933-946, doi:10.1016/j.epsl.2004.03.030

Mourão, C., Mata, J., Doucelance, J., Madeira, J., Brum da Silveira, A., Silva, L. & Moreira, M. (2010). Quaternary extrusive calciocarbonatite volcanism on Brava Island (Cape Verde). Journal of African Earth Sciences, 55, 59–74.

Müller, R., Sdrolias, M., & Roest, W., (2008). Age, spreading rates and spreading symmetry of the world's ocean crust, Geochemestry Geophysics Geosystems, 9(Q04006).

Nascimento A. (2015) Post disaster needs assessment: Fogo volcanic eruption 2014-2015. https://www.gfdrr.org/en/cape-verde-post-disaster-needs-assessment-volcano-eruption-2014-2015

Neave, D. A., & Putirka, K. D. (2017). A new clinopyroxene-liquid barometer, and implications for magma storage pressures under Icelandic rift zones. *American Mineralogist*, *102*(4), 777-794.

Nikogosian IK, Elliott T, Touret JLR (2002) Melt evolution beneath thick lithosphere: a magmatic inclusion study of La Palma, Canary Islands. Chemical Geology 183: 169-193.

Nimis, P. (1995). A clinopyroxene geobarometer for basaltic systems based on crystal-structure modelling. *Contibutions to Mineralogy and Petrology* **121**: 115-125.

O'Mongain, A., Ottemoller, L., Baptie, B., Galloway, D., & Booth, D. (2007). Seismic activity associated with a probable submarine eruption near Tristan da Cunha, July 2004–July 2006. *Seismological Research Letters*, *78*(3), 375-382.

Ogg, J.G., (1995). Magnetic polarity time scale of the Phanerozoic, *in Global Earth Physics: A handbook of physical constants. AGU Ref. Shelf, vol. 1*, edited by T.J. Ahrens, p 240-270. Washington D.C.

Paris, R., Giachetti, T., Chevalier, J., Guillou, H. and Frank, N., (2011). Tsunami deposits in Santiago Island (Cape Verde archipelago) as possible evidence of a massive flank failure of Fogos volcano. Sedimentary Geology, 239(3-4), pp.129-145.

Paris, R., Ramalho, R. S., Madeira, J., Ávila, S., May, S. M., Rixhon, G.,Engel, M., Brückner, H., Herzog, M., Schukraft, G., Pérez-Torrado, F. J., Rodrigues-González, A., Carracedo, J.C. & Giachetti, T. (2018). Mega-tsunami conglomerates and flank collapses of ocean island volcanoes. *Marine Geology*, *395*, 168-187.

Peltier, A., Bachèlery, P. and Staudacher, T., (2009). Magma transport and storage at Piton de La Fournaise (La Réunion) between 1972 and 2007: A review of geophysical and geochemical data. Journal of Volcanology and Geothermal Research, 184(1-2), pp.93-108.

Pérez, M., Dionis, S., Fernandes, P., Barrancos, J., Rodríguez, F., Bandomo, Z., Hernández, P., Melián, G., Silva, S., Padilla, G., Padrón, E., Cabral, J., Calvo, D., Asensio-Ramos, M., Pereira, J., Gonçalves, A., Barros, I., & Semedo, H., (2015). Precursory signals of the 2014-15 Fogo eruption (Cape Verde) detected by surface CO_2 emission and heat flow observations. Geophysical Research Abstracts Vol. 17, 2015, EGU General Assembly 2015.

Pim, J., Peirce, C., Watts, A. B., Grevemeyer, I. and Krabbenhöft, A., (2008). Crustal structure and origin of the Cape Verde Rise. Earth and Planetary Science Letters, 272(1), 422-428.

Plesner, S., Holm, P. M., & Wilson, J. R. (2003). 40Ar–39Ar geochronology of Santo Antão, Cape Verde Islands. Journal of Volcanology and Geothermal Research, 120(1-2), 103-121.

Poland, M.P., Miklius, A. and Montgomery-Brown, E.K., (2015). Magma supply, storage, and transport at shield-stage. Charact. Hawaii. Volcanoes, 179(1801), pp.179-234.

Putirka, K. D. (2017). Down the crater: where magmas are stored and why they erupt. Elements, 13(1), 11-16.

Putirka, K. (2008) Thermometers and barometers for volcanic systems. *Reviews in Mineralogy and Geochemistry, 69*, 61-120.

Putirka K, Mikaelian H, Ryerson FJ, Shaw H (2003) New clinopyroxene-liquid thermobarometers for mafic, evolved and volatile-bearing lava compositions, with applications to lavas from Tibet and the Snake River Plain, ID. Am Mineral 88:1542–1554

Putirka K (1999) Clinopyroxene + liquid equilibria to 100 kbar and 2450 K. Contrib Mineral Petrol 135: 151-163

1158 Putirka K (1997) Magma transport at Hawaii: Inferences based on igneous thermobarometry. Geology 25: 69-72

1159 Putirka K, Johnson M, Kinzler R, Longhi J, Walker D (1996) Thermobarometry of mafic igneous rocks based on
1160 clinopyroxene-liquid equilibria, 0-30 kbar. Contrib Mineral Petrol 123: 92-108

1161 Putirka K, Condit C (2003) A cross section of a magma conduit system at the margins of the Colorado Plateau.
1162 Geology 31:701-704

1163 Quilty, P. G., & Wheller, G. E. (2000). Heard Island and the McDonald Islands: a window into the Kerguelen
1164 Plateau. In *Papers and Proceedings of the Royal Society of Tasmania* (Vol. 133, No. 2, pp. 1-12).

1165 Ranero CR, Torne M, Banda E (1995) Gravity and multichannel seismic reflection constraints on the lithospheric
1166 structure of the Canary Swell. Mar Geophys Res 17:519–534

1167 Ramalho, R. S., Winckler, G., Madeira, J., Helffrich, G. R., Hipólito, A., Quartau, R., Adena, K. & Schaefer, J. M.
1168 (2015). Hazard potential of volcanic flank collapses raised by new megatsunami evidence. *Science advances*, *1*(9),
1169 e1500456.

1170 Ramalho, R. A. dos Santos (2011). Vertical Movements of Ocean Island Volcanoes: Insights from a Stationary
1171 Plate. In Building the Cape Verde Islands (pp. 177-197). Springer, Berlin, Heidelberg.

1172 Ramalho, R. S., Helffrich, G., Cosca, M., Vance, D., Hoffmann, D., & Schmidt, D. N. (2010c). Vertical movements
1173 of ocean island volcanoes: insights from a stationary plate environment. Marine Geology, 275(1-4), 84-95.

1174 Ramalho, R., Helffrich, G., Schmidt, D. & Vance, D. (2010b). Tracers of uplift and subsidence in the Cape Verde
1175 Archipelago. J. Geol. Soc. Lond. 167, pp. 519-538.

1176 Ramalho, R., Helffrich, G., Cosca, M.,Vance, D., Hoffmann, D. & Schmidt, D. (2010a). Episodic swell growth
1177 inferred from variable uplift of the Cape Verde hotspot islands. Nature Geoscience, Vol. 3, pp. 774-777.

1178 Renzulli, A. and Santi, P., (2000). Two-stage fractionation history of the alkali basalt-trachyte series of Sete Cidades
1179 volcano (São Miguel Island, Azores). *European Journal of Mineralogy*, *12*(2), pp.469-494.

1180 Ribeiro, O. (1960). A ilha do Fogo e as suas Erupções. Memórias Série Geográfica I. Lisboa: Junta de Investigações
1181 do Ultramar.

1182 Richter, N., Favalli, M., de Zeeuw-van Dalfsen, E., Fornaciai, A., Fernandes, R. M. D. S., Pérez, N. M., Levy, J.,
1183 Silva, S.V. & Walter, T. R. (2016). Lava flow hazard at Fogo Volcano, Cabo Verde, before and after the 2014-2015
1184 eruption. *Natural Hazards & Earth System Sciences*, *16*(8).

1185 Risby, O. & Sandback, B. (2014) Mapping report Fogo, Cape Verde. Uppsala University.

1186 Roest, W. R., Danobeitia, J. J., Verhoef, J., & Collette, B. J. (1992). Magnetic anomalies in the Canary Basin and the
1187 Mesozoic evolution of the central North Atlantic. *Marine Geophysical Researches*, *14*(1), 1-24.

1188 Rona, P. A. (1971). Bathymetry off central northwest Africa. In Deep Sea Research and Oceanographic Abstracts
1189 Vol. 18, No. 3, pp. 321-327. Elsevier.

1190 Ryabchikov, J. D.; Ntaflos, T.; Kurat, G.; Kogarko, L. N. (1995) Glass-bearing xenoliths from Cape Verde:
1191 evidence for a hot rising mantle jet. *Mineralogy and Petrology*, *55*(4), 217-237.

Ryan, W.B.; Carbotte, S.M.; Coplan, J.O.; O'Hara, S.; Melkonian, A.; Arko, R.; Weissel, R.A.; Ferrini, V.; Goodwillie, A.; Nitsche, F.; Bonczkowski, J. (2009) Global multi- resolution topography synthesis. *Geochemistry, Geophysics, Geosystems*, *10*, 3.

Rydeblad, E. (2018). Mineral Constraints on the Source Lithologies at Fogo, Cape Verde. Unpublished MSc thesis, Uppsala University. ISSN 1650-6553 ; 433. urn:nbn:se:uu:diva-354077

Sakai H, Des Marias DJ, Ueda A, Moore JG (1984) Concentrations and isotope ratios of carbon, nitrogen and sulfur in ocean-floor basalts. Geochim Cosmochim Acta 48:2433–2441

Samrock L.K., Wartho, J-A., Hansteen, T.H. (2019). ^{40}Ar-^{39}Ar dating of the active phonolitic Cadamosto Seamount (CapeVerde): Indications for periodic volcanic activity and a possible relationship to global sea level changes. Lithos

Sandwell, D. T., & Smith, W. H. (1997). Marine gravity anomaly from Geosat and ERS 1 satellite altimetry. *Journal of Geophysical Research: Solid Earth*, *102*(B5), 10039-10054.

Schwarz, S. & Klügel, A. (2004). Melt extraction pathways and stagnation depths beneath the Maderia and Desertas rift zones (NE Atlantic) inferred from barometric studies. *Contributions to Mineralogy and Petrology* **147**: 228-240.

Serralheiro, A. (1976). A geologia da Ihla de Santiago (Cabo Verde). *Boletim do museu e laboratório mineralógico e geológico da Faculdade de Ciências* 14: 157-369.

Serralheiro, A., (1970). Geologia da Ilha de Maio (Cabo Verde). Junta de Investigações do Ultramar.

Seifert, R., Malfait, W. J., Petitgirard, S., & Sanchez-Valle, C. (2013). Density of phonolitic magmas and time scales of crystal fractionation in magma chambers. *Earth and Planetary Science Letters*, *381*, 12-20.

Silva, L., Le Bas, M. & Robertson, A. (1981). An oceanic carbonatite volcano on Santiago, Cape Verde Islands. Nature, 294, 644–645.

Silva, R., Havskov, J., Bean, C. and Wallenstein, N., (2012). Seismic swarms, fault plane solutions, and stress tensors for São Miguel Island central region (Azores). *Journal of Seismology*, *16*(3), pp.389-407.

Silva, S.; Calvari, S.; Hernandez, P.; Pérez, N.; Ganci, G.; Alfama, V.; Barrancos, J.; Cabral, J.; Cardoso, N.; Dionis, S.; Fernandes, P.; Melian, G.; Pereira, J.; Semedo, H.; Padilla, G. & Rodriguez. F., (2017). Tracking the hidden growth of a lava flow field: the 2014-15 eruption of Fogo volcano (Cape Verde). Geophysical Research Abstracts Vol. 19, EGU 2017-14514, 201. EGU General Assembly 2017.

Silva, S., Cardoso, N., Alfama, A., Cabral, J., Semedo, H., Pérez, N., Dionis, S., Hernández, P., Barrancos, J., Melián, G., Pereira, J. & Rodríguez, R., (2015). Chronology of the 2014 volcanic eruption on the island of Fogo, Cape Verde. Geophysical Research Abstracts Vol. 17, 2015 EGU General Assembly 2015.

Skolotnev, S. G., Turko, N. N., Sokolov, S. Y., Peyve, A. A., Tsukanov, N. V., Kolodyazhnyi, S. Y., Eskin, A. E. (2007). New data on the geological structure of the junction of the Cape Verde rise, Cape Verde abyssal basin, and bathymetrists seamounts (Central atlantic ocean). In *Doklady Earth Sciences* (Vol. 416, No. 1, pp. 1037-1041). MAIK Nauka/Interperiodica.

Skolotnev, S. G., Kolodyazhny, S. Y., Tsukanov, N. V., Chamov, N. P., & Sokolov, S. Y. (2009). Neotectonic morphotructures in the junction zone of the Cape Verde Rise and Cape Verde Abyssal Plain, Central Atlantic. *Geotectonics*, *43*(1), 51-66.

Sparks, R. S. J., & Cashman, K. V. (2017). Dynamic magma systems: Implications for forecasting volcanic activity. *Elements*, *13*(1), 35-40.

Stephenson, J., Budd, G. M., Manning, J., & Hansbro, P. (2005). Major eruption-induced changes to the McDonald Islands, southern Indian Ocean. *Antarctic Science*, *17*(2), 259-266.

Stillman, C., Furnes, H., Le Bas, M., Robertson, A. & Zielonka, J. (1982). The geological history of Maio, Cape Verde Islands. Journal of the Geological Society, Vol. 139, nº3, pp. 347-361. Londres.

Stock, M. J., Bagnardi, M., Neave, D. A., Maclennan, J., Bernard, B., Buisman, I., Gleeson, L.M. & Geist, D. (2018). Integrated petrological and geophysical constraints on magma system architecture in the western Galápagos Archipelago: insights from Wolf volcano. *Geochemistry, Geophysics, Geosystems*, *19*(12), 4722-4743.

Streck, M. J. (2008). Mineral textures and zoning as evidence for open system processes. *Reviews in Mineralogy and Geochemistry*, *69*(1), 595-622.

Tenzer, R., Bagherbandi, M., & Vajda, P. (2013). Global model of the upper mantle lateral density structure based on combining seismic and isostatic models. *Geosciences Journal*, *17*(1), 65-73.

Texier-Teixeira, P., Chouraqui, F., Perrillat-Collomb, A., Lavigne, F., Cadag, J. R., & Grancher, D. (2014). Reducing volcanic risk on Fogo Volcano, Cape Verde, through a participatory approach: which outcome?. *Natural Hazards and Earth System Sciences*, *14*(9), 2347-2358.

Till, C. B. (2017). A review and update of mantle thermobarometry for primitive arc magmas. *American Mineralogist*, *102*(5), 931-947.

Torres, P. C., Madeira, J., Silva, L. C., Brum da Silveira, A., Serralheiro, A. and Mota Gomes, A., (1997). Carta geológica das erupções históricas da Ilha do Fogo: revisão e actualização. In "A erupção vulcânica de 1995 na ilha do Fogo, Cabo Verde"; Edição do Instituto de Investigação Científica Tropical e Ministério da Ciência e Tecnologia: 119-132.

Torres, P. C., Madeira, J., Silva, L. C., da Silveira, A. B., Serralheiro, A., & Gomes, A. M. (1998). Carta Geológica das Erupções Históricas da Ilha do Fogo (Cabo Verde): revisão e actualização. *Comunicações do Instituto Geológico e Mineiro*, *84*, A193-196.

Torres, P., Silva, L., Serralheiro, A., Tassinari, C., & Munhá, J., (2002). Enquadramento geocronológico pelo método K/Ar das principais sequências vulcano-estratigráficas da Ilha do Sal - Cabo Verde, Garcia de Orta, Serviços Geológicos, 18(1-2), 9–13.

Turbeville, B. N., Wolff, J. A., & Le Bas, M. J. (1987). An oceanic nephelinite–phonolite–carbonatite association, Brava, Cape Verde Islands. *Eos*, *68*, 1522.

Vales, D., Dias, N.A., Rio, I., Matias, L., Silveira, G., Madeira, J., Weber, M., Carrilho, F. and Haberland, C., (2014). Intraplate seismicity across the Cape Verde swell: A contribution from a temporary seismic network. Tectonophysics, 636, pp.325-337.

Verhoef, J., Collette, B.J., Dañobeitia, J.J., Roeser, H.A., Roest, W.R., (1991). Magnetic anomalies off West-Africa (20–38° N). Marine Geophysical Research 13 (2), 81–103.

Weidendorfer, D., Schmidt, M. W., & Mattsson, H. B. (2016). Fractional crystallization of Si-undersaturated alkaline magmas leading to unmixing of carbonatites on Brava Island (Cape Verde) and a general model of carbonatite genesis in alkaline magma suites. *Contributions to Mineralogy and Petrology*, *171*(5), 43.

Weit, A., Trumbull, R.B., Keiding, J.K., Geissler, W.H., Gibson, S.A. and Veksler, I.V., (2017). The magmatic system beneath the Tristan da Cunha Island: Insights from thermobarometry, melting models and geophysics. Tectonophysics, 716, pp.64-76.

Welsch, B., Hammer, J., Baronnet, A., Jacob, S., Hellebrand, E., & Sinton, J. (2016). Clinopyroxene in postshield Haleakala ankaramite: 2. Texture, compositional zoning and supersaturation in the magma. *Contributions to Mineralogy and Petrology*, *171*(1), 6.

White, R. S. (1984). Atlantic oceanic crust: seismic structure of a slow-spreading ridge. *Geological Society, London, Special Publications*, *13*(1), 101-111.

Williams, C., Hill, I., Young, R. & White, R. (1990). Fracture zones across the Cape Verde Rise, NE Atlantic. Journal of Geological Society of London, 1

Wilson, D., Peirce, C., Watts, A., Grevemeyer, I., Krabbenhoeft, A., (2010). Uplift at litho- spheric swells-I: seismic and gravity constraints on the crust and uppermost mantle structure of the Cape Verde mid-plate swell. Geophysical Journal International 182, 531–550.

Wilson, D., Peirce, C., Watts, A., Grevemeyer, I., (2013). Uplift at lithospheric swells-II: is the Cape Verde mid-plate swell supported by a lithosphere of varying mechanical strength? Geophysical Journal International 193, 798–819.

Worsley, P. (2015). Physical geology of the Fogo volcano (Cape Verde Islands) and its 2014–2015 eruption. *Geology Today*, *31*(4), 153-159.

Wunderman, R. (2003). Summary of recent volcanic activity. *Bulletin of Volcanology*, *65*(6), 458-459.

Zanon, V., Kueppers, U., Pacheco, J.M. and Cruz, I., (2013). Volcanism from fissure zones and the Caldeira central volcano of Faial Island, Azores archipelago: geochemical processes in multiple feeding systems. *Geological Magazine*, *150*(3), pp.536-555.

Zanon, V. and Pimentel, A., (2015). Spatio-temporal constraints on magma storage and ascent conditions in a transtensional tectonic setting: the case of the Terceira Island (Azores). *American Mineralogist*, *100*(4), pp.795-805.

Zhao Z-F, Zheng Y-F (2003) Calculation of oxygen isotope fractionation in magmatic rocks. Chem Geol 193:59–80

Figure captions:

Figure 1. Bathymetric and topographic map of the Cape Verde Archipelago as well as the Cadamosto Seamount, and islands of Brava, Fogo and Santiago. Note the existence of a "northern chain" composed of the islands of Santo Antão, São Vicente, Santa Luzia and islets, and São Nicolau, and a "southern chain" composed of the islands Santiago, Fogo and Brava and the Cadamosto Seamount. Relatively deep water separates most islands. Sources: Ryan et al., 2009; www.geomapapp.org; Hansteen et al., 2014.

Figure 2. Complied stratigraphy of DSDP Site 368, the Cape Verde Rise and the Cape Verde islands. Several kilometer thick sequences of sediment are found above the ocean crust throughout the region (Dash et al. 1976; Lancelot et al., 1978; Pim et al., 2008). The Moho is thickened beneath the islands and occurs at depths of 12 to 18 km, becoming deeper towards the East (Dash et al. 1976; Lancelot et al., 1978; Ali & Watts, 2003; Lodge & Helffrich, 2006; Pim et al., 2008).

Figure 3 (a) Map showing fractures zones, magnetic lineations, gravity and magnetism of the Cape Verde Rise. Black lines show fracture zones as mapped by Williams et al. (1990). Magnetic lineations of M4–M25 are plotted after Klitgord and Schouten (1986). The satellite-derived free-air gravity anomalies are shown (Sandwell and Smith, 1997). DSDP Site 368 is labeled. Magnetic quiet zone boundary from Hayes and Rabinowitz (1975). (b) Schematic cross-section NNW to SSE across the Cape Verde Rise following the yellow line (Stillman et al.,1982; Ryan et al., 2009; www.geomapapp.org).

Figure 4. Age distribution of exposed volcanic and intrusive products across the Cape Verde Archipelago. Black bars mark $^{40}Ar/^{39}Ar$ geochronology and He exposure dating whereas grey bars show K/Ar geochronology and other geological inferences. Modified from Holm et al. (2008) and based on the geochonological data of Bernard-Griffiths et al. (1975); Mitchell et al. (1983); Torres et al. (2002); Plesner et al. (2003); Jørgensen and Holm (2002); Duprat et al., (2007); Holm et al. (2008); Foeken et al. (2009); Dyhr and Holm (2010); Madeira et al. (2010); Ramalho et al. (2010c); Samrock et al. (2019). Note the tentative age progression of the oldest exposed rocks in East to the youngest in the West.

Figure 5. Photographs from the islands of Santiago, Fogo and Brava and the Cadamosto Seamount. a) Hyaloclastite from the submarine Flamengos Formation overlain by subaerial lavas of the Pico de Antónia Formation, Santiago. b) The Assomada Formation, Santiago, c) Pillow lavas in hyaloclastite from the Flamengos Formation overlain by a beach conglomerate followed by lavas of the Pico de Antónia Formation, Santiago, d) the iconic Pico do Fogo standing on the Chã das Caldeiras plateau,

Fogo, e) Bordeira cliffs that surround the western part of the Chã das Caldeiras, Fogo, f) the volcanic eruption at Fogo in November 2014, g) pillow lavas and hyaloclastites intruded by dike swarms, Brava h) sequence of ignimbrites, Brava, i) phonolitic lava near the summit of the Cadamosto Seamount (M80/3-033ROV), and j) steep cliffs of a crater at the Cadamosto Seamount (M80/3-033ROV).

Figure 6. Geological and topographic map of Santiago after Serralheiro, 1976; Ryan et al., 2009; www.geomapapp.org. The Flamengos Formation is exposed along river valleys and in highly eroded areas. The Pico da Antonía Formation is wide spread and represents the shield building stage of volcanism. An erosional phase was followed by lavas of the Assomada Formation that flowed into valleys and the Monte das Vacas scoria cones.

Figure 7. Geological and topographic map of Fogo after Torres et al., 1998; Ryan et al., 2009; www.geomapapp.org; Carracedo et al., 2015. The shield volcano is composed of the Monte Amarelo Group volcanism and a large landslide created the Bordeira cliffs delineating the Cha das Caldeiras plateau that hosts the Pico do Fogo and recent volcanic eruptions.

Figure 8. Geological and topographic map of Brava after Madeira et al., 2010; Ryan et al., 2009; www.geomapapp.org. The island core complex is composed of alkaline and carbonatite intrusive rocks, whereas the volcanic rocks are mostly nephelinite to phonolite.

Figure 9. Compositional classification of the volcanic rocks from Santiago, Fogo, Brava and the Cadamosto Seamount after LeMaitre et al. 2002. Santiago and Fogo host (mela)nephelinite, basanite and tephrite to basalt and even tephriphonolite at Fogo. In contrast Brava and the Cadamosto Seamount host dominantly phonolite and syenite. Data are unnormalized. Data sources: Kokfelt, 1998; Barker et al., 2009, 2012; Hildner et al., 2011, 2012; Magnusson, 2016; Weidendorfer et al., 2016.

Figure 10. Clinopyroxene Mg# histograms for Santiago, Fogo, Brava and the Cadamosto Seamount. All locations host diopside-augite, whereas Brava and the Cadamosto Seamount display highest abundances of aegirine-augite. Data sources: Barker et al., 2009, 2012; Hildner et al., 2011, 2012; Weidendorfer et al., 2016; Rydeblad, 2018.

Figure 11. Clinopyroxene mineral chemistry for Santiago, Fogo, Brava and the Cadamosto Seamount. The clinopyroxene crystals from Santiago and Fogo display a distinct trend from the clinopyroxene found

at Brava and the Cadamosto Seamount. Data sources: Barker et al., 2009, 2012; Hildner et al., 2011, 2012; Weidendorfer et al., 2016; Rydeblad, 2018.

Figure 12. Zonation in clinopyroxene from Santiago, Fogo and the Cadamosto Seamount, shown by Mg# (mol%), TiO_2 and MnO content. Santiago Coastal group of the Flamengos Formation (121-306; Barker et al., 2009); Fogo eruption 1847 (CVF07 pyroxene 11; Rydeblad, 2018); Cadamosto Seamount (D885 J1; Barker et al., 2012). Data sources: Barker et al., 2009, 2012; Hildner et al., 2011, 2012; Weidendorfer et al., 2016; Rydeblad, 2018.

Figure 13. Multicomponent equilibrium ΔDiHd versus temperature for diopside-augite from Santiago, Fogo, Brava and the Cadamosto Seamount calculated after Mollo et al. (2013).

Figure 14. Thermobarometry for Santiago, Fogo, Brava and the Cadamosto Seamount. Data sources: Barker et al., 2009, 2012; Hildner et al., 2011, 2012; Rydeblad, 2018. The Moho is from Lodge & Helffrich 2006 and Pim et al. 2008.

Figure 15 Crystallization conditions; temperature and pressure, with composition for zoned clinopyroxene from Fogo; a) Prehistoric eruption CVF05 pyroxene 8, b) Eruption in 1785 CVF08 pyroxene 15, c) Eruption in 1799 CVF09 pyroxene 5 and d) Eruption in 1847 CVF06 pyroxene 7.

Figure 16. Crystallisation depth and model for the magma plumbing system beneath Santiago, Fogo, Brava and the Cadamosto Seamount. The shallow magma storage system is illustrated by fluid inclusion barometry as well as seismicity, deformation and the active hydrothermal systems. Data sources: Da Silva et al., 1999; Amelung & Day, 2002; Barker et al., 2009, 2012; Ryan et al., 2009; www.geomapapp.org; Heleno et al., 2006; Grevemeyer et al., 2010; Hildner et al., 2011, 2012; Faria & Fonseca, 2014; Rydeblad, 2018. The Moho is from Lodge & Helffrich 2006 and Pim et al. 2008.

Figure 17. Schematic of the magma storage systems for Ocean Islands globally including results from clinopyroxene-melt thermobarometry, fluid inclusions, melt inclusions, experimental petrology deformation and seismicity. Cape Verde; Da Silva et al 1999; Amelung & Day 2002; Lodge & Helffrich, 2006; Pim et al., 2008; Barker et al., 2009, 2012; Grevemeyer et al., 2010; Hildner et al., 2011, 2012; Faria & Fonseca 2014; Fernandes & Faria, 2015; Vales et al., 2015; Jenkins et al., 2017; Leva et al.,

2019; Mata et al., 2017; this study. Canary Islands; Klügel et al., 2000; 2005; Galipp et al., 2006; Longpré et al., 2008, 2014; Aulinas et al., 2010; Barker et al., 2015; González et al., 2013. Madeira; Schwarz & Klügel 2004; Klügel & Klein, 2006. The Azores; Renzulli & Santi 2000; Beier et al., 2006; Dias et al., 2007; Silva et al 2012; Jeffery et al., 2016; Madureira et al., 2008; Zanon et al., 2013; Zanon & Pimentel 2015. Tristan da Cunha; Geissler et al., 2016; Weit et al., 2017. Ascension; Klinghofer et al., 2001; Hanson et al., 1996; Chamberlain et al., 2016. Hawaii; Putirka et al. 1996, Putirka 1997; Chatterjee et al., 2005; Poland et al 2015; Hammer et al., 2016. Galapagos; Stock et al., 2018. Reunion; Bureau et al., 1998; Famin et al., 2009; Peltier et al. 2009; Di Muro et al., 2014; Fontaine et al., 2014. Kerguelen; Freise et al., 2003.

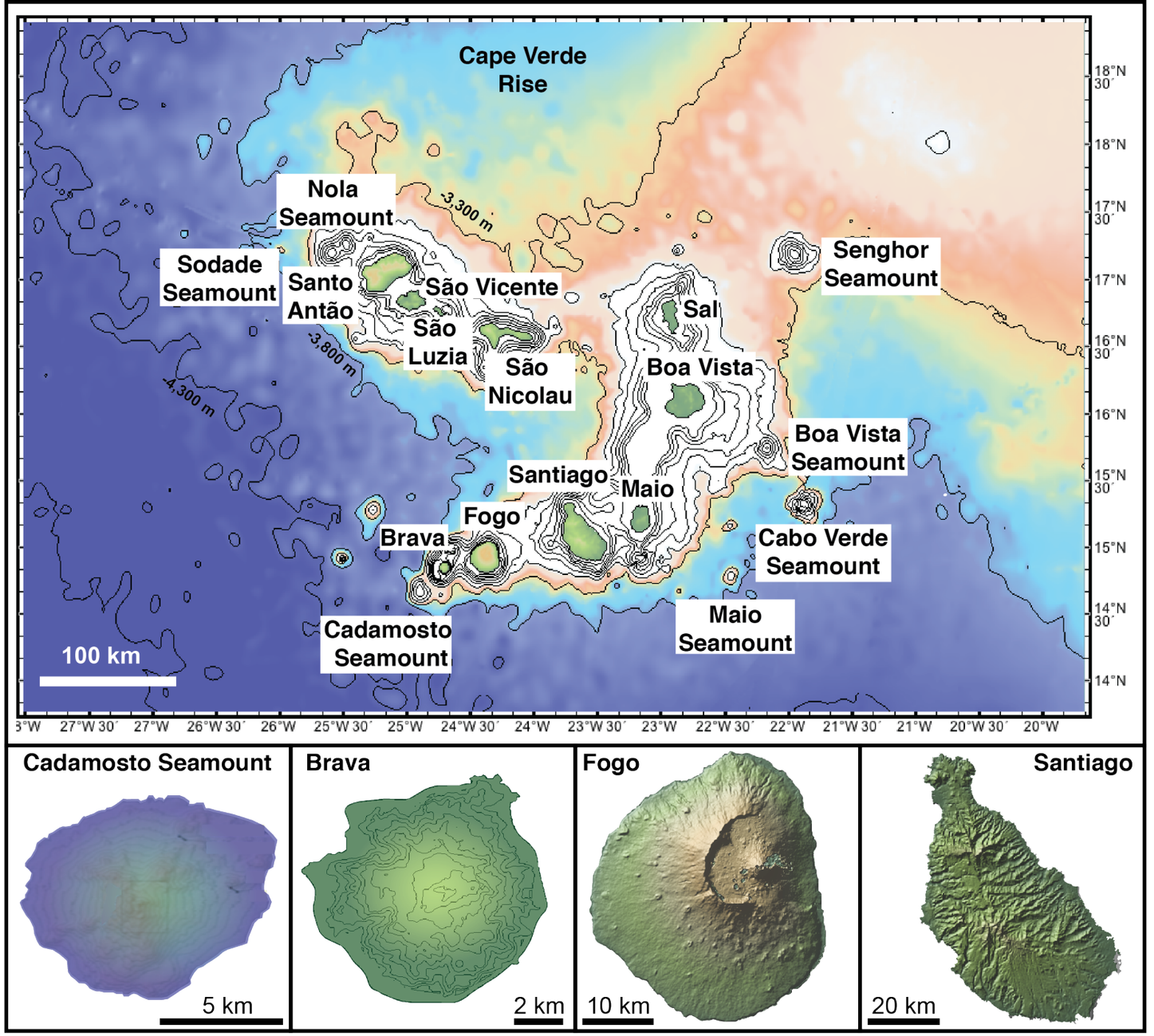
Cape Verde Rise
Nola Seamount
-3,300 m
Sodade Seamount
Santo Antão
São Vicente
São Luzia
São Nicolau
Sal
Boa Vista
Senghor Seamount
-3,800 m
-4,300 m
Boa Vista Seamount
Santiago
Maio
Fogo
Brava
Cabo Verde Seamount
Maio Seamount
Cadamosto Seamount
100 km
18°N 30´
18°N
17°N 30´
17°N
16°N 30´
16°N
15°N 30´
15°N
14°N 30´
14°N
27°W 30´
27°W
26°W 30´
26°W
25°W 30´
25°W
24°W 30´
24°W
23°W 30´
23°W
22°W 30´
22°W
21°W 30´
21°W
20°W 30´
20°W

Cadamosto Seamount
5 km
Brava
2 km
Fogo
10 km
Santiago
20 km

A

DSDP368

Magnetic quiet zone boundary

B

Horsts

Grabens

Graben

Horst

Elevation, m

-3800 -3600 -3400 -3200 -3000 -2800

-0 20 40 60 80 100 120 140 160

Distance, km

Gravity anomalies

Fracture lines

Palaeomagnetic lineations

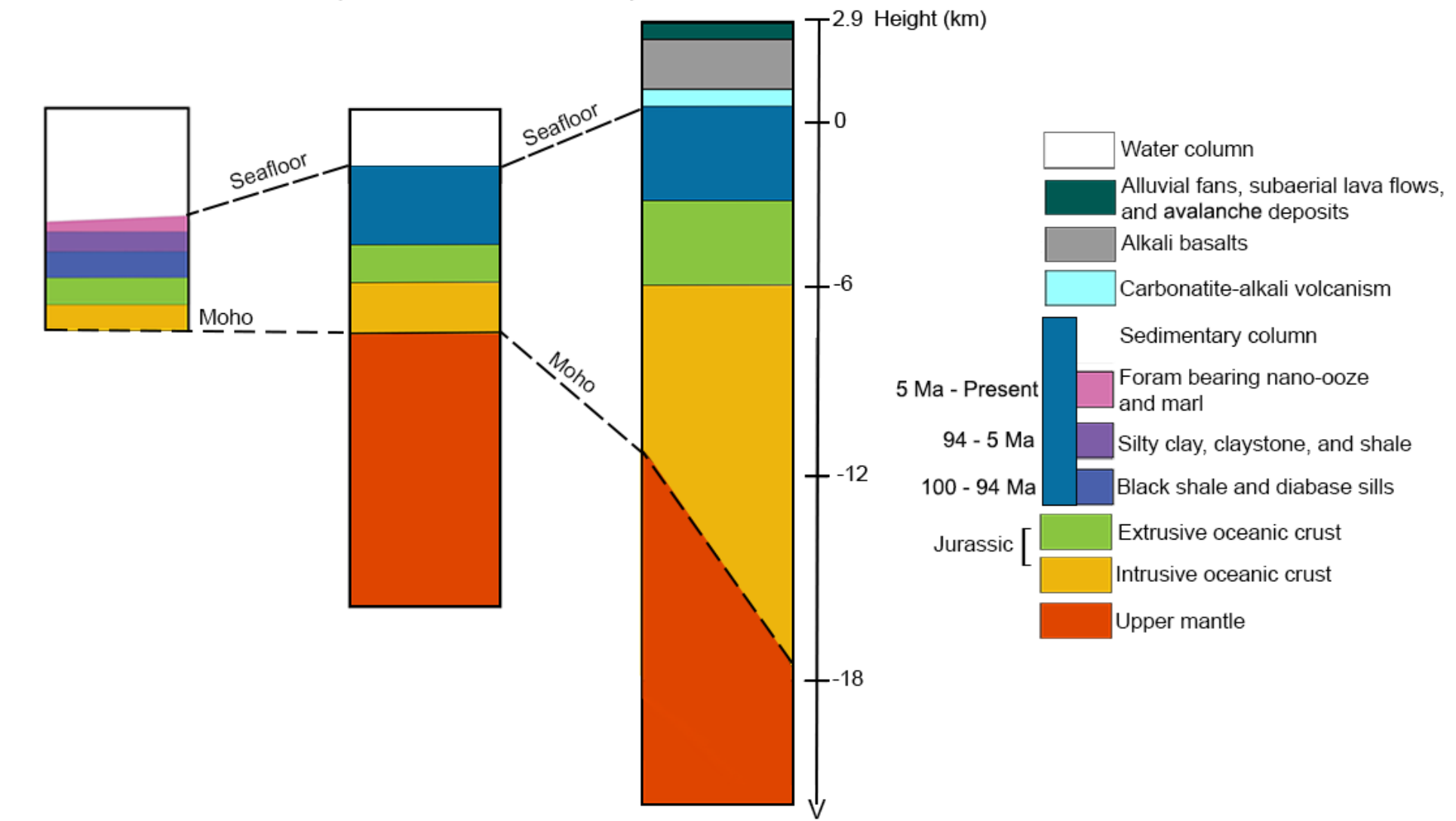
DSDP site 368
Cape Verde Rise
Cape Verde Islands
2.9 Height (km)
0
-6
-12
-18
Seafloor
Seafloor
Moho
Moho
Water column
Alluvial fans, subaerial lava flows, and avalanche deposits
Alkali basalts
Carbonatite-alkali volcanism
Sedimentary column
5 Ma - Present
Foram bearing nano-ooze and marl
94 - 5 Ma
Silty clay, claystone, and shale
100 - 94 Ma
Black shale and diabase sills
Jurassic
Extrusive oceanic crust
Intrusive oceanic crust
Upper mantle

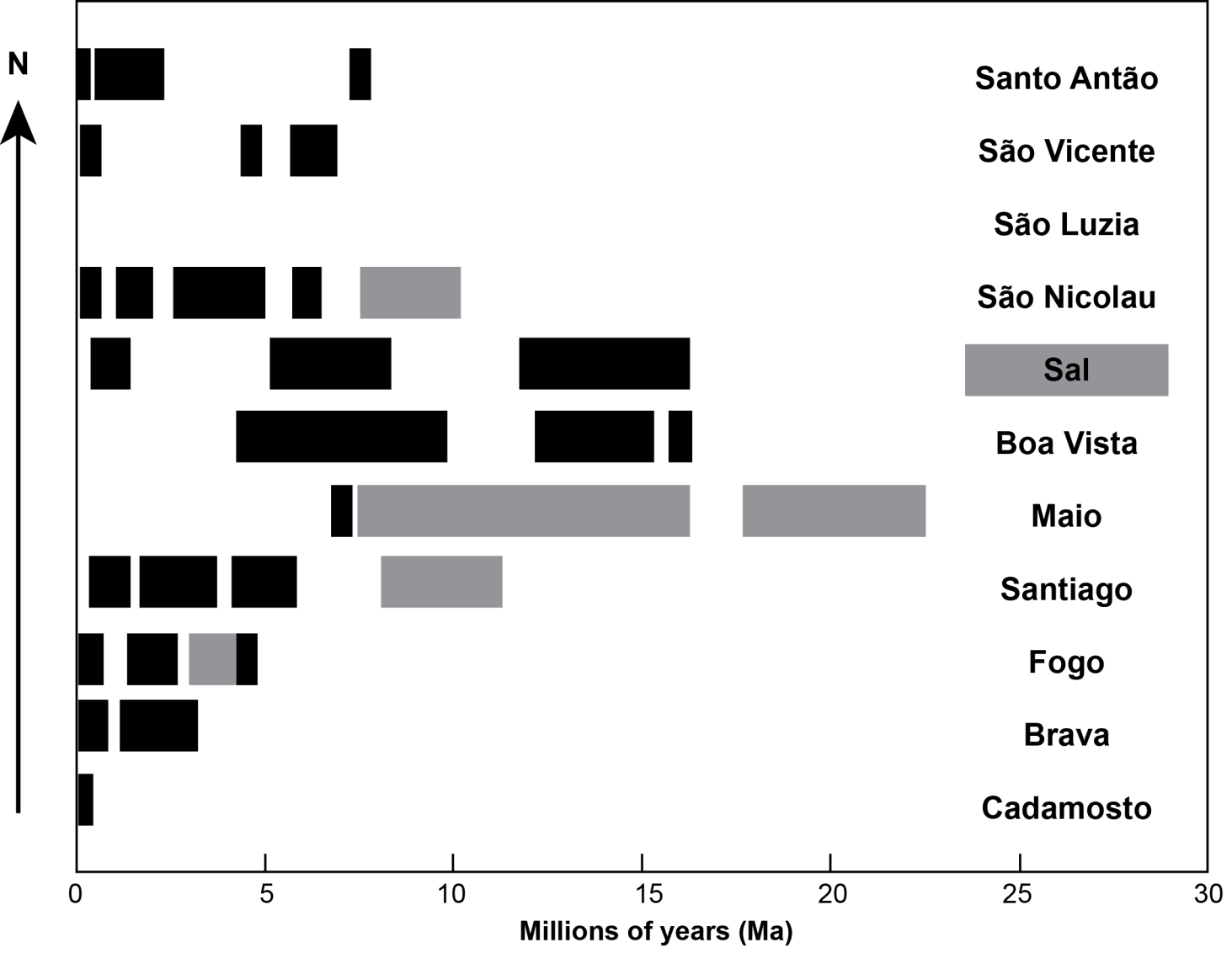
N
Santo Antão
São Vicente
São Luzia
São Nicolau
Sal
Boa Vista
Maio
Santiago
Fogo
Brava
Cadamosto
0
5
10
15
20
25
30
Millions of years (Ma)

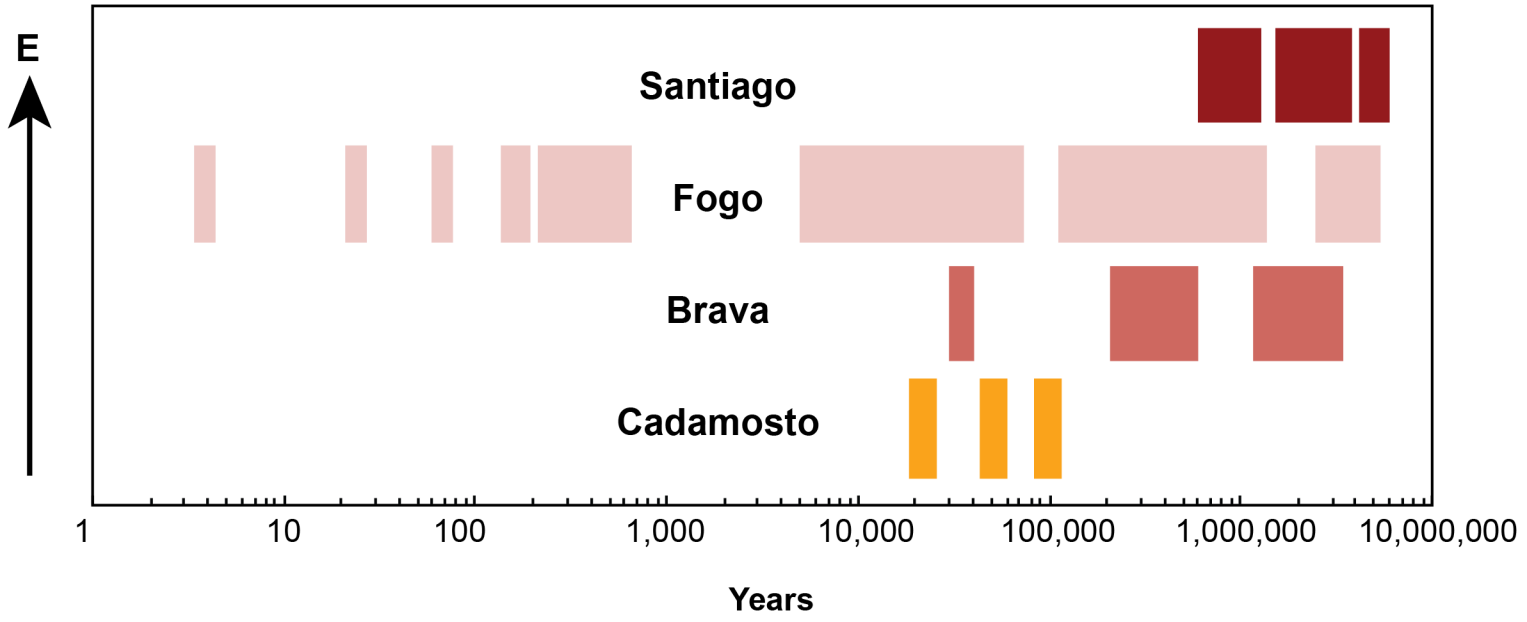
E
Santiago
Fogo
Brava
Cadamosto
1
10
100
1,000
10,000
100,000
1,000,000
10,000,000
Years


a)
Pico da Antonia Formation
Santiago
Flamengos Formation
b)
Assomada Formation, Santiago
c)
Flamengos & Pico da Antonia, Santiago
d)
Pico do Fogo
e)
Bordeira cliffs, Fogo
f)
Fogo 2014
g)
Brava submarine volcanics
h)
Brava Ignimbrites
Cadamosto Seamount: Phonolitic lava
i)
j)
Cadamosto Seamount: Pillow lavas

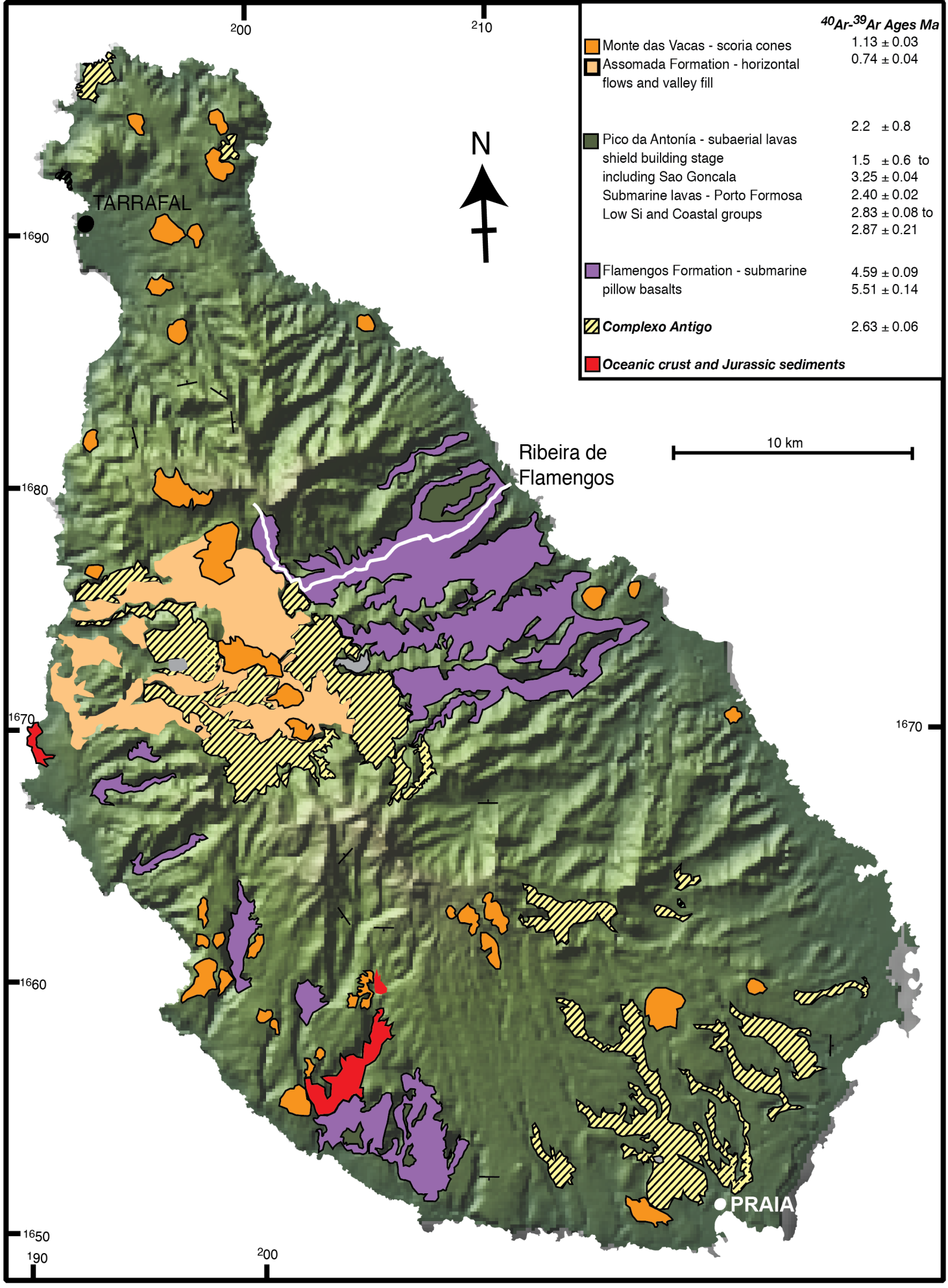
200
210
1690
1680
1670
1660
1650
190
200
1670
N
TARRAFAL
Ribeira de
Flamengos
10 km
PRAIA
^{40}Ar-^{39}Ar Ages Ma
Monte das Vacas - scoria cones
1.13 ± 0.03
Assomada Formation - horizontal flows and valley fill
0.74 ± 0.04
Pico da Antonía - subaerial lavas shield building stage
2.2 ± 0.8
including Sao Goncala
1.5 ± 0.6 to 3.25 ± 0.04
Submarine lavas - Porto Formosa
2.40 ± 0.02
Low Si and Coastal groups
2.83 ± 0.08 to 2.87 ± 0.21
Flamengos Formation - submarine pillow basalts
4.59 ± 0.09
5.51 ± 0.14
Complexo Antigo
2.63 ± 0.06
Oceanic crust and Jurassic sediments

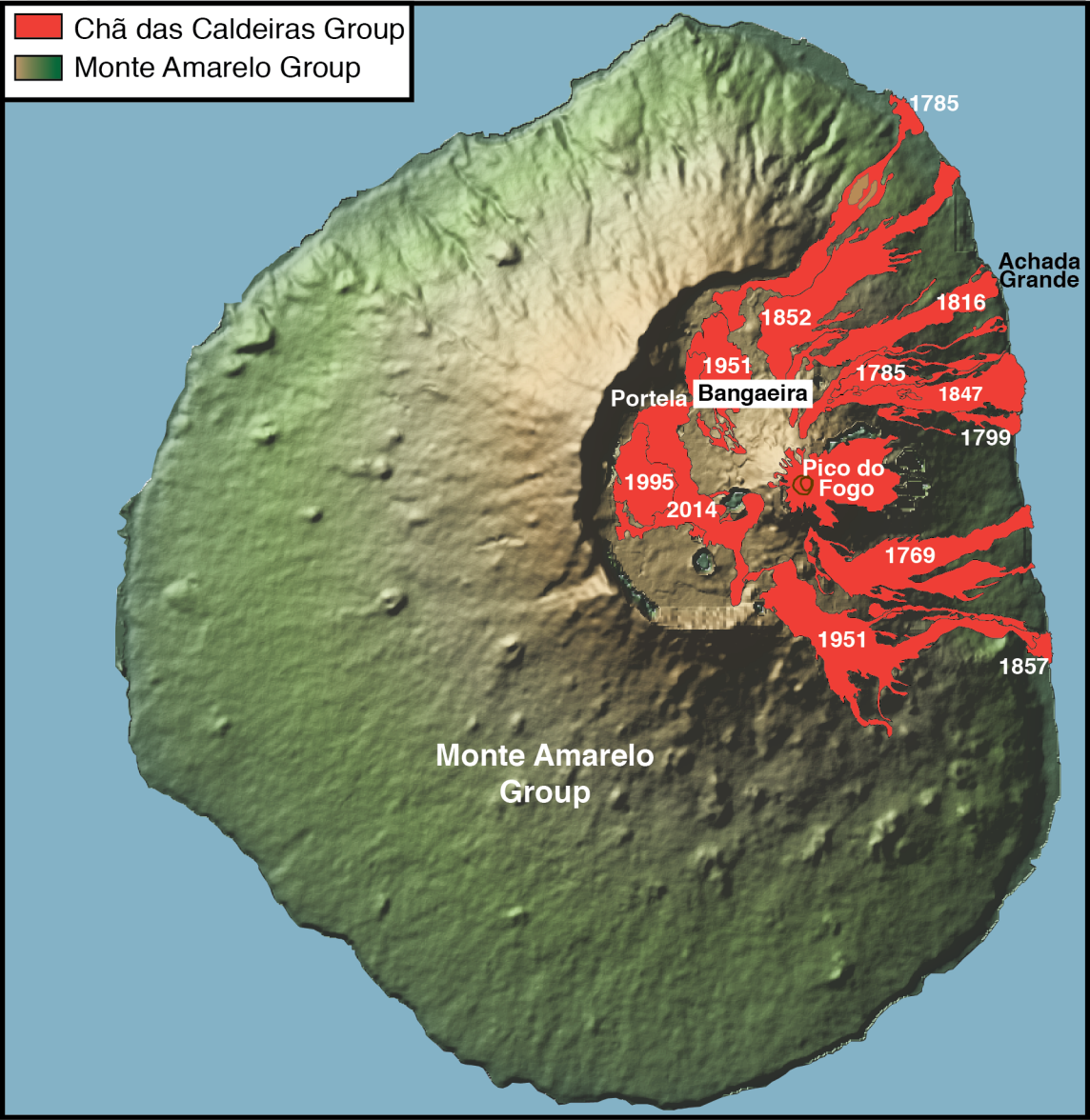
Chã das Caldeiras Group
Monte Amarelo Group
1785
Achada Grande
1816
1852
1951
1785
1847
Portela
Bangaeira
1799
Pico do Fogo
1995
2014
1769
1951
1857
Monte Amarelo Group

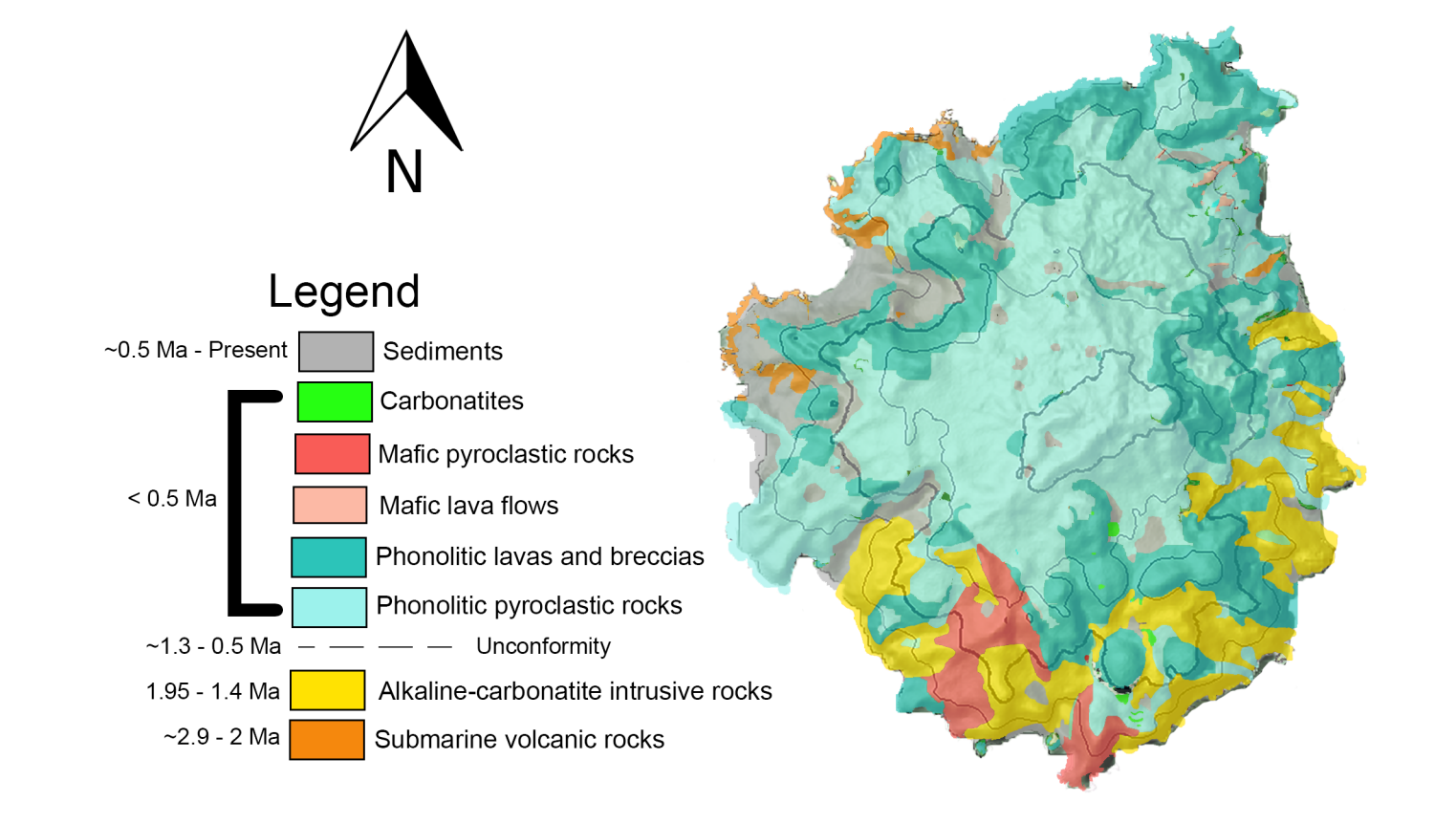
N
Legend
~0.5 Ma - Present
Sediments
< 0.5 Ma
Carbonatites
Mafic pyroclastic rocks
Mafic lava flows
Phonolitic lavas and breccias
Phonolitic pyroclastic rocks
~1.3 - 0.5 Ma
Unconformity
1.95 - 1.4 Ma
Alkaline-carbonatite intrusive rocks
~2.9 - 2 Ma
Submarine volcanic rocks

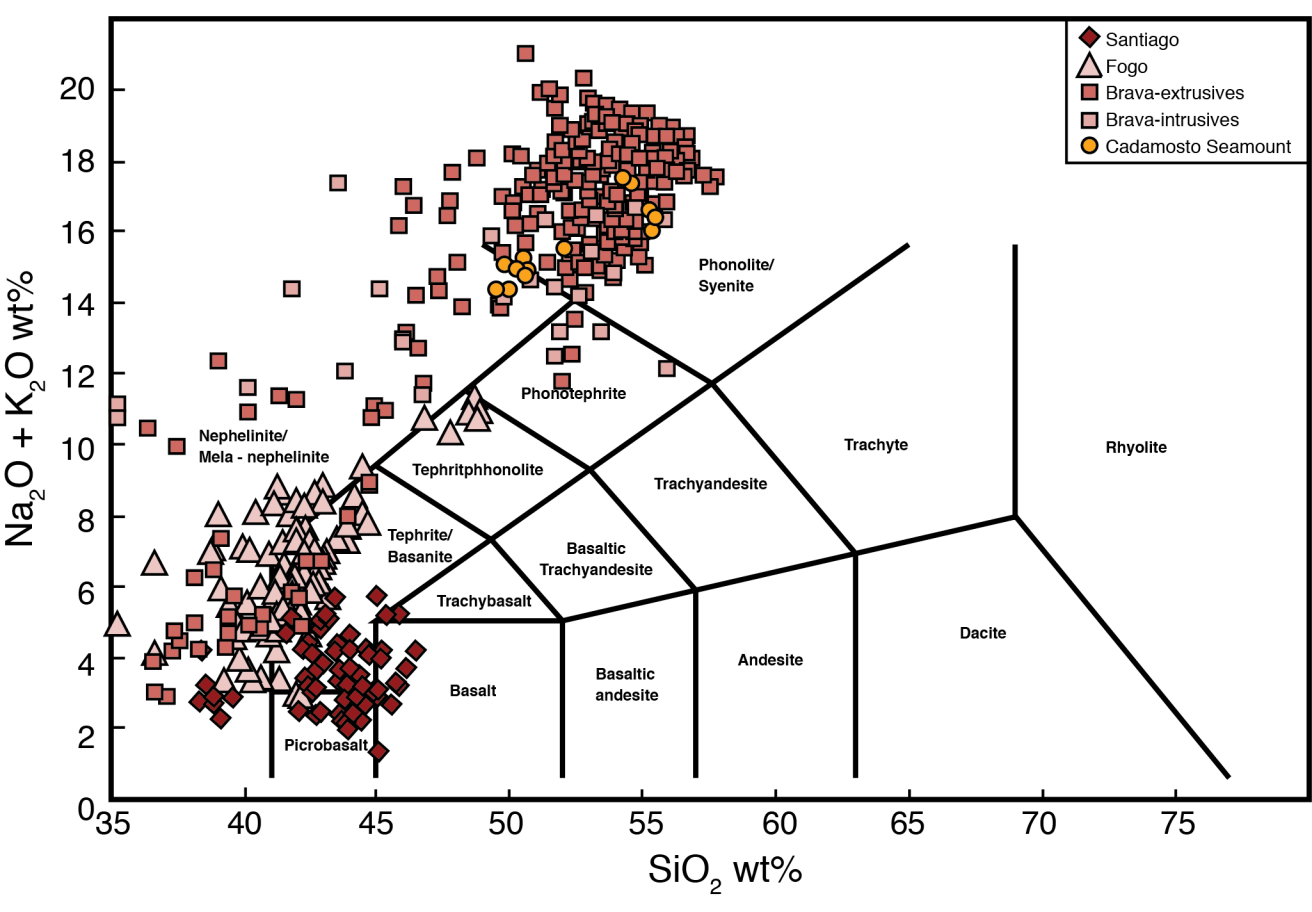
Santiago
Fogo
Brava-extrusives
Brava-intrusives
Cadamosto Seamount
Phonolite/
Syenite
Phonotephrite
Nephelinite/
Mela - nephelinite
Tephritphhonolite
Trachyte
Rhyolite
Trachyandesite
Tephrite/
Basanite
Basaltic
Trachyandesite
Trachybasalt
Dacite
Andesite
Basaltic
andesite
Basalt
Picrobasalt
$Na_2O + K_2O$ wt%
SiO_2 wt%
0
2
4
6
8
10
12
14
16
18
20
35
40
45
50
55
60
65
70
75

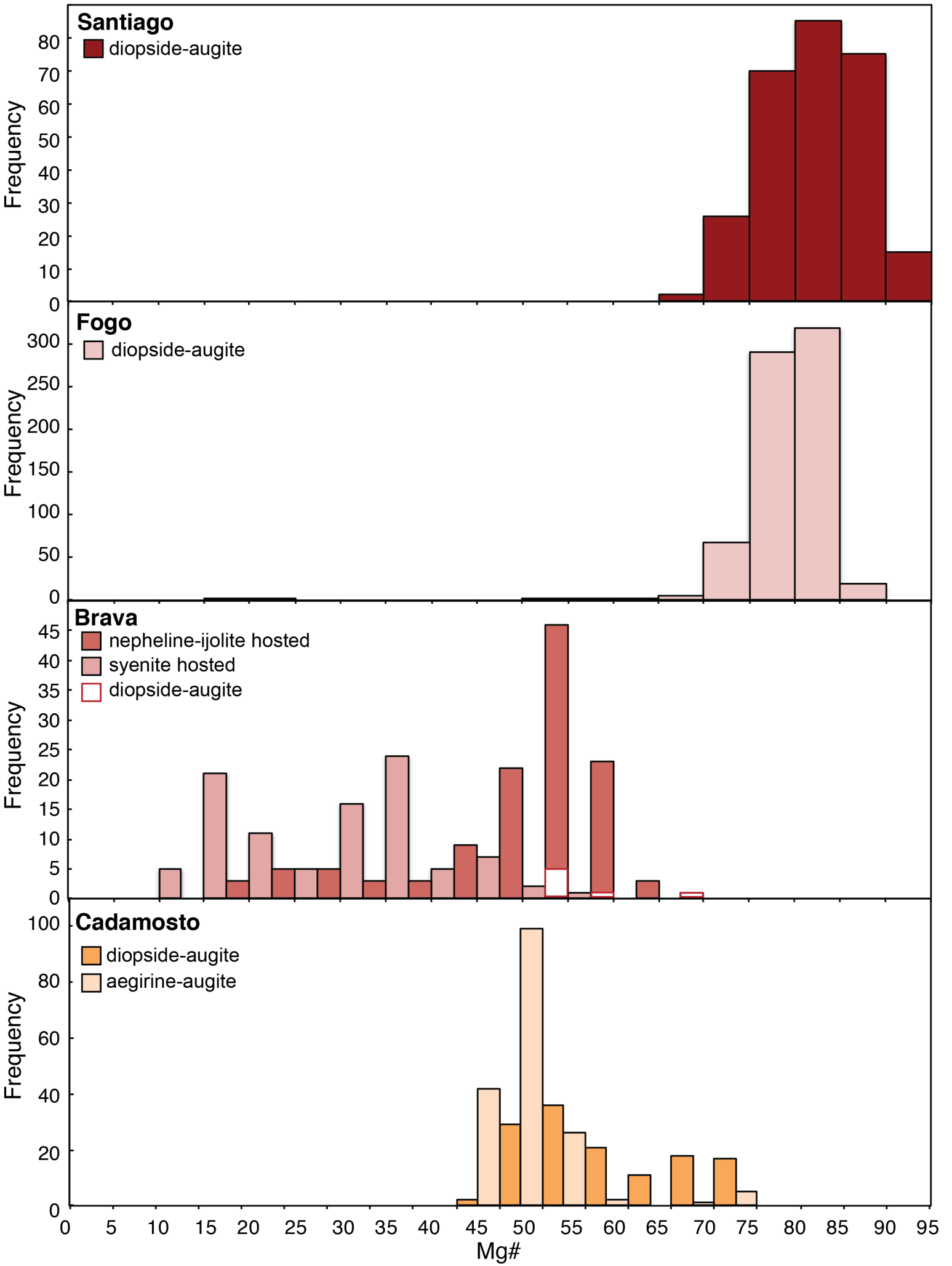
Santiago
diopside-augite
Frequency
Fogo
diopside-augite
Frequency
Brava
nepheline-ijolite hosted
syenite hosted
diopside-augite
Frequency
Cadamosto
diopside-augite
aegirine-augite
Frequency
Mg#

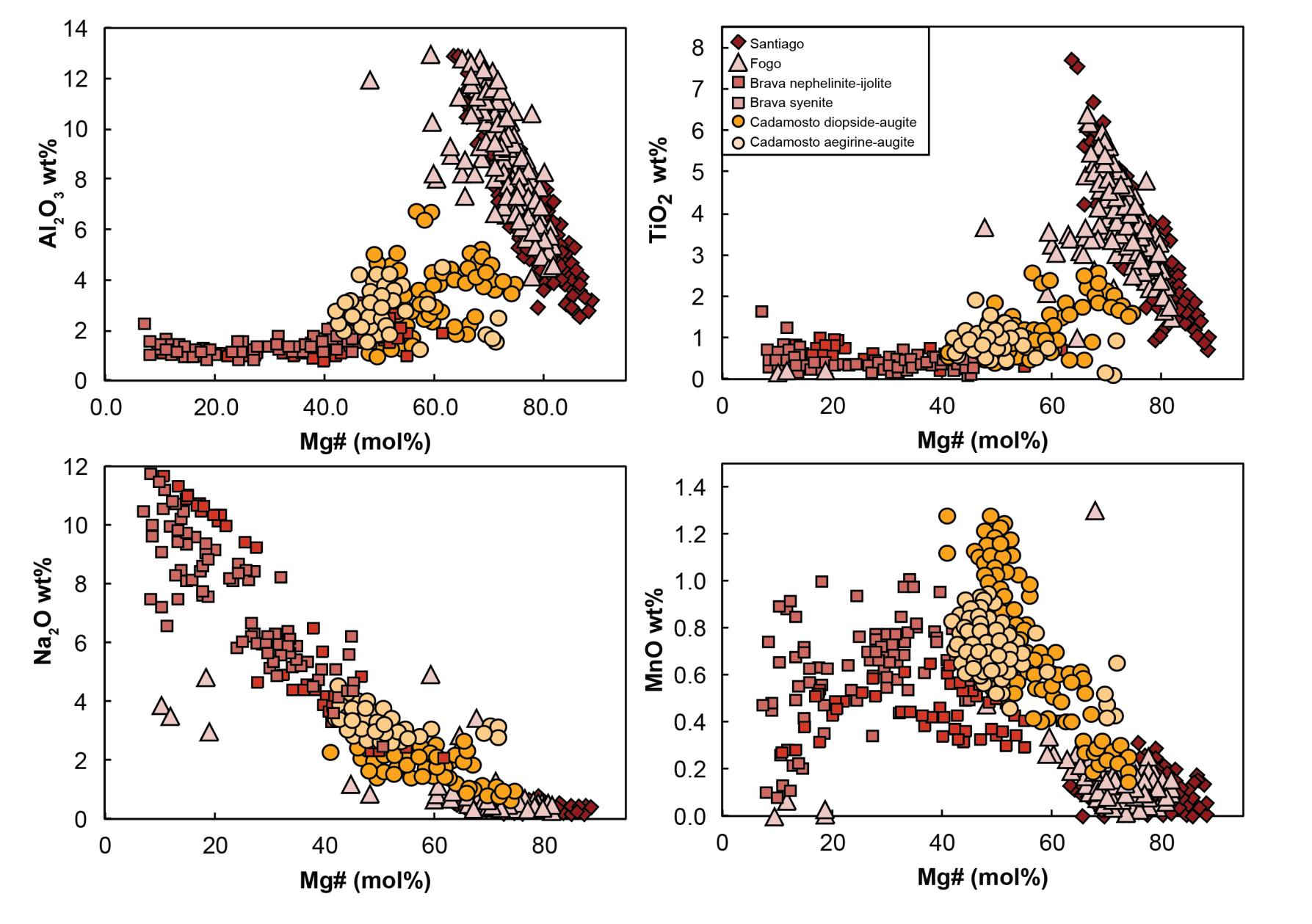
Al2O3 wt%
Mg# (mol%)
TiO2 wt%
Mg# (mol%)
Na2O wt%
Mg# (mol%)
MnO wt%
Mg# (mol%)
Santiago
Fogo
Brava nephelinite-ijolite
Brava syenite
Cadamosto diopside-augite
Cadamosto aegirine-augite

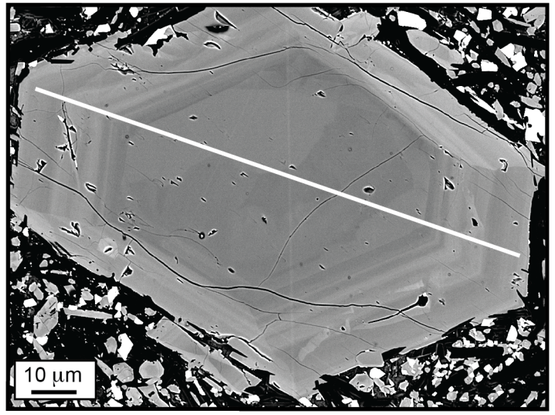
10 µm

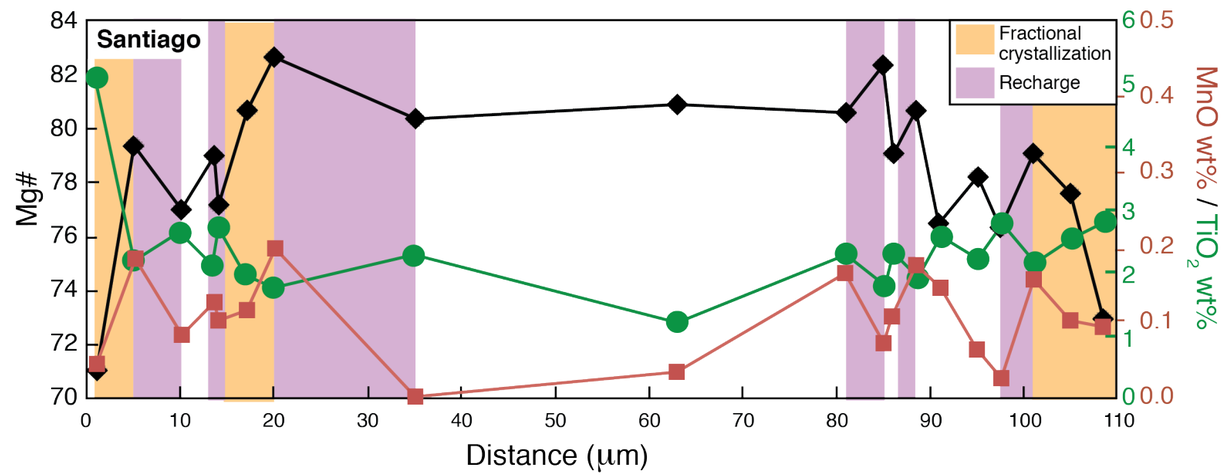
Santiago
Fractional crystallization
Recharge
Mg#
MnO wt% / TiO2 wt%
Distance (µm)

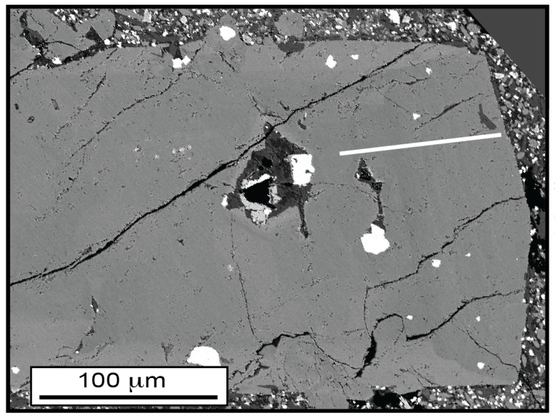
100 µm

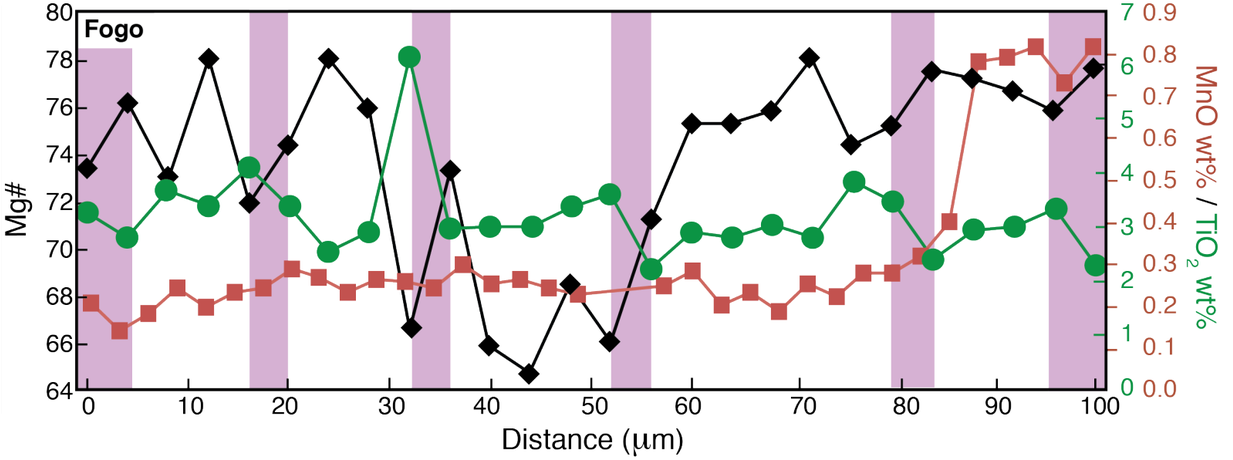
Fogo
Mg#
MnO wt% / TiO2 wt%
Distance (µm)

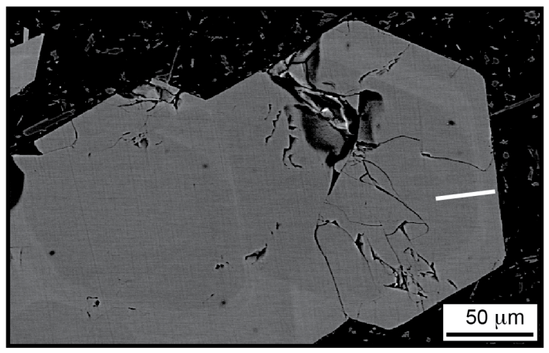
50 µm

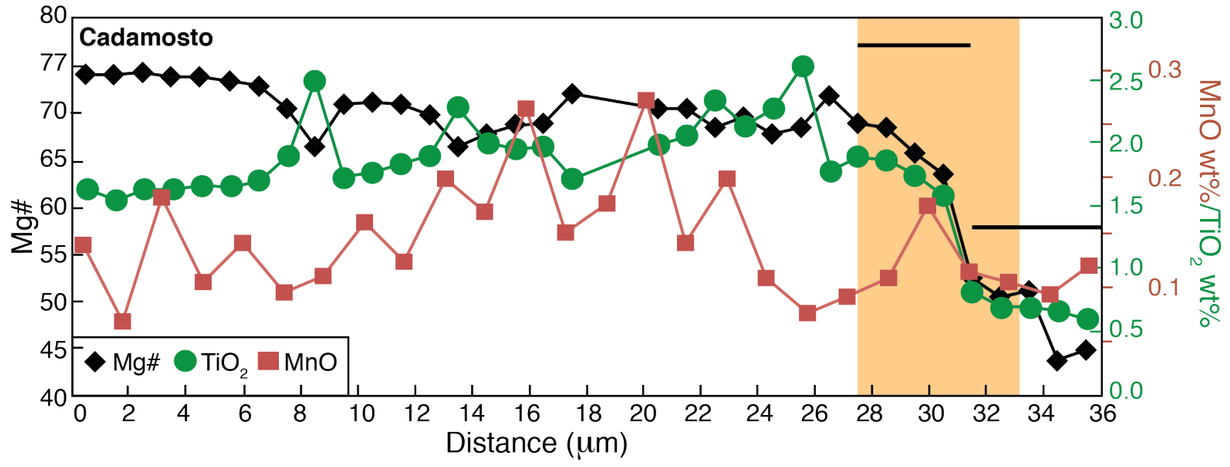
Cadamosto
Mg#
TiO2
MnO
MnO wt%/TiO2 wt%
Distance (µm)

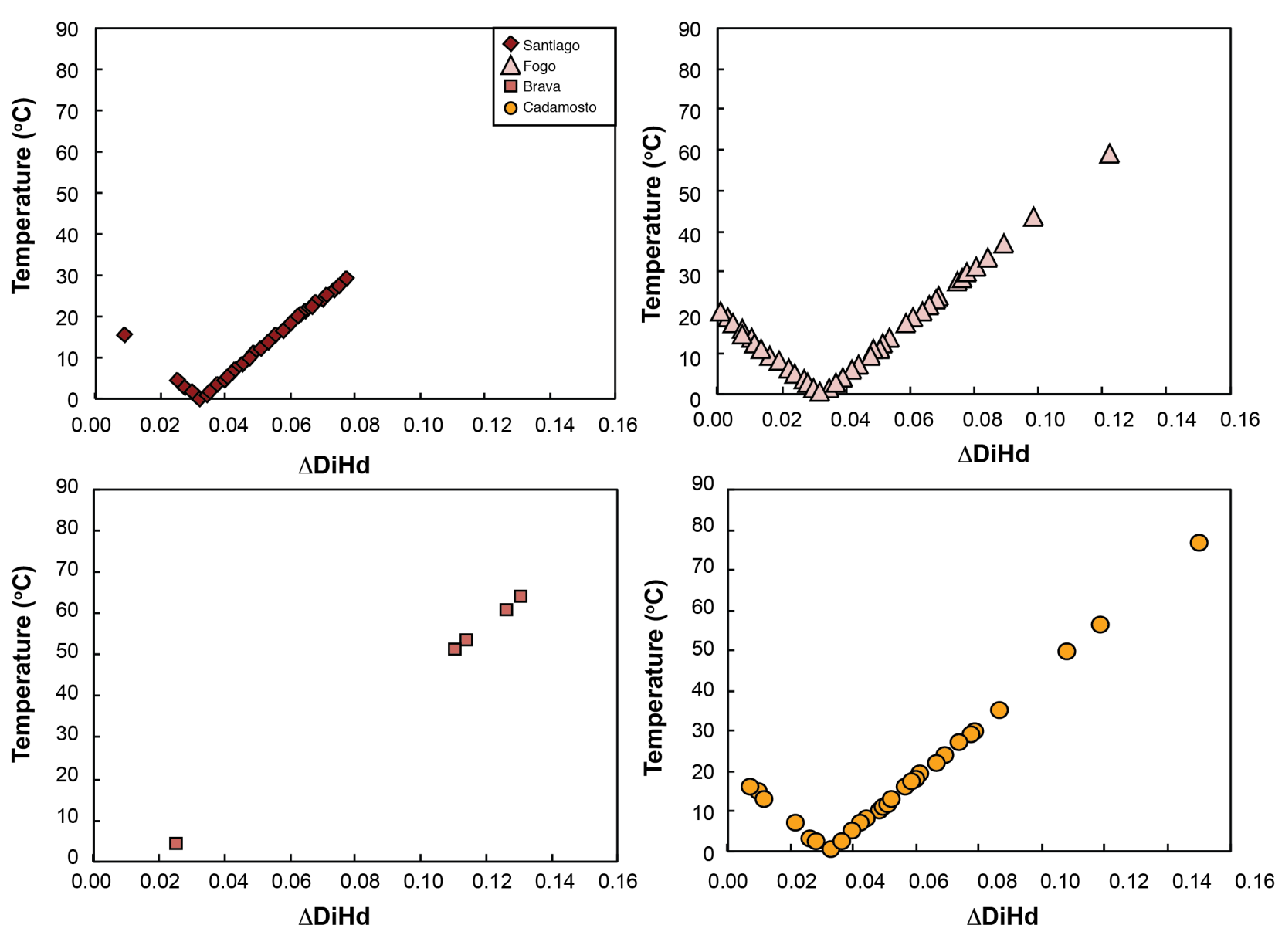
Santiago
Fogo
Brava
Cadamosto
Temperature (°C)
ΔDiHd
0
10
20
30
40
50
60
70
80
90
0.00
0.02
0.04
0.06
0.08
0.10
0.12
0.14
0.16

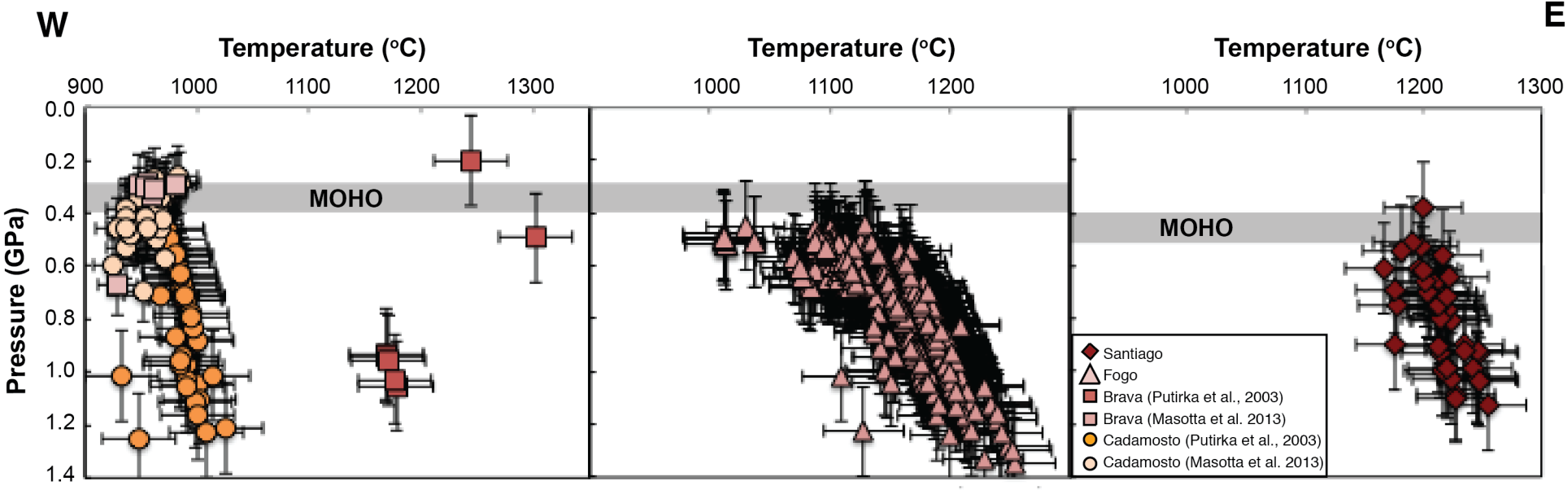
W
E
Temperature (°C)
900
1000
1100
1200
1300
Pressure (GPa)
0.0
0.2
0.4
0.6
0.8
1.0
1.2
1.4
MOHO
Santiago
Fogo
Brava (Putirka et al., 2003)
Brava (Masotta et al. 2013)
Cadamosto (Putirka et al., 2003)
Cadamosto (Masotta et al. 2013)

(a)

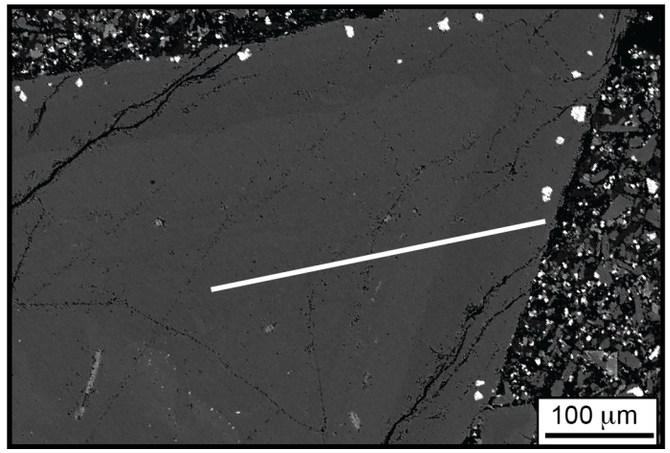
100 μm

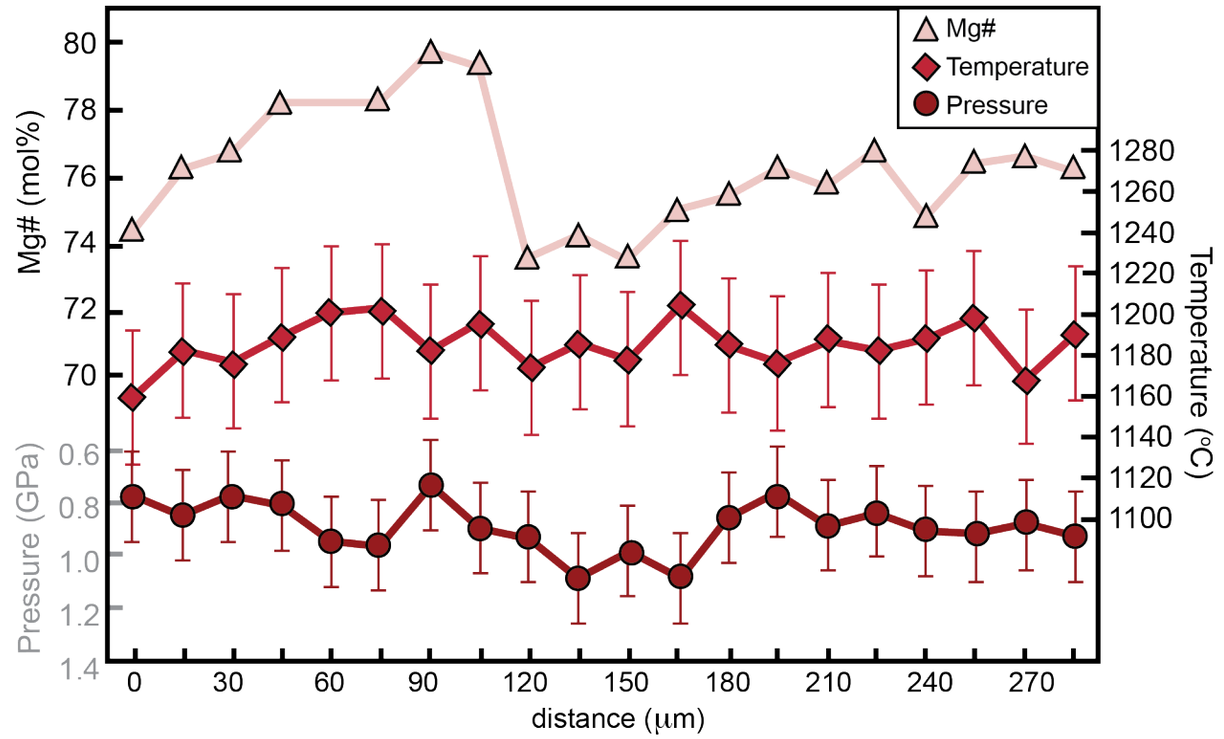
Mg#
Temperature
Pressure
Mg# (mol%)
Pressure (GPa)
Temperature (°C)
distance (μm)

(b)

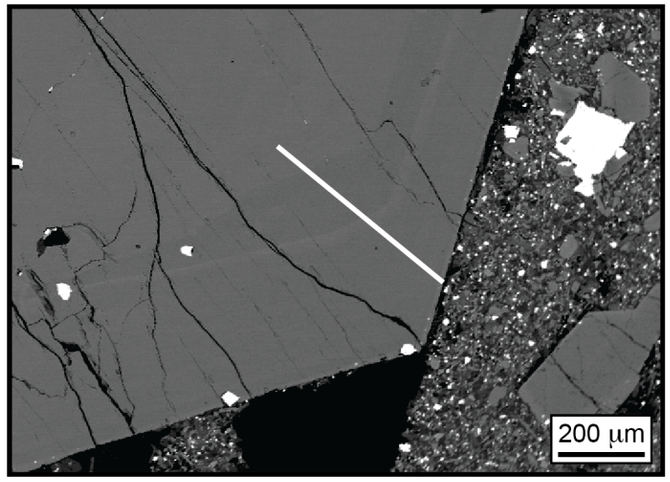
200 μm

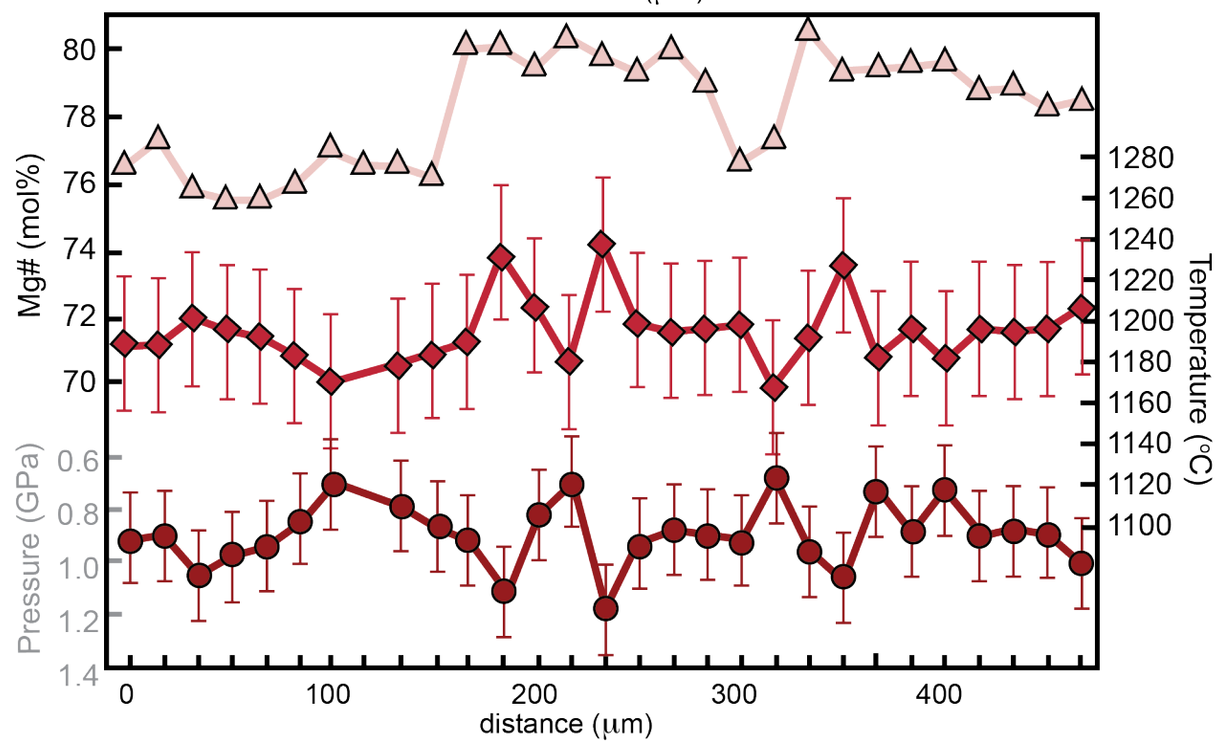
Mg# (mol%)
Pressure (GPa)
Temperature (°C)
distance (μm)

(c)

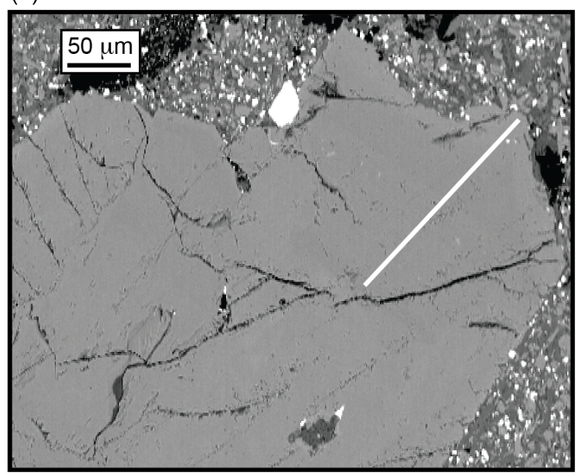
50 μm

(d)

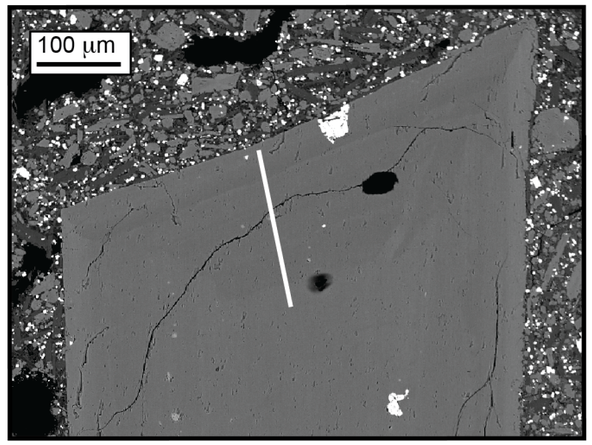
100 μm

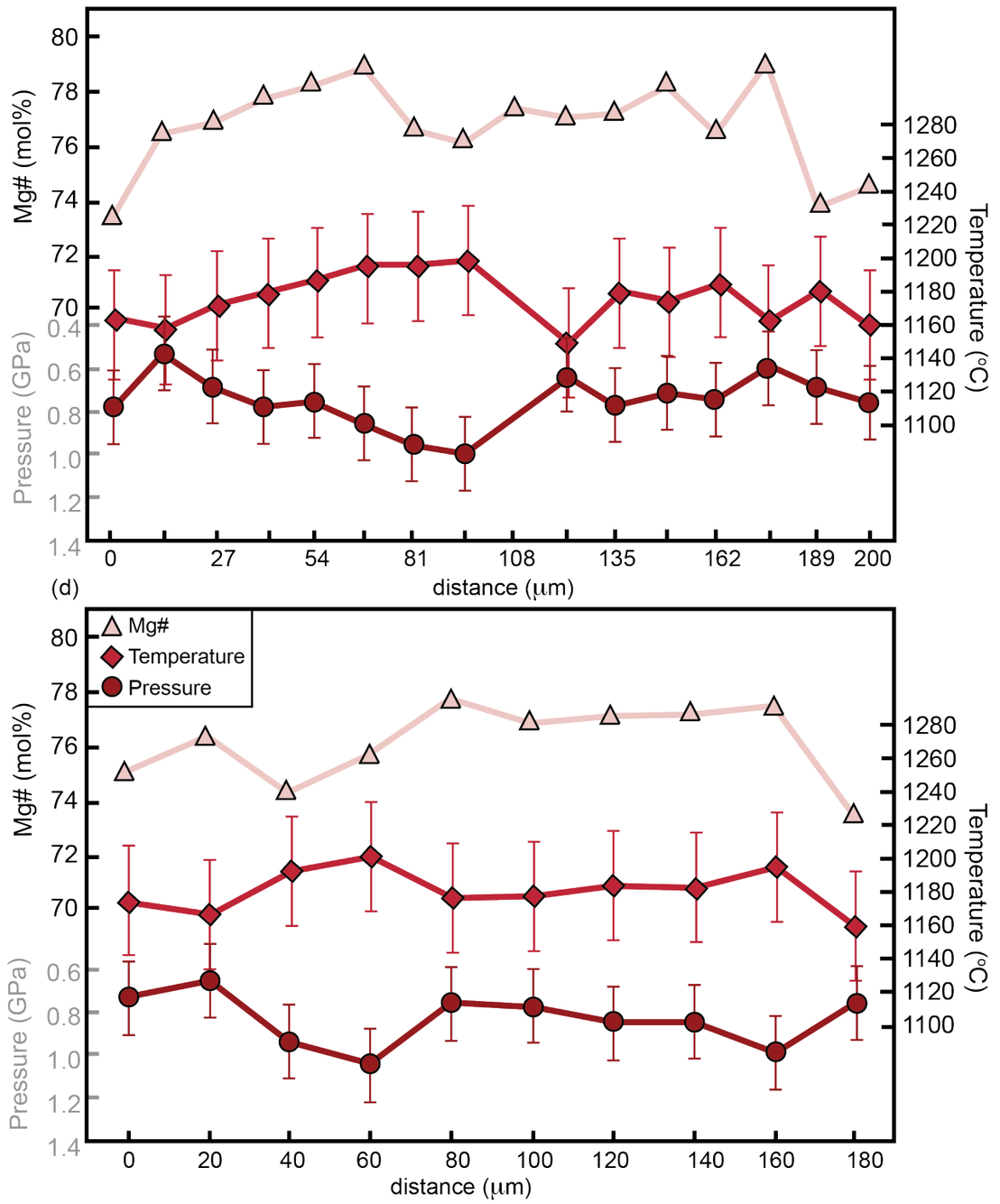
Mg# (mol%)
Pressure (GPa)
Temperature (°C)
distance (μm)
Mg#
Temperature
Pressure
80
78
76
74
72
70
0.4
0.6
0.8
1.0
1.2
1.4
1280
1260
1240
1220
1200
1180
1160
1140
1120
1100
0
27
54
81
108
135
162
189
200
0
20
40
60
80
100
120
140
160
180

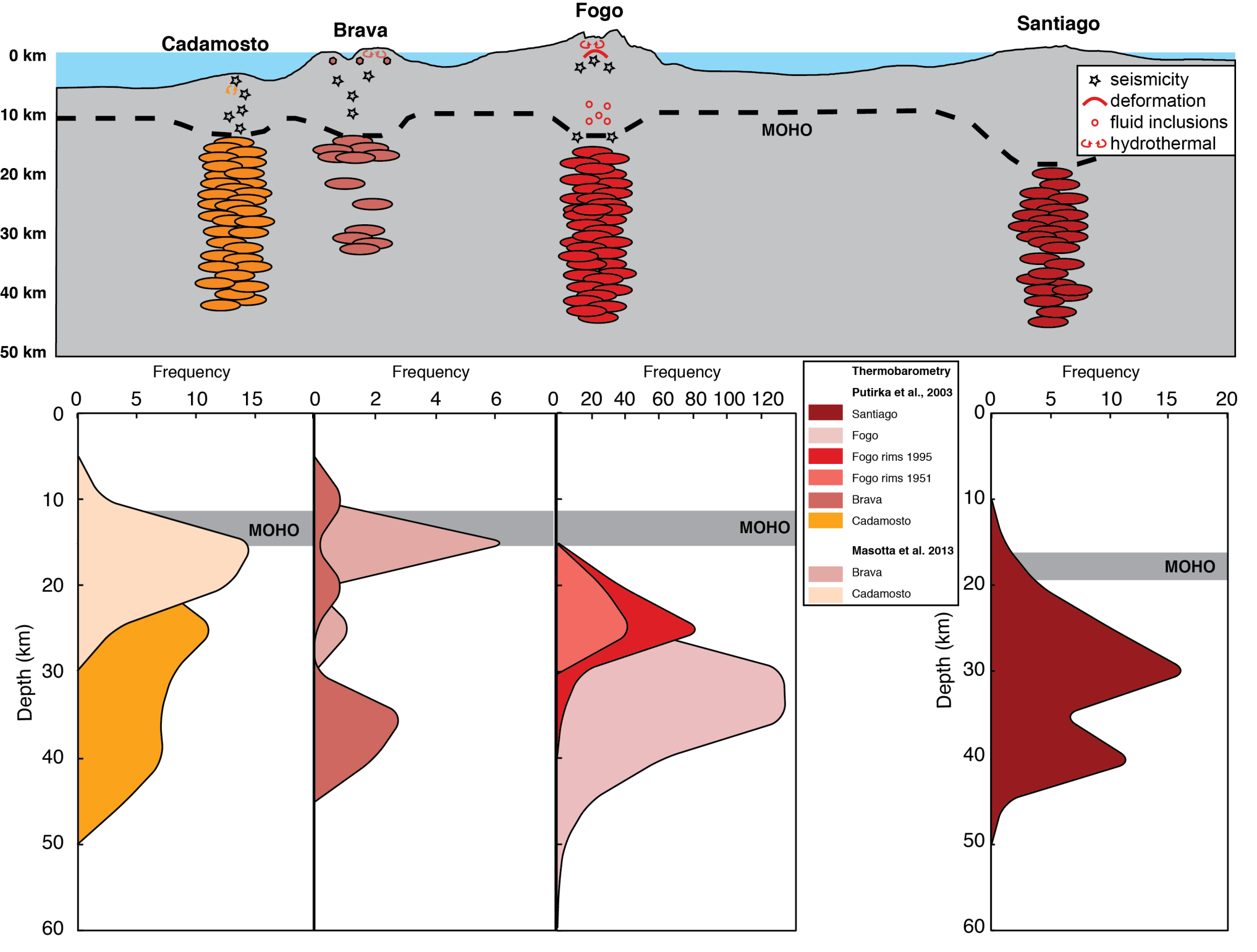
Cadamosto
Brava
Fogo
Santiago
0 km
10 km
20 km
30 km
40 km
50 km
MOHO
seismicity
deformation
fluid inclusions
hydrothermal
Frequency
Depth (km)
MOHO
Thermobarometry
Putirka et al., 2003
Santiago
Fogo
Fogo rims 1995
Fogo rims 1951
Brava
Cadamosto
Masotta et al. 2013
Brava
Cadamosto

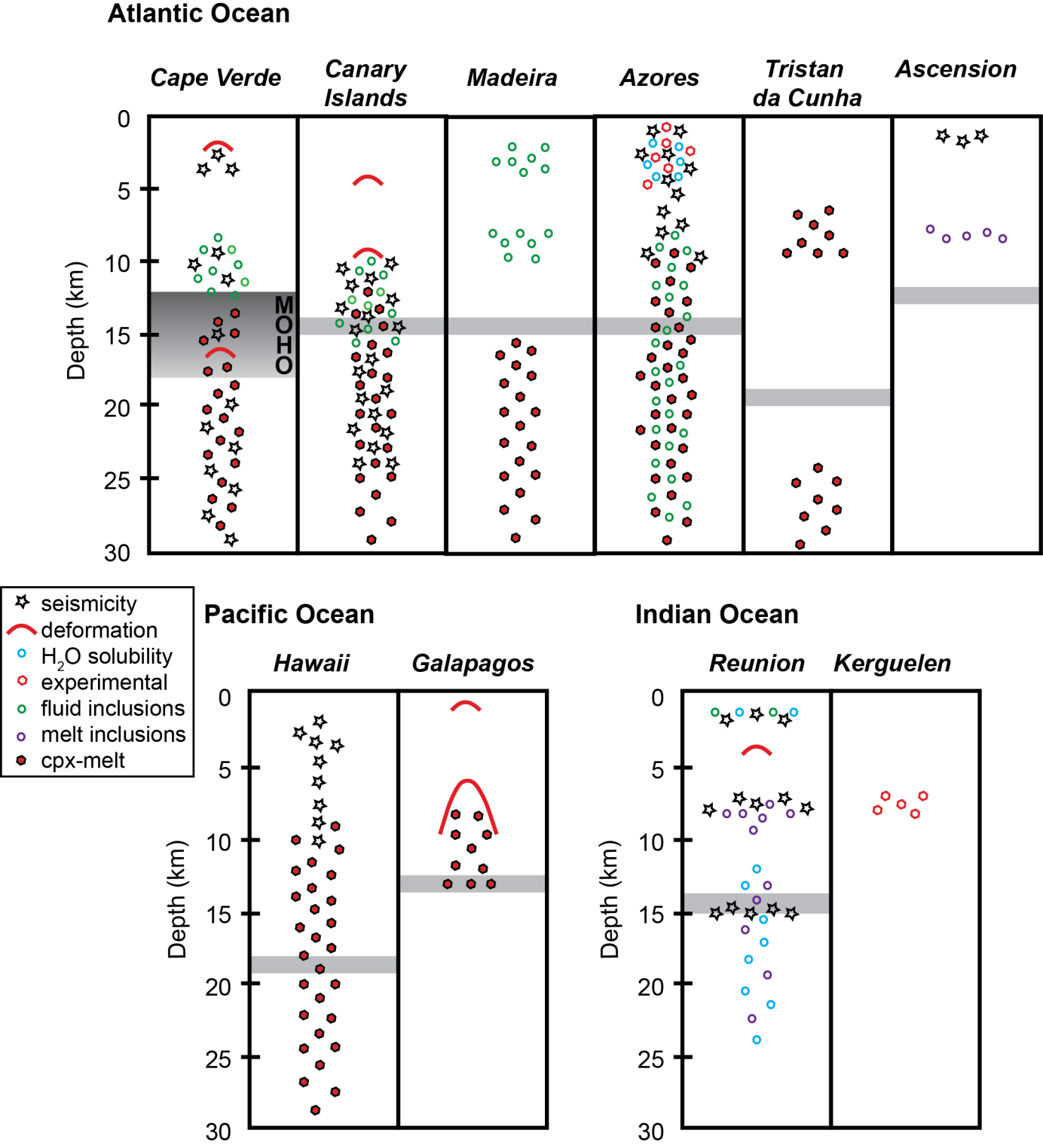
Atlantic Ocean
Cape Verde
Canary Islands
Madeira
Azores
Tristan da Cunha
Ascension
Depth (km)
0
5
10
15
20
25
30
MOHO
seismicity
deformation
H2O solubility
experimental
fluid inclusions
melt inclusions
cpx-melt
Pacific Ocean
Hawaii
Galapagos
Indian Ocean
Reunion
Kerguelen

Atlantic Ocean

Cape Verde	Canary Islands	Madeira	Azores	Tristan da Cunha	Ascension
1 to 5 km seismicity, deformation	4.5 km deformation	2 to 4 km fluid inclusions	2 to 4 km water solubility, fractionation, seismicity	earthquakes prior to eruptions	1.5 to 2 km seismicity
8 to 13 km fluid inclusions, seismicity	10 to 16 km fluid inclusions, deformation	8 to 10 km fluid inclusions	>8 km fluid inclusions, cpx-melt, seismicity	6 to 10 km cpx-melt	8.5 km melt inclusions
12 to 18 km Moho	14 km Moho	14 to 15 km Moho	14 km Moho	19 km Moho	12 to 13 km Moho
13 to 46 km cpx-melt, seismicity, deformation	12 to 45 km cpx-melt, seismicity	15 to 35 km cpx-melt	<30 km cpx-melt, fsp-ol melt, fluid inclusions	24 to 36 km cpx-melt	
da Silva et al 1999; Amelung & Day 2002; Lodge & Helffrich, 2006; Pim et al., 2008; Barker et al., 2009, 2012; Grevemeyer et al., 2010; Hildner et al., 2011, 2012; Faria & Fonseca 2014; Fernandez & Faria, 2015; Vales et al., 2015; Jenkins et al., 2017; Leva et al., 2019; Mata et al., 2017; this study.	Klügel et al., 2000; 2005; Galipp et al., 2006; Longpre et al., 2008, 2014; Aulinas et al., 2010; Barker et al., 2015; Gonzalez et al., 2013.	Schwarz et al., 2004; Klügel & Klein, 2006	Renzulli & Santi 2000; Beier et al., 2006; Dias et al., 2007; Silva et al 2012; Jeffery et al., 2016; Madureira et al., 2008; Zanon et al., 2013; Zanon & Pimentel 2015	Geissler et al., 2016; Weit et al., 2017	Klinghofer et al., 2001; Hanson et al., 1996; Chamberlin et al., 2016

Pacific Ocean		**Indian Ocean**	
Hawaii	**Galapagos**	**Reunion**	**Kerguelen**
2 to 4 km (<10 km) seismicity	1 km deformation	0.5 to 2.5 km water solubility, melt inclusions, seismicity	
9 to 18 km cpx-melt	8 to 13 km cpx-melt, deformation	7 to 14 km water solubility, melt inclusions, seismicity	6 to 8 km experimental
18 to 19 km Moho	13 km Moho	14 to 15 km Moho	
19 to 46 km cpx-melt		15 to 24 km water solubility, melt inclusions, seismicity	
Putirka 1996, 1997; Chatterjee et al., 2005; Poland et al 2015; Hammer et al., 2016	Stock et al., 2018	Bureau et al., 1998; Famin et al., 2009; Peltier et al. 2009; Di Muro et al., 2014; Fontaine et al., 2014	Freise et al., 2003